A Study of the Effects of Heterogeneities on Immiscible Displacements and Their Representation in Numerical Simulators

by

JOHN RAYMOND WAGGONER, B.S. in Petroleum Engineering

THESIS

Presented to the Faculty of the Graduate School of

The University of Texas at Austin

in Partial Fulfillment

of the Requirements

for the Degree of

Master of Science in Petroleum Engineering

THE UNIVERSITY OF TEXAS AT AUSTIN

December, 1985

ACKNOWLEDGEMENTS

ABSTRACT

Reservoir characterization is the process of discretizing the continuous geologic description of a reservoir into grid blocks for input into a numerical reservoir simulator. The accuracy of this discretization process is of great importance since the simulation results are often used to make important and expensive decisions. This thesis looks at the effects of some common permeability heterogeneities, namely systematically graded permeability and cross bedding, which occur in common geologic depositional units such as channel sands and barrier bar sands. After this qualitative discussion of the effects of flow rate, permeability contrast, viscosity ratio, and cross bedding on water saturation profiles in heterogeneous porous media, this study examines the use of pseudo functions, such as pseudo fractional flow, to represent the heterogeneity in a one dimensional, homogeneous reservoir. Three analytical methods of calculating pseudo fractional flow, Dykstra-Parsons, Hearn, and Vertical Equilibrium, are compared to simulation results to evaluate their effectiveness in representing heterogeneities.

This study concludes, in part, that the extent of vertical communication in the reservoir determines which of the pseudo curve calculation methods will best represent the heterogeneity, and that a previously proposed dimensionless number, R_L, adequately determines the extent of vertical communication in the reservoir.

TABLE OF CONTENTS

LIST OF FIGURES

CHAPTER I

INTRODUCTION

For most of the oil industry, oil recovery is the primary concern. Different groups within a company, however, have different areas of interest which work together to achieve the maximum possible recovery. The reservoir engineering group, for example, is concerned with optimizing oil recovery by adjusting well flow rates and designing well stimulation treatments. One tool that the reservoir engineer may use is a numerical reservoir simulator which the simulation group maintains. The simulation group is concerned with developing and operating the program to solve the engineer's problem with a high degree of confidence in the solution. The weak point in any simulator is the input data. Errors here can have anywhere from an insignificant to a catastrophic effect depending on the sensitivity of the program to a given piece of data. Clearly the simulation group should identify those parameters which are the most sensitive and try to minimize the errors.

The reservoir description is a set of input data which is very difficult to determine and thus can cast much uncertainty upon the simulator output. Generating a reasonable reservoir description for input to a simulator is the job of the reservoir characterization group. The geology group develops descriptions of the reservoir rock based on cores, well logs, and knowledge of typical behavior within a depositional unit.

The primary aim of this study is the reservoir characterization group which, as the above indicates, lies between the simulation group and the geology group. Geology

is a study of the continuum of nature, while simulations require a discrete description with single properties representing an often large volume. The job of the reservoir characterization group, therefore, is to provide the simulators with a discrete description of the reservoir which maintains the continuous geological description.

In all processes which take input and produce output, the quality of the output is directly proportional to the quality of the input. Therefore, the first step in developing a good discrete reservoir description is obtaining a good continuous, or grid-independent, description, the creation of which is a joint effort between geologists, geostatisticians, and reservoir engineers examining well log data, core data, seismic data, pressure transient tests, and statistics derived from knowledge of data in the well and perhaps an estimate of the depositional system. When the most likely grid independent description is developed, it is then necessary to overlay the desired grid to be used in the simulation. The cost of the simulation per grid block and the degree of accuracy desired are the main points to consider when determining the number and size of the grid block mesh.

Once the mesh is laid over the reservoir description, it will usually become obvious that each grid block contains a great deal of detail, Fig I-1, which must be reduced to effective, or pseudo, properties for input to the simulator. This complex process, called parameter assignment, is an averaging of effects in such a way that the original detail is well represented. This can obviously be a very simple or difficult task, depending on the type of detail or heterogeneity. The simple case occurs when the grid block encloses a homogeneous region. In a detailed reservoir description, this will probably never happen. The difficulty occurs when the grid block contains shale streaks, several depositional unit boundaries, or even a single depositional unit with no
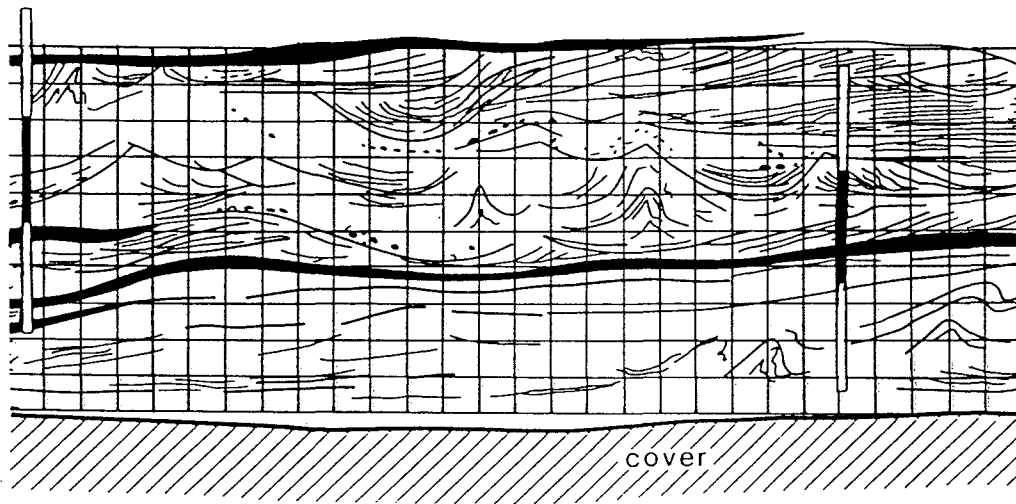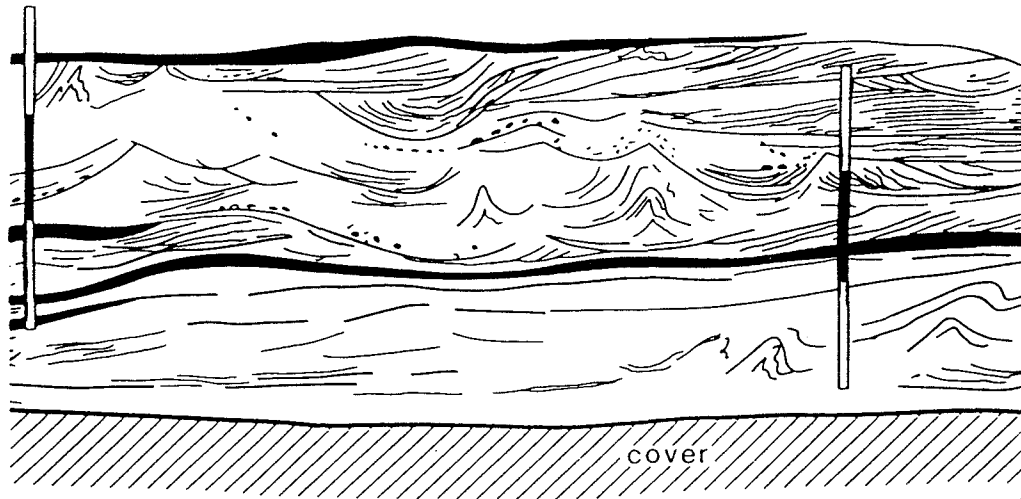
Shale Drape
Erosional Contact
Shale-siltstone
Sandstone

Figure I-1 : Illustration of Realistic Geologic Detail With
and Without Simulation Grid Overlayed

boundaries, the latter of which is the subject of this study. The first two are subjects for future research.

The current work studies the grid block representation of two common depositional units: barrier bar sands and channel sands, both of which can be represented by a systematically stratified system with a linear permeability distribution. The aim is to qualitatively evaluate immiscible displacements in the system (Chapter III), and then quantitatively represent the heterogeneity as a pseudo fractional flow curve (Chapter IV). The first section, Chapter III, investigates the effect of these realistic heterogeneities on waterflood recovery, and looks at the effect of flow rate, permeability ratio, viscosity ratio, and cross-bedding. The second section, Chapter IV, examines the generation of pseudo curves as a way to represent the oil displacement behavior of these depositional units in a single coarse grid block. The pseudo curves are generated from a two dimensional (2-D) cross sectional, compressible, IMPES (IMplicit Pressure Explicit Saturation) simulation which calculates and outputs the pseudo fractional flow curves at various times in the flood. These pseudo curves are compared to curves generated by the Vertical Equilibrium (VE), Hearn and continuous Dykstra-Parsons (DP) theories to evaluate under what conditions of vertical permeability one of these analytical methods may be used without loss of accuracy. It is supposed that these pseudo curves will be able to accurately represent the simulated heterogeneity with a single grid block in a much larger field simulation. The work for these two sections was carried out at different times using different simulation models and computers. Both of these sections are limited to waterfloods of a 2-D vertical cross-section of a single deposition with unit width. No attempt has been made to extend the results to full 3-D behavior which is clearly of great interest. The two

studies are also restricted to looking at saturation profiles or computed pseudo curves as output. A discussion of the system studied and the simulator used will be delayed until the beginning of each chapter. Before describing the work at hand, however, it is important to survey the literature to see what has been published on this subject.

CHAPTER II

LITERATURE REVIEW

The literature reflects the industry acceptance, by lack of published alternatives, of some classic theories concerning immiscible displacements in heterogeneous layered systems. More recently, several authors have modified these theories to reflect more realistic heterogeneities, while others have employed simulations to examine conditions which are too complex for analytical methods. This chapter will briefly review these published articles.

Perhaps the most recognized analytical description of immiscible displacements in a homogeneous porous media was published by S.E. Buckley and M.C. Leverett (BL) in 1942[1]. In 1952, H.J. Welge[2] developed a graphical method to the BL solution that makes working the problem much easier. Both of these papers were based on the same system, namely a homogeneous, isotropic, one-dimensional (1-D) porous media. The two phases are immiscible, incompressible, and isothermal with no phase pressure difference, or capillary pressure. Even with these restrictions, however, the BL theory has been of great use in describing immiscible displacements and forms the basis for much of the industry's understanding of displacement processes. The BL theory is very well described by the original paper and subsequent references by Collins[3], Craig[4], Dake[5] and Lake[6].

Stratified, or layered, systems were apparently first studied analytically by H. Dykstra and R.L. Parsons (DP) in a paper[7] presented in 1948. Their system consisted of two or more homogeneous, isotropic, 1-D layers with an impermeable lamina

between each layer preventing crossflow of fluids. The two-phase immiscible, incompressible, isothermal displacement in each layer assumed a constant relative permeability to water (k_{rw}) behind the front, and a constant relative permeability to water (k_{ro}) ahead of the front, describing what is commonly called a piston-like displacement. Capillary pressure was neglected. The total flow rate into the system was kept constant. The injection and production ends of the system are planes of constant pressure, although the pressures at each end are not constant since the pressure drop across the system must vary during the flood. Although these restrictions are severe, this system has been the basis for most subsequent studies on stratified systems, as it provides the mechanism for studying stratified reservoirs that was not present before.

The DP theory makes no restrictions on the mobility ratio, M, of the two phases. When M = 1.0, however, a simpler solution is available. In 1949, W.E. Stiles[8] published his work on a unit mobility ratio stratified displacement in a system identical to the DP system described above. Although he assumed unit mobility ratio in the derivation, he later applied these equations to non-unit mobility ratios. The reader should be aware that this inconsistency might lead to some errors when the equations are applied to non-unit mobility ratio cases. The Stiles method is, however, valid when M = 1.0.

The DP solution takes the form of an equation which calculates the front position in all layers when the most permeable unswept layer breaks through. From the known front position in each layer, it is possible to calculate a number of waterflood variables, such as cumulative and incremental fluid injected and produced, and water/oil ratio at the production end. While this data is very important, it is also sparse due to the

discrete times at which the calculations are made. Recently, Zapata[9] in 1979 and Reznic et al.[10] in 1984 have extended the DP theory to a continuous basis where the front positions can be calculated based on any reference layer and at any front position within that layer. This makes it possible to calculate data points at a large number of data points instead of being limited by the number of layers. These analytical extensions of the classical DP theory have greatly enhanced the usefulness of DP theory in the research of stratified systems.

DP theory assumes that the layers do not communicate with each other, except at the injection and production ends. For most realistic systems, however, the layers do communicate to some degree, thus creating the need for stratified models which include crossflow. The absence of an analytical extension to the DP theory which includes crossflow attests to the difficulty of analytical treatment. Several authors have sacrificed knowledge of front positions during the flood in favor of pseudo functions which incorporate the effects of crossflow.

Pseudo functions, generally pseudo relative permeabilities, have the ability to represent complex behavior in a simplified manner, and have been used routinely as a way of representing 3-D behavior in a 2-D simulator. The main benefit is that the 2-D simulation can be an order of magnitude cheaper in computer time and man hours than the 3-D simulation, without a significant loss of accuracy. Coats et al.[11] discusses this problem thoroughly. This same benefit can be realized when simulating a 2-D cross section with a 1-D simulation or analytical BL analysis, if the proper pseudo functions can be derived.

Several authors have reported their methods for deriving pseudo functions. Of particular note are Coats *et al.*[12] and Hearn[13], both in 1971. Both of these studies employ a stratified system in which fluid is allowed unrestricted vertical movement, which describes a reservoir in which the layers are in infinite communication with neighboring layers. The difference between these analytical studies arises from elimination of gravity and capillary forces in the Hearn paper, so that the Hearn theory is a special case of the vertical equilibrium (VE) theory presented by Coats *et al.* Vertical equilibrium has been well described in the literature by Coats[12], Jones[14], and Lake[15]. The Hearn model is discussed in the original paper, and has been modified for mobility ratios greater than one by Zapata in 1979. See these references for details.

The Hearn and VE theories assume a system with infinite crossflow. The DP theory assumes zero crossflow. Between these extremes lies a wide range of crossflow conditions for which no analytical solution has been presented. Berruin and Morse[16] in 1979 simulated stratified systems with both a systematic and a random placement of layer permeabilities chosen from a log-normal distribution. For cases with crossflow, the vertical permeability was set equal to the horizontal permeability, indicating a case where the crossflow is between the extremes of zero and infinity. This work concluded that a randomly stratified system could be accurately represented by a homogeneous system with the same flow capacity. No conclusions were drawn on representing a systematically stratified system quantitatively.

CHAPTER III

THE EFFECT OF DEPOSITIONAL STRUCTURES ON RECOVERY

III.A - Introduction

Our motivation for this work comes from the observation that depositional structures affect oil recoveries. We generally notice this observation only when oil recovery has been adversly affected and we are looking for a scapegoat. It is possible, however, for the depositional structure to actually improve on a recovery estimate made without knowledge of the deposition. Obviously our knowledge of depositional structures and fluid flow through these structures is of great importance in making accurate predictions of oil recovery and fluid movement.

Nature is not so nice as to give us a finite number of depositional structures to investigate. However, geologists have. Their classifications have enabled us to identify structures that we find in an oil field, and, therefore, to recognize which structures occur most commonly. Two common structures, a barrier bar sand and a channel sand, will be the focus of this study, largely due to the ease with which they can be represented in a simulation. Within a given structure, we are still faced with an infinite variety of flow characteristics, such as permeability, porosity, and bedding.

III.B - System Studied

Barrier bars and channel sands are both described as fining sequences by geologists, meaning that the grain size is increasing or decreasing vertically. To an

engineer, this means that the permeability is graded, or monotonically increasing or decreasing, due to the grain size changes. Permeability will change with grain size in two ways. First, a smaller grain size means smaller pore throats which indicates a lower permeability. Second, as grain size decreases, more silt and shale is deposited due to the lower energy of deposition. This will tend to plug some of the already small pore throats and reduce permeability.

Geologists have not quantified the fining process, so we must guess at the magnitude of the permeability grading. Therefore, the contrast between the highest permeability and the lowest permeability (k_{max}/k_{min}) is one of the variables to study. Only k_{max}/k_{min} values of 10 and 1 are included in this study.

Permeability represented in the (k_{max}/k_{min}) ratio is horizontal permeability, k_h. Historically, horizontal and vertical permeability anisotropy has not been quantified, so that there is no body of knowledge defining the proper value for vertical permeability, k_v. Two different options have been used here to represent k_v. The first is to set k_v to a constant value across a cross-section. While this ignores the changing grain size, it can represent the observation that permeability normal to bedding planes tends to be less than permeability parallel to bedding planes. To include the fining grain size, the second option assigns the vertical permeability at a given point to equal some fraction of the horizontal permeability at that same point. The fraction used in this study was 1.0, but this is obviously an area for increased geological research.

The fining sequence described by geologists is continuous. A numerical simulator requires a discrete approximation to this continuity. In this study, the vertical dimension was divided into 10 equal thickness layers with permeabilities increasing

linearly from top to bottom (channel sand) or from bottom to top (barrier bar sand), Fig. III-1a. The vertical permeability can be different from the horizontal permeability to reflect anisotropy found in most fields. The system is horizontal to remove the complications caused by a dipping reservoir. Barrier bars are larger geologic structures than channel sands. Therefore, the barrier bar is modelled as 3000' x 100', while the channel sand is 300' x 10', each with the same number of grid blocks in each direction. Simulation results show that modelling a barrier bar as 300' x 10' or a channel sand as 3000' x 100' does not change the results, as long as the number of grid blocks in each direction remains the same.

III.C - Simulator Used

For this study, an incompressible, 2-phase, 2-dimensional cross-sectional simulator from Dr. Tom Lasseter at Schlumberger-Doll Research was used to generate saturation profiles in a variety of conditions. Capillary pressure was neglected and the same relative permeability curve, Fig. III-1b, applies to all cases. The choice of relative permeability curve was arbitrary. Porosity was also constant, at 20%.

III.D - Parameters Studied

This study investigates the effects of three of the most significant fluid flow parameters - flow rate, permeability contrast, and viscosity - and one geological consideration - cross bedding. The flow rate investigated is the injected flow rate. The actual flow rate in a layer will be significantly less than this since the well rate is divided amongst all the layers. The injected flow-rate is quoted in units of linear feet of reservoir per day, ft/day, or equivalently, $q/A\phi$. This unit actually describes the

Figure III-1a : Waterflood Heterogeneities
Depositional Unit Description

Channel Sand

k1 = kmin = 10.0 md
k2 = 20.0
k3 = 30.0
k4 = 40.0
k5 = 50.0 k_h
k6 = 60.0
k7 = 70.0 k_v
k8 = 80.0
k9 = 90.0
k10 = kmax = 100.0

Barrier Bar Sand

k1 = kmax = 100.0 md
k2 = 90.0
k3 = 80.0
k4 = 70.0
k5 = 60.0 k_h
k6 = 50.0
k7 = 40.0 k_v
k8 = 30.0
k9 = 20.0
k10 = kmin = 10.0
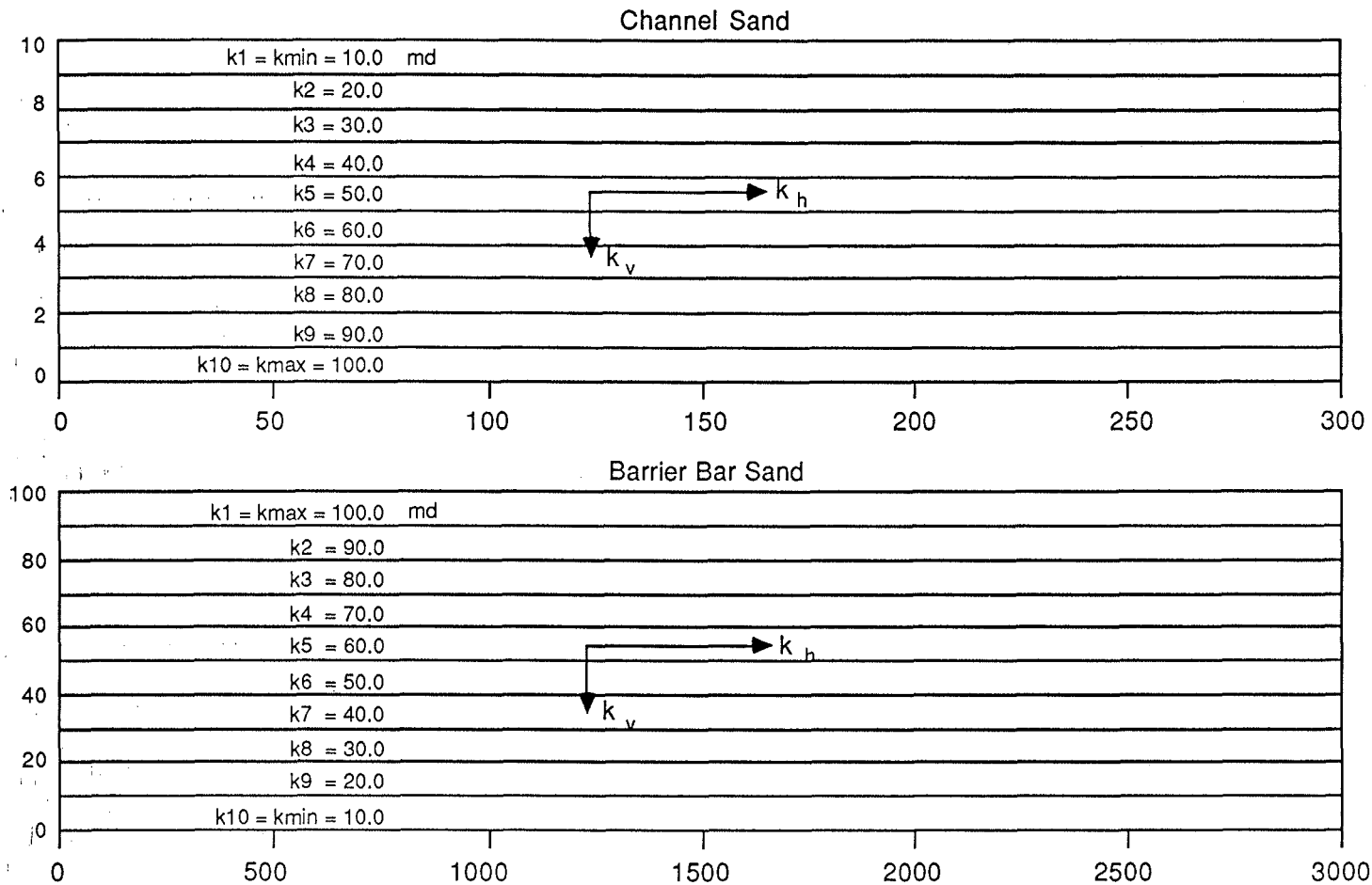
Relative Permeability Curves
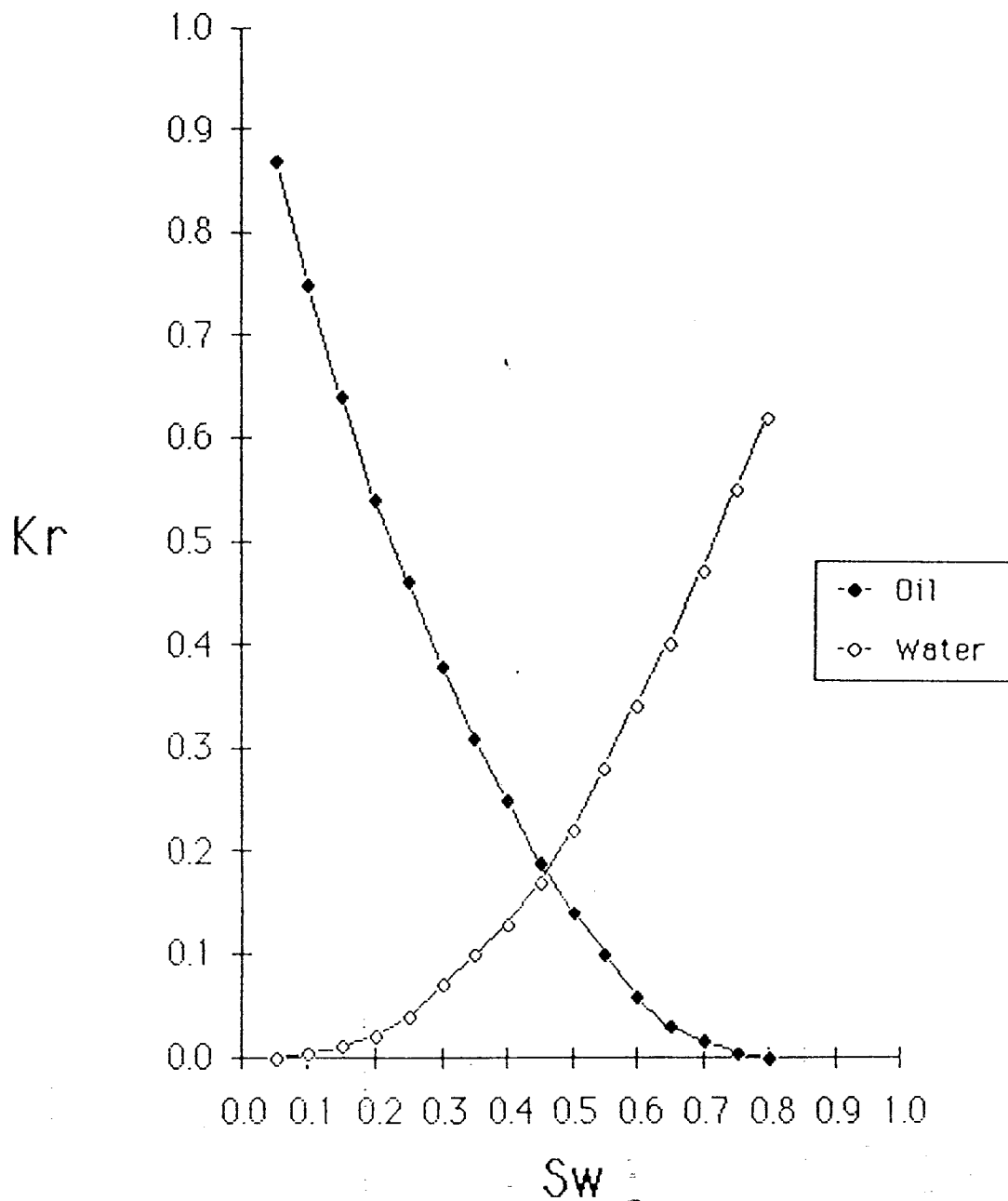
Figure III-1b : Input Relative Permeability Curves

velocity of a piston-like front traveling through a homogeneous system. This velocity unit is a constant multiple of the flow rate unit. The usefullness of the unit is that at any time during the flood, the position of this idealized front is obtained by multiplying the time by the velocity. The heterogeneous systems with a smeared front that we are interested in here clearly will have different velocities in each layer and thus will not have a single front position. However, the benefit of displaying injected flow rate as a velocity is that a comparison to the idealized displacement described above can be made quickly. Calling the parameter a velocity would lead to confusion since that velocity does not actually exist within the system.

Permeability contrast is the ratio of the maximum layer permeability to the minimum layer permeability, k_{max}/k_{min}. In our graded permeability system, this means top/bottom for a barrier bar and bottom/top for a channel sand. This k_{max}/k_{min} ratio is, therefore, a measure of the heterogeneity of the graded system. This is obviously not a unique measure of heterogeneity that can be applied to systems with a non-linear permeability grading. It is also not a very common measure of heterogeneity. However, the Dykstra-Parsons coefficient, V_{DP}, can be calculated well only when the permeabilities are log-normally distributed. Since this permeability distribution is linear, V_{DP} cannot be calculated with accuracy (a value of 0.68 can be estimated, however).

The viscosity effect is measured by the ratio of oil viscosity to water viscosity, μ_o/μ_w. This effect will also be represented by the end-point mobility ratio, M, defined as:

$$M = \frac{\lambda_{rw}^o}{\lambda_{ro}^o} = \frac{k_{rw}^o}{k_{ro}^o} \frac{\mu_o}{\mu_w} \qquad \text{(III-1)}$$

where

M = end-point mobility ratio

k_{rw}^o = water relative permeability at residual oil saturation

k_{ro}^o = oil relative permeability at residual water saturation

μ_w = water viscosity

μ_o = oil viscosity

The viscosity ratio was chosen as the parameter to represent the viscosity effect instead of the mobility ratio in order to illustrate that the effects are due to viscosity changes and not to changes in the relative permeability curves. Changes in this parameter were achieved by altering the oil viscosity alone.

Cross bedding occurs when bedding planes are deposited at some angle to the horizontal. Since fluid is flowing across the bedding planes instead of parallel to them, the flow patterns may be redirected and affect displacement efficiency. The effects of cross bedding were seen by rotating the grid system as described later.

Each of these parameters were assigned base case values which remained constant until that parameter was studied. This avoids problems such as additive or

competing effects which mask the true response of the system to the one parameter. Each parameter assumed only one value different from the base case. More thorough studies should investigate the parameters which have the greatest effect on oil displacement.

III.E - Results

Base Case - The base case displacement is shown in the upper panel on the next several figures. A deviation of one of the study parameters is shown in the lower panel. Most of the parameter variations have two figures associated with it, representing dimensionless times of $t_D=1/3$ PV and $t_D=2/3$ PV, where t_D is defined such that at $t_D = 1$ moveable pore volume [1 PV = $A \cdot L \cdot \phi \cdot (1-S_{or}-S_{wr})$], the front in a homogeneous, piston-like displacement is located at the production end of the system.. Unless otherwise stated, flood direction is from left to right. Notice that some of the saturation fronts are more irregular than might be expected. This is largely unexplained, but may be due to the coarse saturation divisions and minor instabilities in the solution. It is not seen as a major problem since only qualitative judgements are being made and the irregularities are small.

Before we look at the effects of varying individual properties, let's discuss the differences between the barrier bar and channel sand under the base case conditions. At first glance, the two displacements (Figs. III-2 and III-3) appear to be inverse images of each other. Closer inspection at $t_D=1/3$ PV (Fig. III-2) reveals, however, that the barrier bar has been affected by gravity pulling the water down, leading to more curvature, or slumping, at the front. The channel sand shows that water has run under the oil to move the front position in the high permeability layer further toward the

Figure III-2 : Waterflood Heterogeneities
Depositional Unit Variation

t_D = 1/3 PV — Channel Sand — Time = 99.93 Days

t_D = 1/3 PV — Barrier Bar Sand — Time = 1000.00 Days

Water Saturation

18
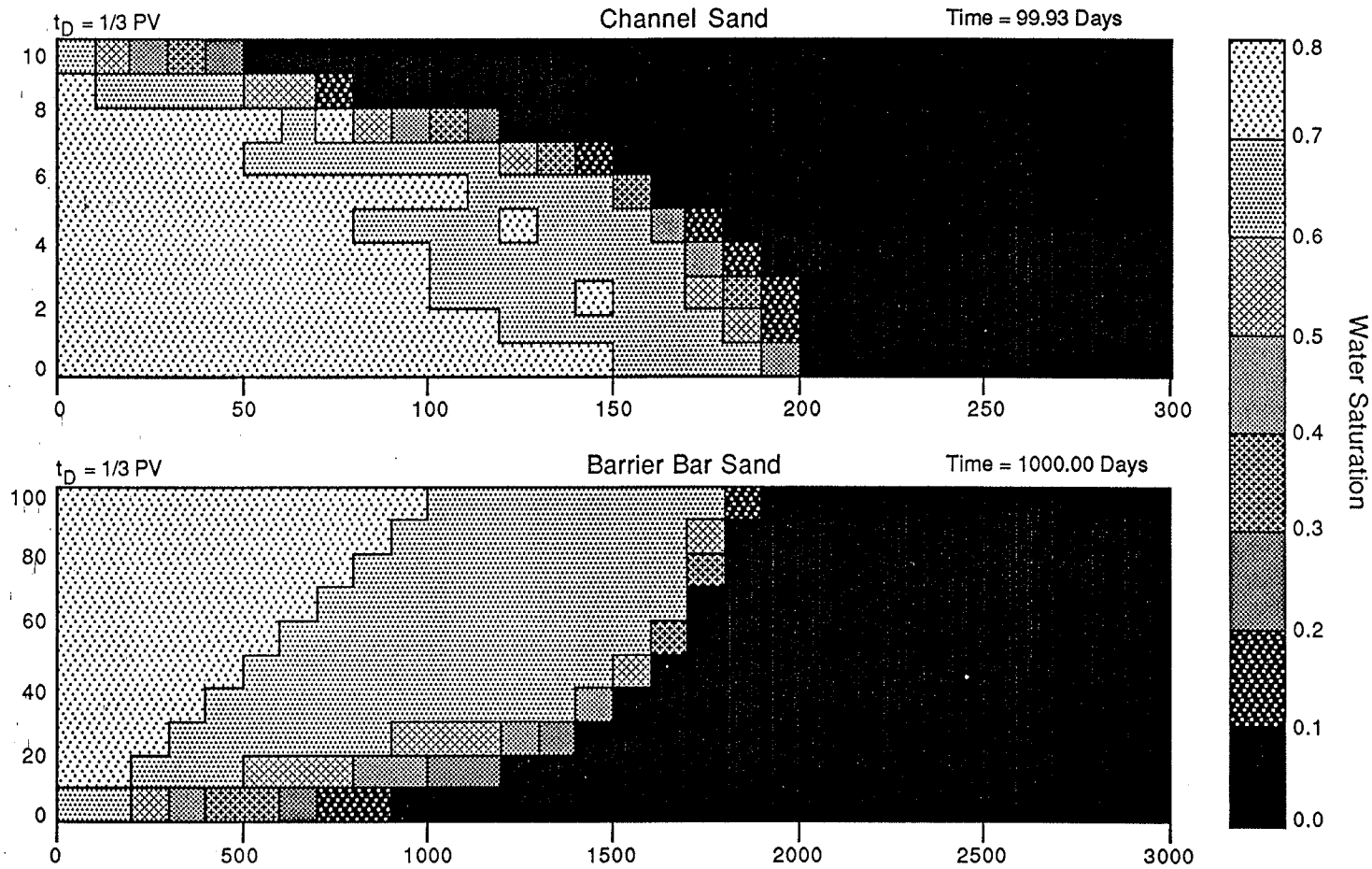
Figure III-3 : Waterflood Heterogeneities
Depositional Unit Variation
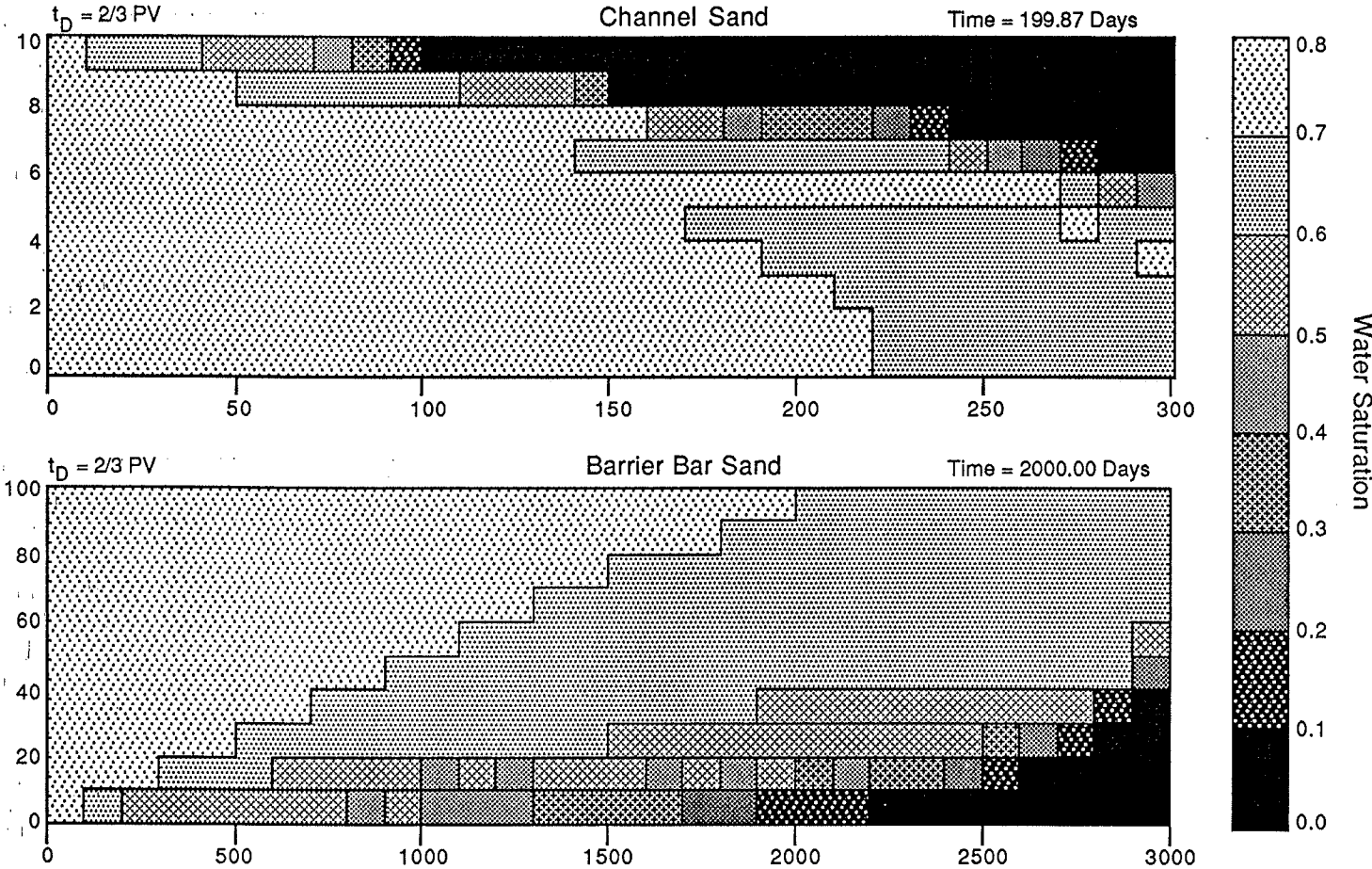
producer, thus reducing the curvature at the front. At $t_D = 2/3$ PV (Fig. III-3), the area of original oil saturation is smaller in the barrier bar than in the channel sand. This leads us to conclude that the barrier bar permeability configuration is slightly more favorable to oil recovery than the channel sand configuration. The degree of favorability, though, is quite variable, and depends primarily on a dimensionless group called the gravity number, N_g. N_g is defined by Dake[5] as the ratio of gravity forces to viscous forces, or :

$$N_g = \frac{k\, k_{rw}^o\, A\, \Delta\rho\, g\, \sin\alpha}{q_t\, \mu_w} \qquad : \text{Consistent Units} \qquad (\text{III-2})$$

or

$$N_g = \frac{4.9\text{E-}4\, k\, k_{rw}^o\, A\, \Delta\gamma\, \sin\alpha}{q_t\, \mu_w} \qquad : \text{Field Units}$$

where

$\quad N_g \quad = \quad$ Gravity number

$\quad k \quad = \quad$ absolute rock permeability (md)

$\quad k_{rw}^o \quad = \quad$ water relative permeability at residual oil saturation

$\quad A \quad = \quad$ cross sectional area (ft^2)

$\quad \mu_w \quad = \quad$ water viscosity (cp)

$\quad q_t \quad = \quad$ total flow rate (bbl/D)

$\quad \Delta\gamma \quad = \quad$ specific gravity difference (oil-water)

$\quad \alpha \quad = \quad$ dip angle (0 = horizontal)

$\quad \Delta\rho \quad = \quad$ density difference (oil-water)

For our base case, $N_g = 0.951$. A larger N_g will cause a greater difference than that observed in the previous figures. A smaller N_g will reduce the difference and, in the limit, they will be exact inverse images since gravity would have no effect.

Flow Rate Effect - The effect of flow rate can be predicted by the gravity number. When q=10 ft/day instead of 1 ft/day, $N_g = 0.095$ instead of $N_g = 0.951$. Figures III-4, III-5, III-10, and III-11 show that the barrier bar is nearly an inverse image of the channel sand with the higher flow rate. This indicates that an order of magnitude decrease in N_g can make a difference in the oil displacement efficiency and points out the importance of identifying depositional units and estimating N_g in field applications. A better displacement is noticed in barrier bars at lower flow rates so that gravity forces have a chance to help. In a channel sand, however, a higher flow rate is desired to reduce the negative effects of gravity. Incorrect identification of depositional structures, therefore, could have a serious effect on oil recovery predictions.

Permeability Ratio Effect - The variation due to permeability ratio was also predictable. A permeability ratio of 1 indicates a constant permeability profile, and therefore acts like a single layer in a Buckley-Leverett displacement (Figs. III-6, III-7, III-12, and III-13). This displacement is clearly superior to the base case, as you would expect from a more homogeneous system. This points to the fact that the larger the permeability contrast, the poorer the oil displacement will be. Since this is already known, we need not discuss it any more.

Viscosity Ratio Effect - A much more interesting case is the variation of the viscosity ratio (oil/water). When the viscosity ratio is 1.0, the mobility ratio, M, is about 0.7. Therefore, M = 7.0 when the viscosity ratio is 10.0. In a 1-D Buckley-Leverett displacement, this change in M would decrease the saturation at the front and lengthen the tail back toward $1\text{-}S_{or}$. Each layer in this system shows this behavior (Figs. III-8, III-9, III-14, and III-15). When M = 7.0, the distance between $S_w \cong S_{wr}$ (lowest box on S_w scale) and $S_w \cong 1\text{-}S_{or}$ (highest box on S_w scale) is larger than the system length for all layers. With M= 0.7, this same saturation change is well within the system length, indicating a much shorter Buckley-Leverett tail. The inefficiency of the displacement is quite dramatic at $t_D = {}^2/_3 PV$, Figs. III-9 and III-15. Whereas over half of the reservoir falls in the highest saturation category at M = 0.7, only 2% of the reservoir is within this category at M = 7.0. This indicates that the displacement sweep efficiency is very poor.

The difference between the two depositional structures is very important also. In Figs. III-8 & III-14, the barrier bar has displaced more oil than the channel sand. This appears to be due to an increased gravity effect as a result of an increased gravity number. However, since the water viscosity is not changed, N_g remains the same as in the base case. However, the gravity number is made up of gravity forces and viscous forces. The gravity forces are determined by the density difference between the fluids which usually tend to pull the water down and push the oil up. The viscous forces are determined by the flow rate, absolute permeability, and the mobility of a phase (k_{rj}/μ_j,j=oil or water). When the water phase is used, the gravity number can be called the water gravity number, N_{gw}. When the oil phase is used, it is called the oil gravity

number, N_{go}. These two gravity numbers are related by the mobility ratio, M, such that $N_{gw}=N_{go} * M$.

In our case, N_{gw} does not change due to the change in oil viscosity, so that when M increases ten fold, N_{go} decreases ten fold. Since the gravity forces are the same, N_{go} reflects the decreased mobility in the oil phase. With this decreased mobility, the more mobile water phase will tend to by-pass the oil in place, preferring to channel through the high permeability layers. The difference between the barrier bar and the channel sand profiles is that after breakthrough in the channel sand, there are no appreciable forces acting to remove the less mobile oil in the lower permeable layers, Figs. III-8 and III-9. The gravity forces pull the water down and away from the oil which is pushed up, and the oil viscous forces tend to push the water away from the oil. Therefore, a significant amount of oil will always be left in this situation. The barrier bar shows a much better displacement than the channel sand due to gravity forces acting to pull the water down to the low permeability layers where the oil was by-passed before breakthrough, Figs. III-14 and III-15. Even though the oil viscous forces still tend to push the water past the oil, gravity forces in the water act in the opposite direction. Also, since water overlays the by-passed oil, the density difference forces the oil up and into the higher permeability layers where it can be recovered more easily. Notice that N_{gw}, N_{go}, and M are not independent as indicated by the equation above that relates all three. It is not actually necessary to define N_{go} since N_{gw} and M can describe the system as well as N_{gw} and N_{go}. However, the definition of N_{go} does relate this displacement mechanism to the effect of gravity which is helpful for illustrative purposes. This recovery mechanism is very important and should be considered in all recovery estimates.

Figure III-4 : Channel Sand Waterflood
Flow Rate Variation
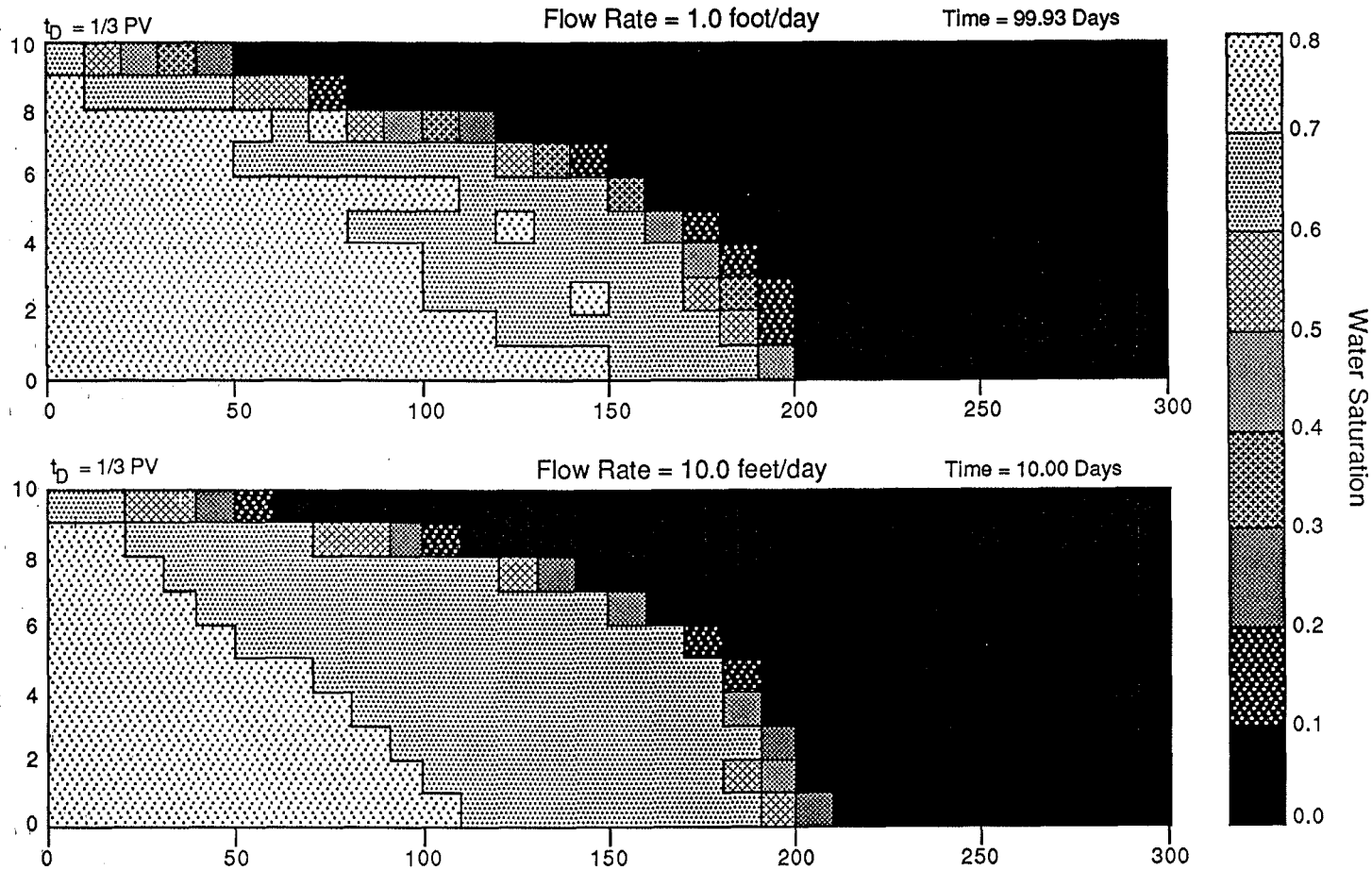
Figure III-5 : Channel Sand Waterflood
Flow Rate Variation
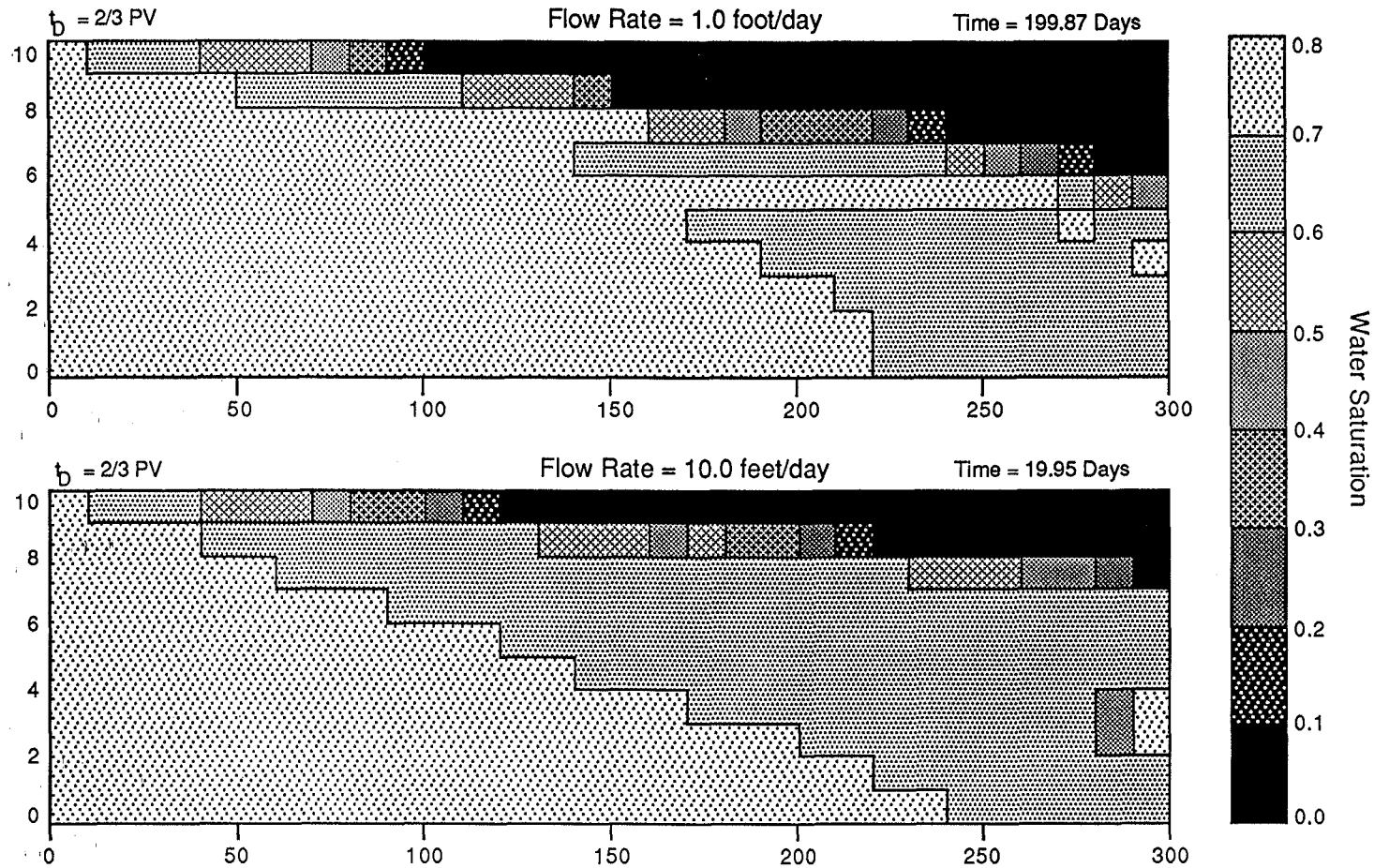
Figure III-6 : Channel Sand Waterflood
Perm Ratio (kmax/kmin) Variation
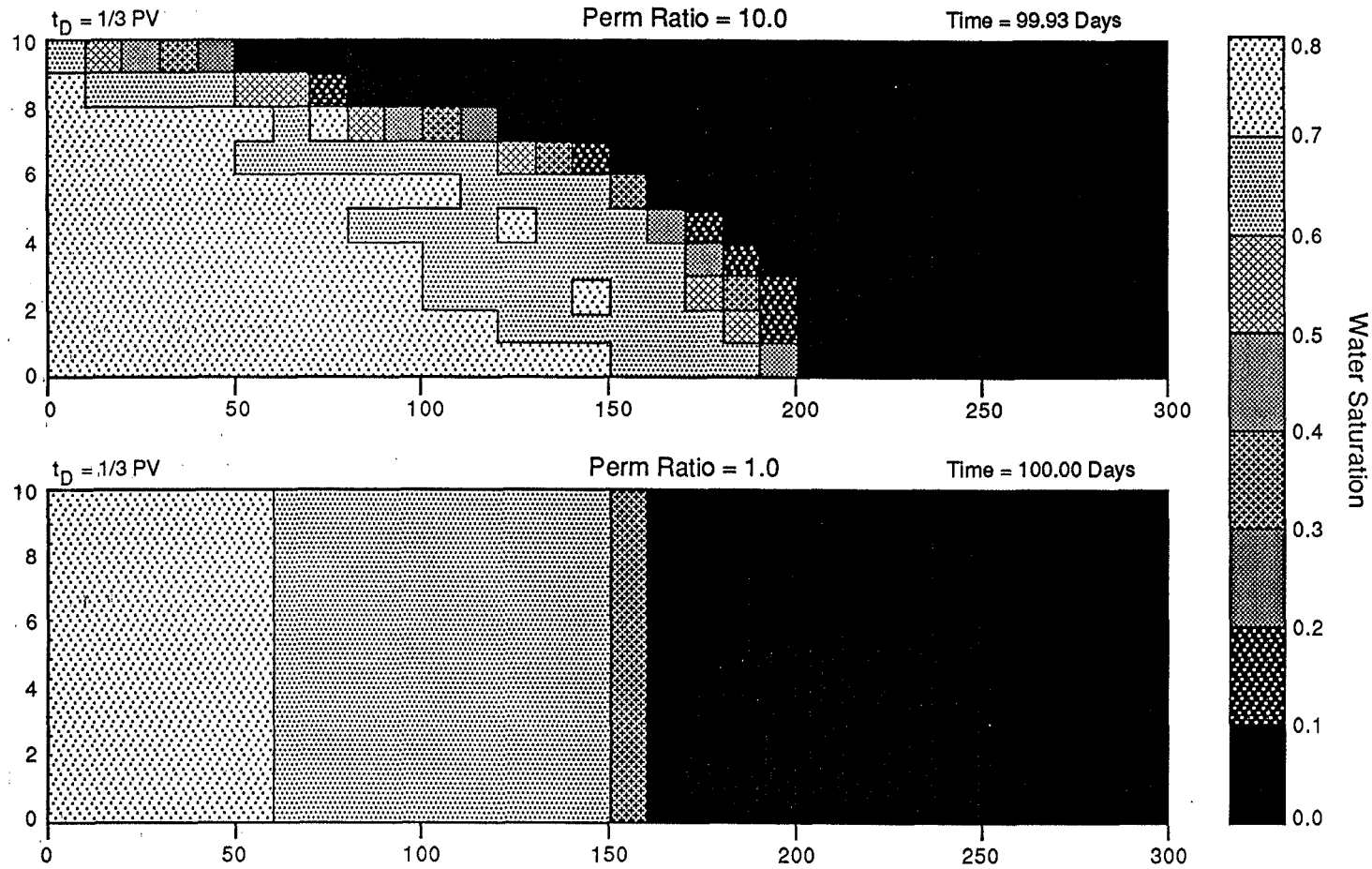
Figure III-7 : Channel Sand Waterflood

Perm Ratio (kmax/kmin) Variation
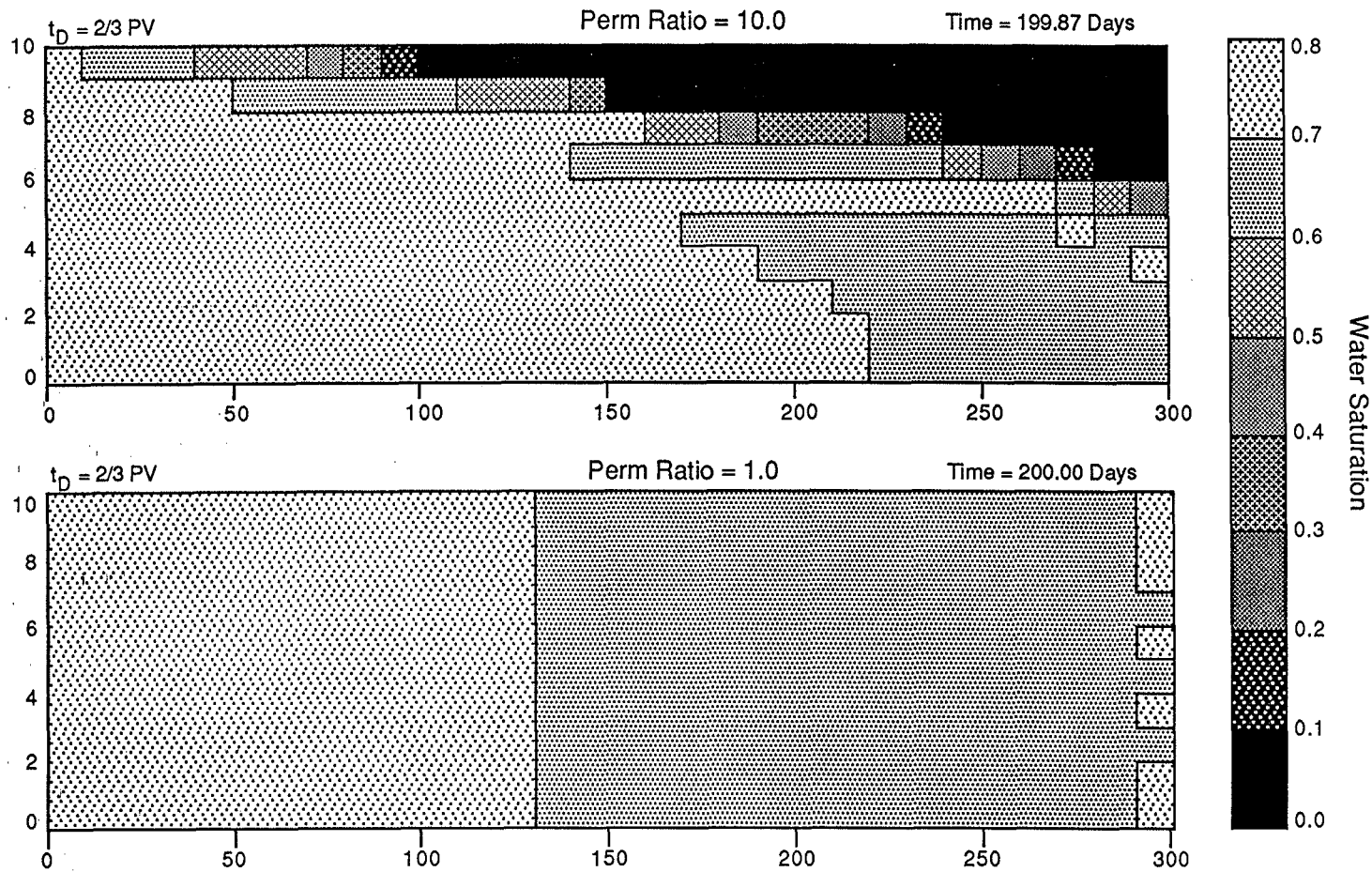
Figure III-8 : Channel Sand Waterflood
Viscosity Ratio (oil/water) Variation
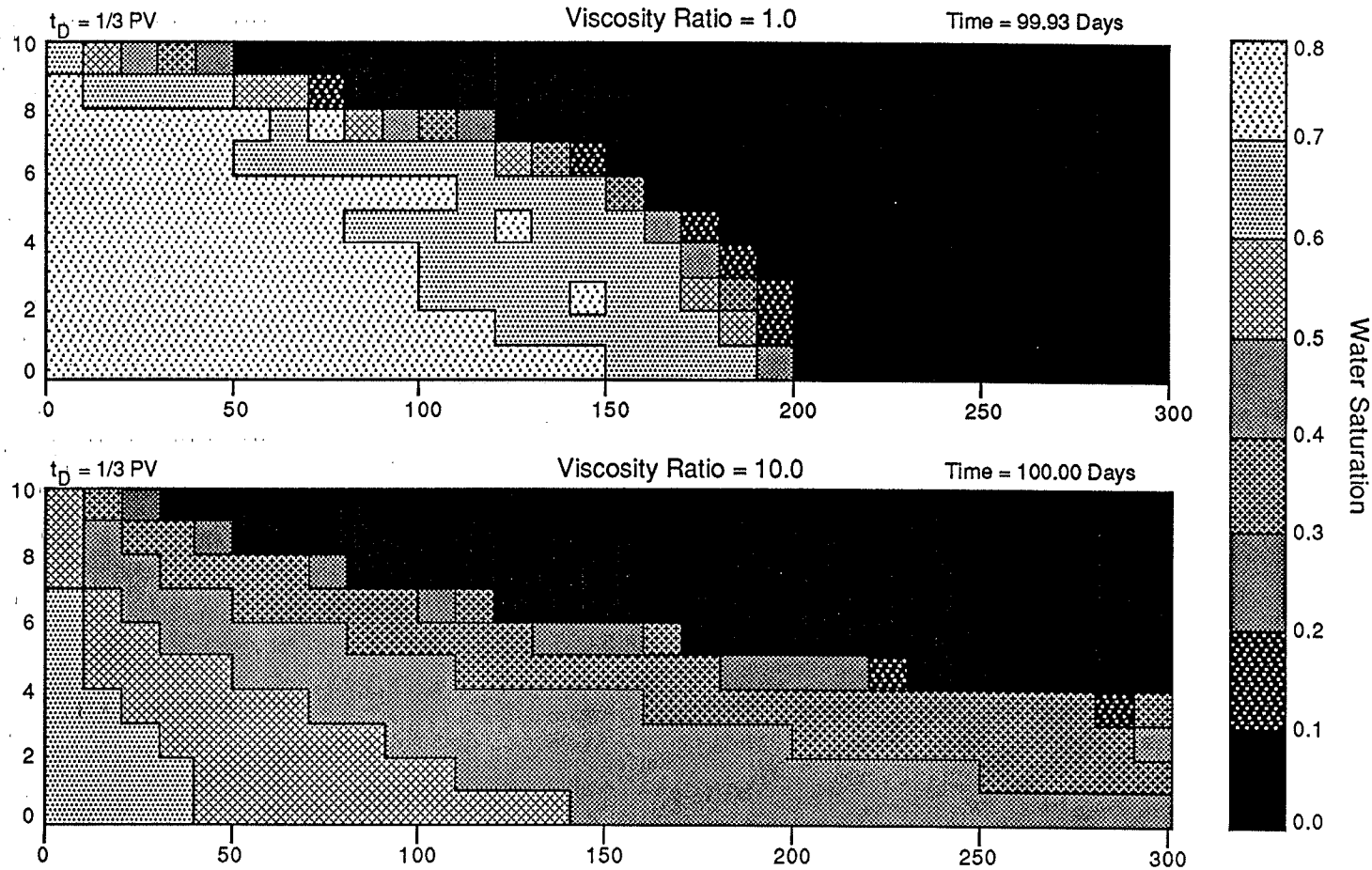
Figure III-9 : Channel Sand Waterflood
Viscosity Ratio (oil/water) Variation
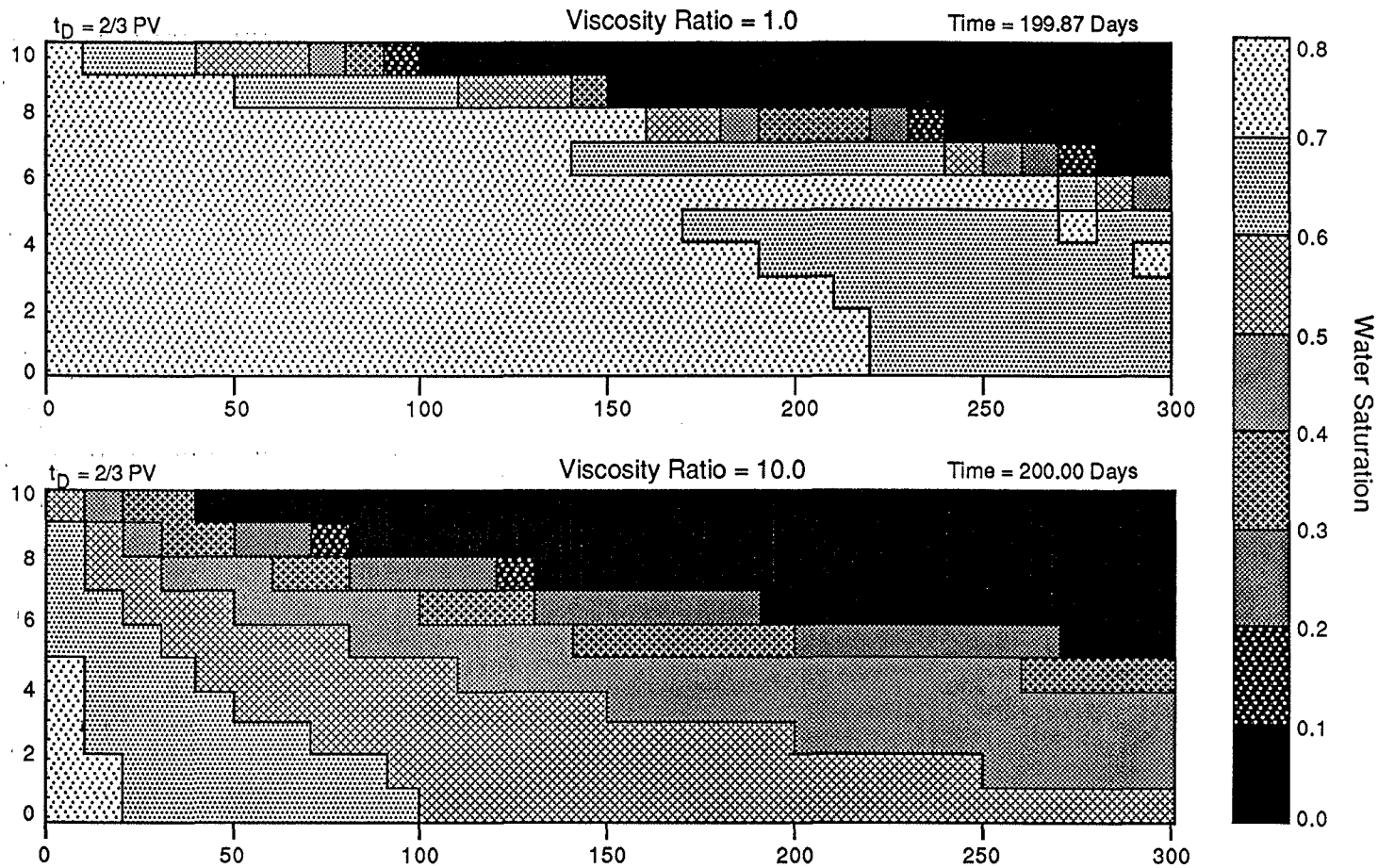
Figure III-10 : Barrier Bar Waterflood
Flow Rate Variation

t_D = 1/3 PV   Flow Rate = 1.0 foot/day   Time = 1000.00 Days

t_D = 1/3 PV   Flow Rate = 10.0 feet/day   Time = 100.00 Days

Water Saturation
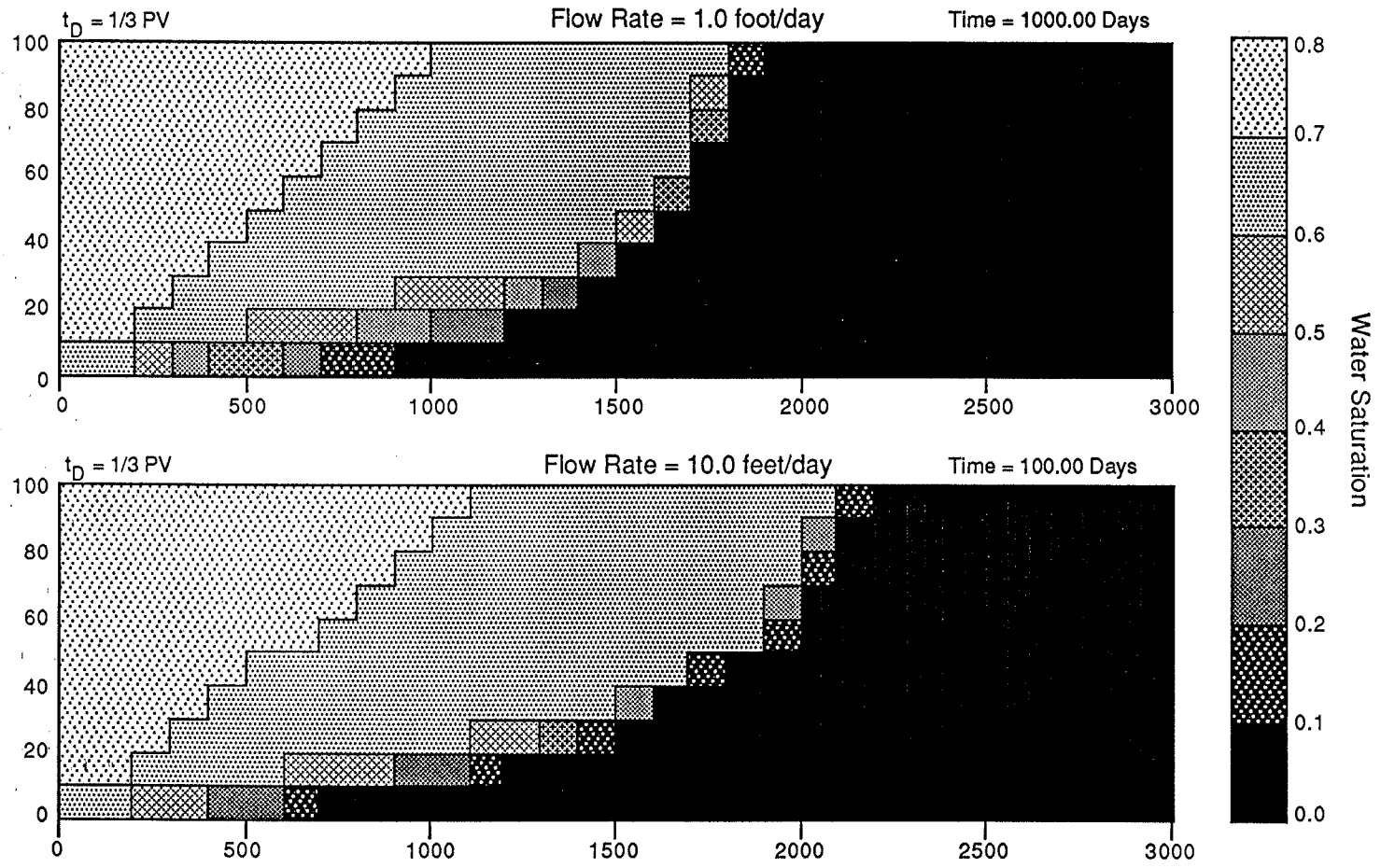
Figure III-11 : Barrier Bar Waterflood
Flow Rate Variation
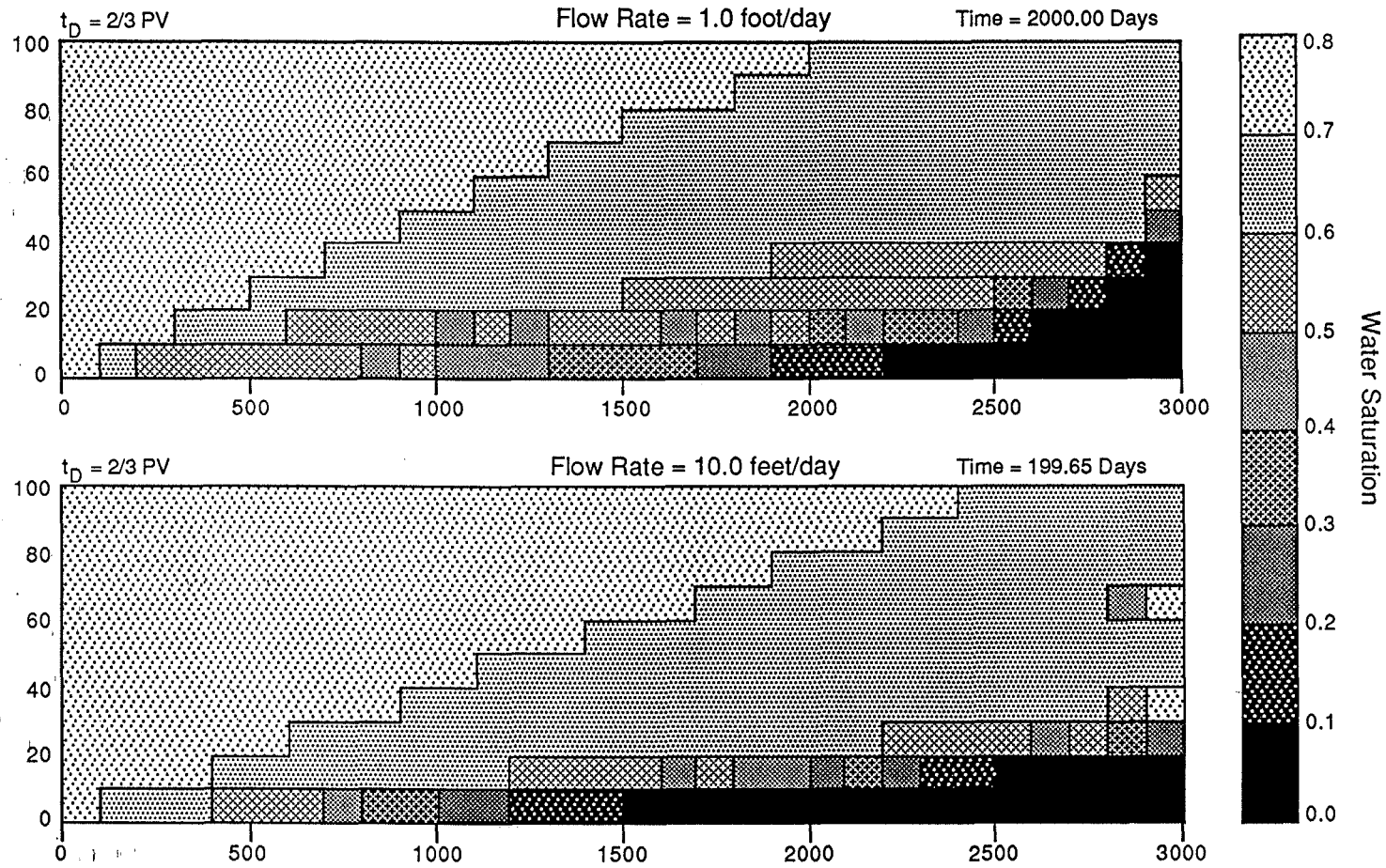
Figure III-12 : Barrier Bar Waterflood
Perm Ratio (kmax/kmin) Variation
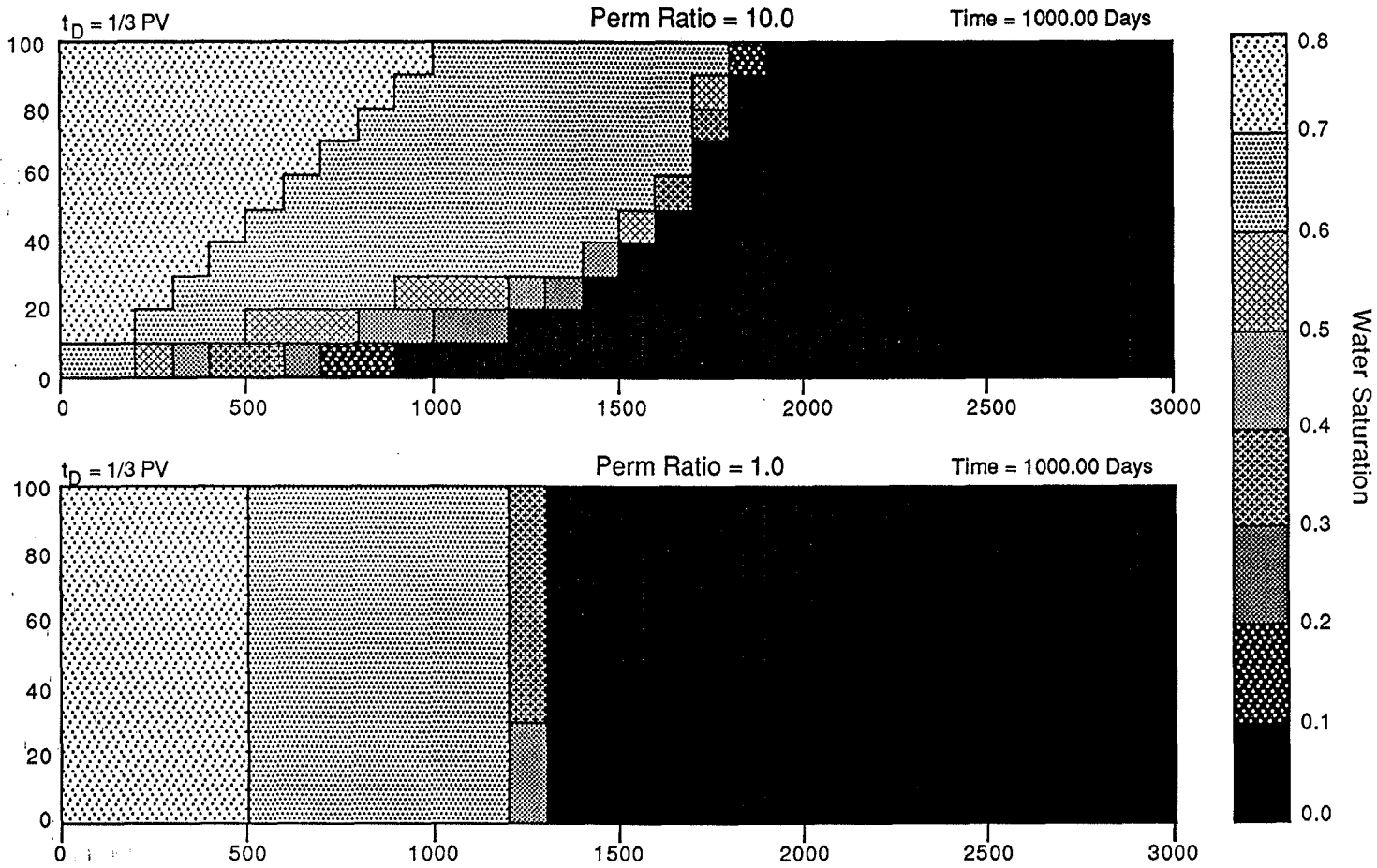
Figure III-13 : Barrier Bar Waterflood
Perm Ratio (kmax/kmin) Variation

t_D = 2/3 PV   Perm Ratio = 10.0   Time = 2000.00 Days

t_D = 2/3 PV   Perm Ratio = 1.0   Time = 2000.00 Days

Water Saturation

0.8
0.7
0.6
0.5
0.4
0.3
0.2
0.1
0.0
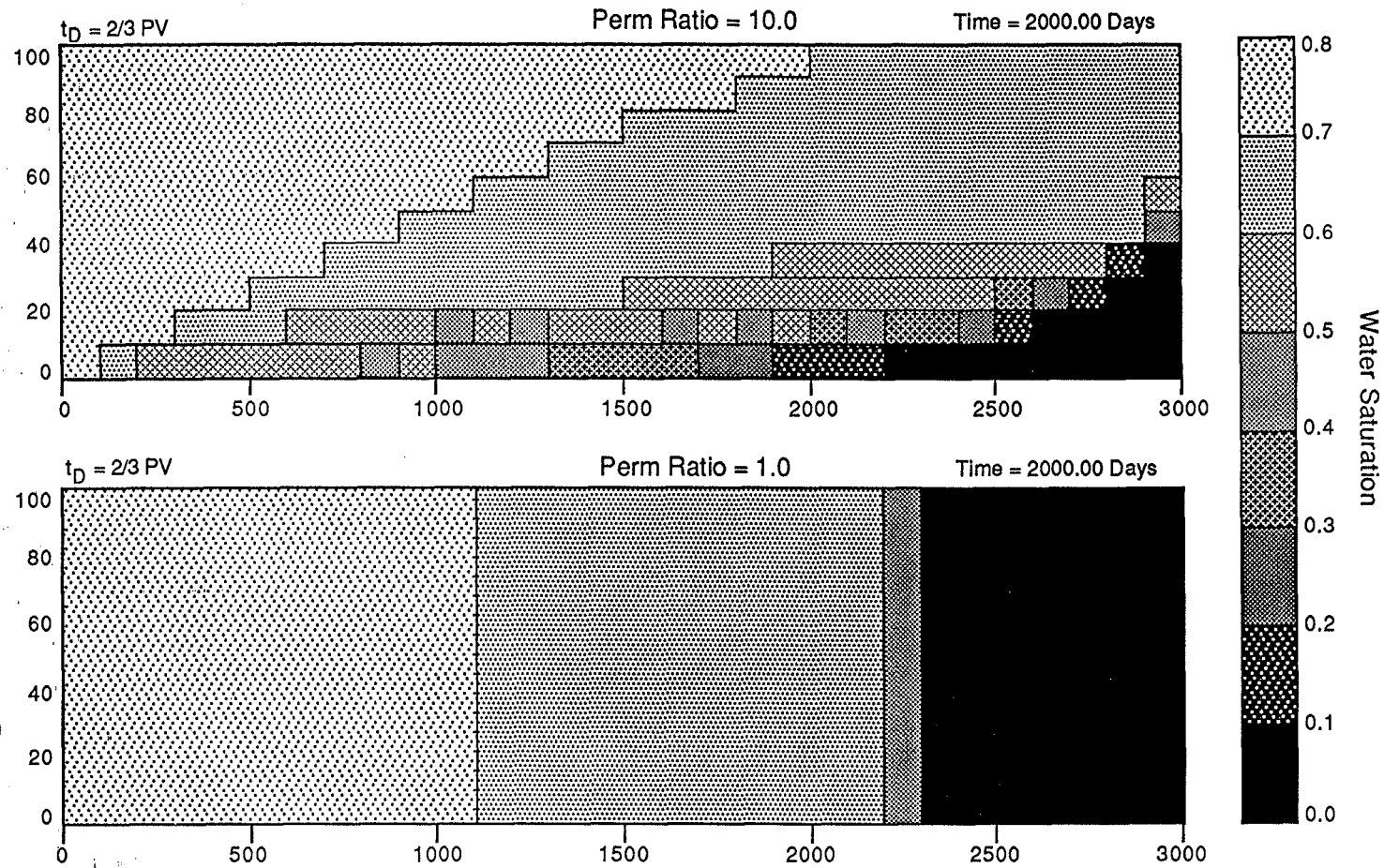
Figure III-14 : Barrier Bar Waterflood
Viscosity Ratio (oil/water) Variation
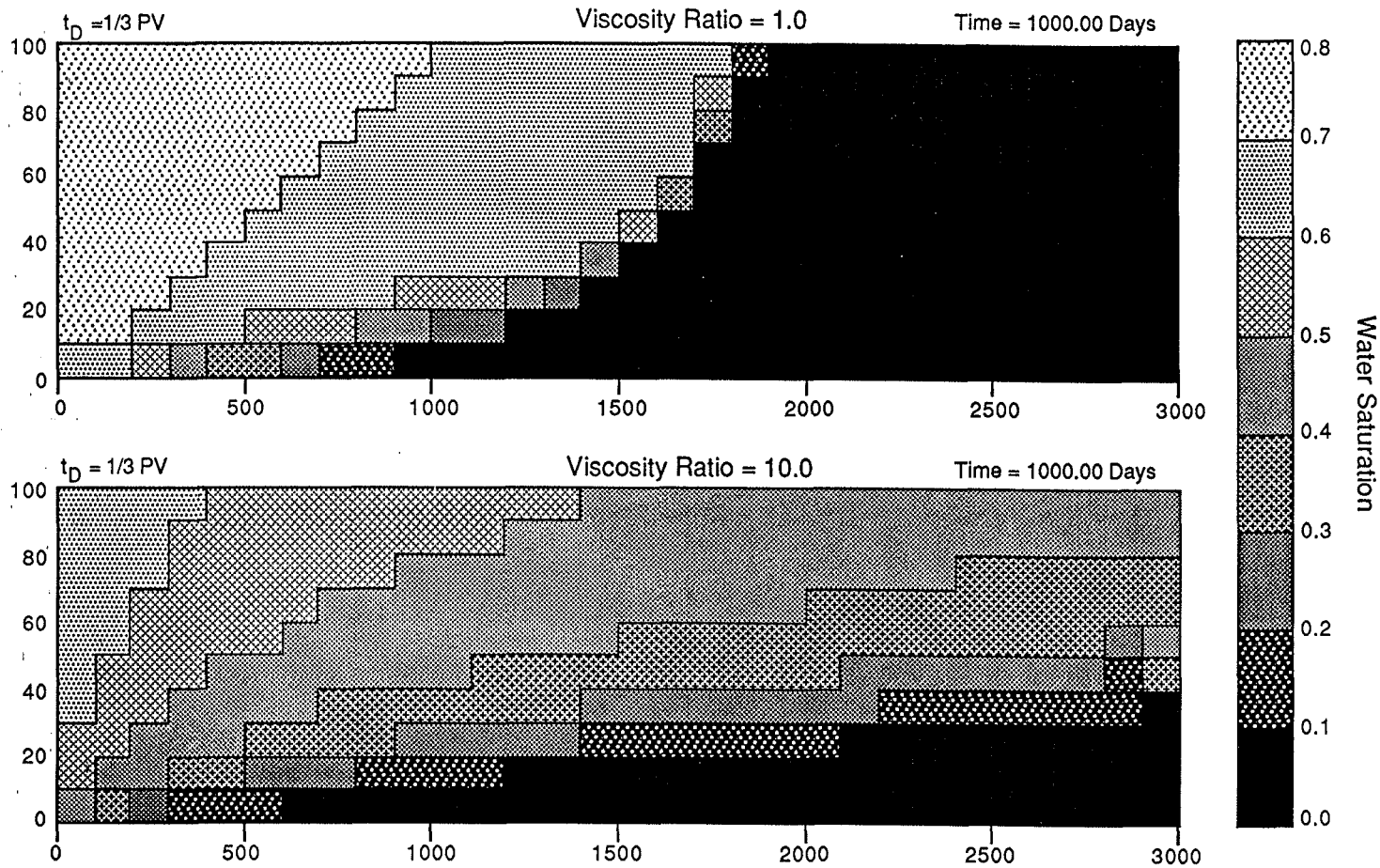
Figure III-15 : Barrier Bar Waterflood
Viscosity Ratio (oil/water) Variation

35
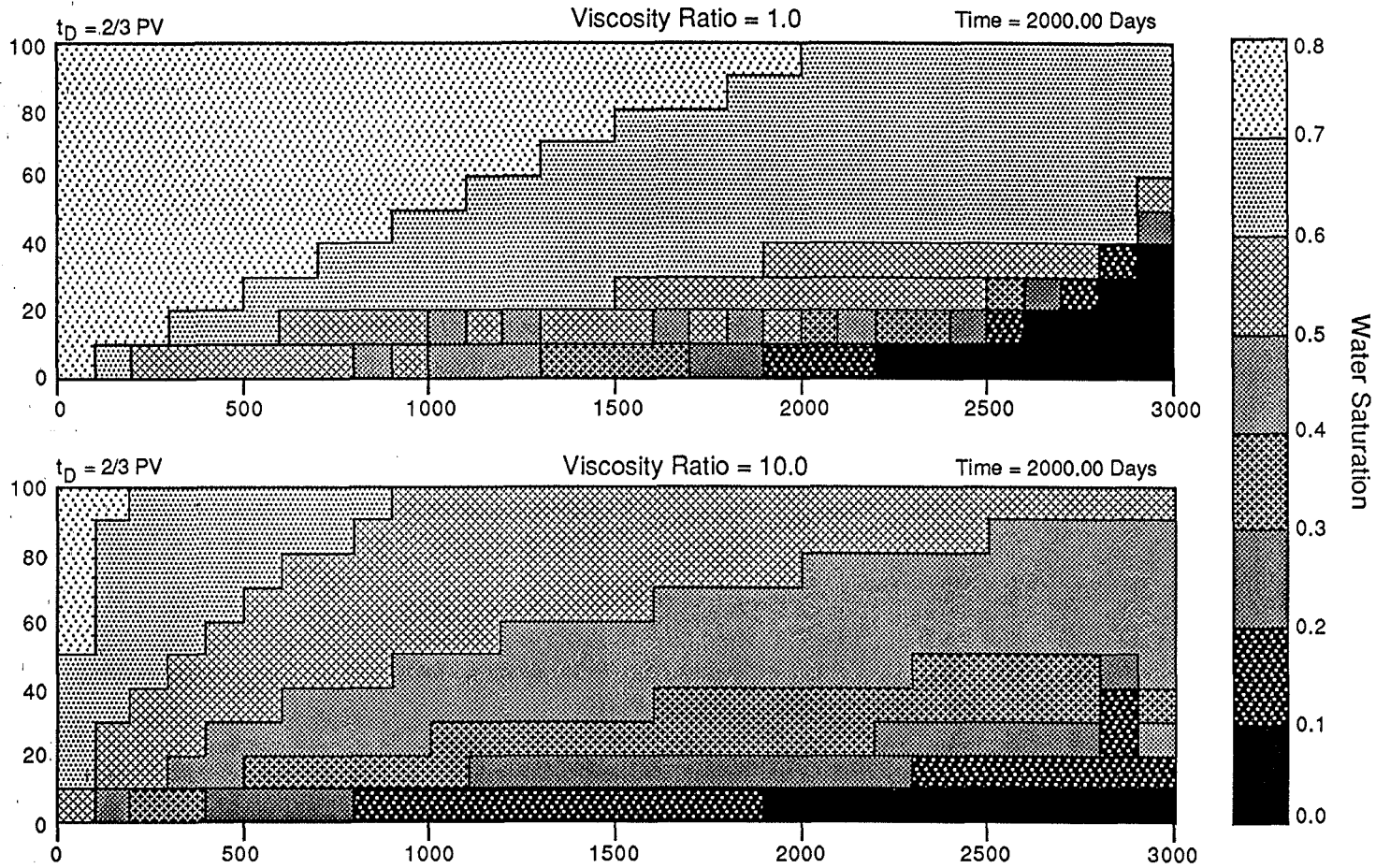
Cross-Bedding Effect - Cross beds are a very common feature of both channel sands and barrier bars, but are very difficult to model in a conventional simulator. Geologically, cross beds are steeply dipping sands separated by a lower permeability bedding plane. A much more geologically correct definition can be found in the paper by Weber[22]. The difficulty in modelling a cross bed comes from the angle at which the beds cross the direction of bulk flow. Kortekaas[23] has represented cross beds as a series of vertical permeable baffles. While this addresses the permeability reduction, it does not address the tilting of the beds. Therefore, a more realistic model was sought.

Treating the cross bed as a dipping reservoir will honor the bedding plane angle properly, but it does not account for the truncated beds which intersect the system boundaries. Also, the wells must be vertical, not perpendicular to the bedding plane as they would be in a rotated system.

Another approach is to use small grid blocks and discretize the bedding planes to best fit the true angle. The x and z permeabilities can be adjusted to approximate the bedding angle and the lower interbed permeability. All of these approximations introduce a great deal of uncertainty as to the realism of the model. A more subtle approximation lies in the derivation of the equations on which the simulator was built. In the derivation, the full permeability tensor is reduced to a diagonal tensor for ease of use. This step requires that the principal axes of permeability coincide with the axis system used in the simulation. The principle axes of permeability are considered to coincide with the bedding planes, so that the attempt to discretize the bedding angles is in error. The magnitude of this error is unknown, as is the solution by including the

full permeability tensor. Another approach is to use a nine-point difference equation instead of the standard five-point. This would allow flow through block corners, but is still a coarse approximation.

To avoid these problems, we used a simulator whose block arrangement is not confined to a grid, nor to square blocks. This allowed us to orient grid blocks along the bedding planes and truncate them along the system boundaries. The blocks are represented by a node list which specifies the block volume, flow properties, and rock properties. The blocks are connected by a node connection list which lists the vertical and center-to-center distances, boundary permeability reduction, and cross sectional area normal to flow between every pair of connected blocks. The injection and production wells are represented by a connection list which provides the distance and flow rate into each block in each well. Using a simulator like this makes it possible to have oddly shaped blocks caused by truncating tilted rectangles against the system boundaries. See Fig. III-16 for a sample grid configuration.

In this study, we examined the effects of grid orientation and flood direction. The bedding planes were oriented 60° from the vertical to represent the average cross bed. Horizontal permeability, k_h, is directed down dip with the direction of flow. Vertical permeability, k_v, is directed across the bedding planes normal to the direction of flow. The permeability ratio is then the ratio of horizontal to vertical permeability, k_h/k_v, and can reflect decreased permeability normal to the bulk flow. Flow parameters were the same as the base case. The bedding plane in the figures looks much steeper due to the aspect ratio compression. A blow-up of the front with the correct aspect ratio is presented with each set to give proper perspective. Figure III-16 shows the grid lines for the cross bedded systems as modelled.

Figure III-16 : Waterflood Heterogeneities
Cross-Bed Unit Description

Cross-Bedded Sand - Expanded Scale θ = 60.00 Degrees

k_v k_h

Cross-Bedded Sand - Normal Scale θ = 60.00 Degrees
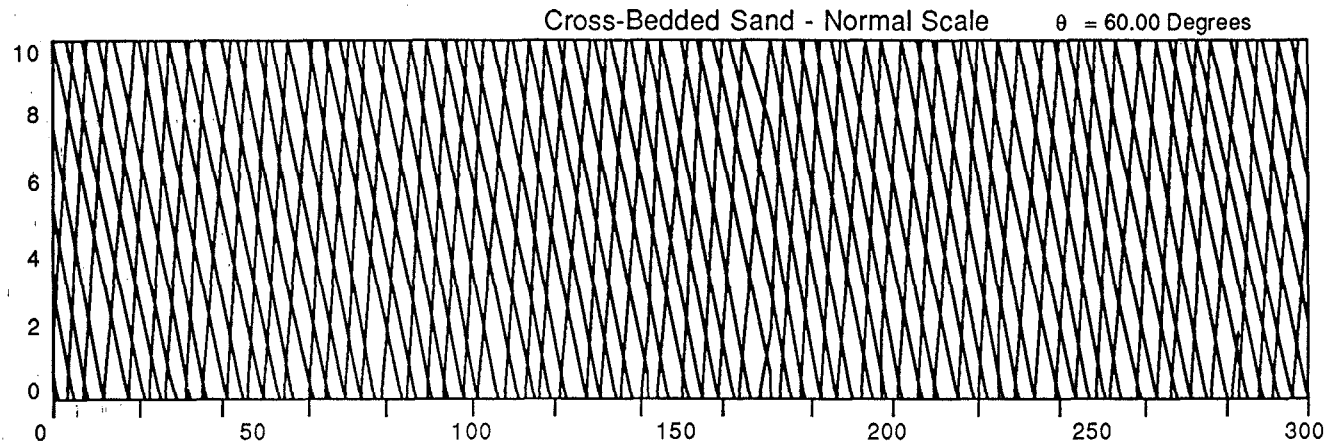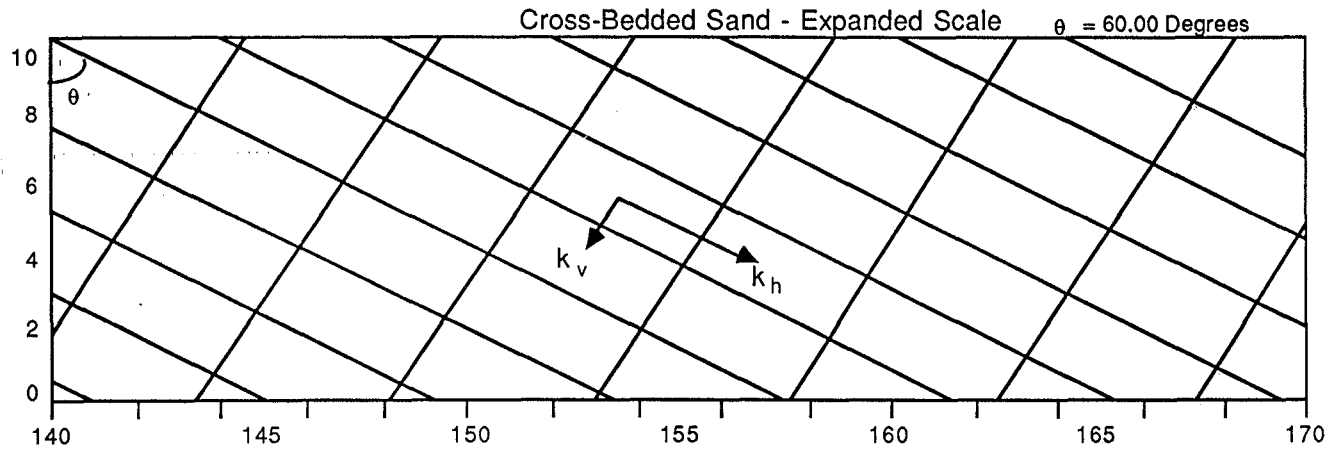
Grid orientation effect is most commonly addressed when representing tilted beds with horizontal grid blocks. With complex procedures, oil recovery curves can match fairly well in the two cases. We define the grid orientation effect as the difference from piston-like displacement when our tilted grid system has isotropic permeabilities and no gravity effect. The upper panels in Figs. III-17 and III-18 show that a case with no gravity and isotropic permeability does well represent piston-like displacement that would be observed using a horizontal grid orientation. This contrasts with the base case in the lower panel, in which gravity is present and the permeability is anisotropic. The preference to flow along a bedding plane is obvious. This action is aided by the gravity forces pulling the water down the beds in this flow direction.

The directionality effect refers to oil displacement differences between flowing from left to right, or down-dip, and flowing from right to left, or up-dip. The theory is that when flooding up-dip, the gravity forces tend to pull water down and across the less permeable bedding boundaries, resulting in a more uniform displacement. Also, since water is overriding the oil, the oil should migrate by gravity segregation into the water zone where it is displaced more easily. These phenomena are not obvious in Figs. III-19 and III-20, however. The blow-ups of the two profiles, Fig. III-20, looks surprisingly similar also. This is probably due to the k_h/k_v ratio causing horizontal viscous forces to dominate the vertical viscous forces, and to a gravity number which is not large enough to overcome the reduced vertical permeability. Future work should study the effects of these two parameters, as well as the viscosity ratio, on the displacement of oil by water.

From this limited study, we can conclude that flood direction may not be important. However, due to the limited scope of the work the generality of this

Figure III-17 : Cross-Bed Sand Waterflood
Grid Orientation Effect

t_D = 1/3 PV

No Gravity - kh/kv =1.0

Time = 100.00 Days
θ = 60.00 Degrees

t_D = 1/3 PV

With Gravity - kh/kv = 10.0

Time = 100.00 Days
θ = 60.00 Degrees

Water Saturation

0.8
0.7
0.6
0.5
0.4
0.3
0.2
0.1
0.0

40
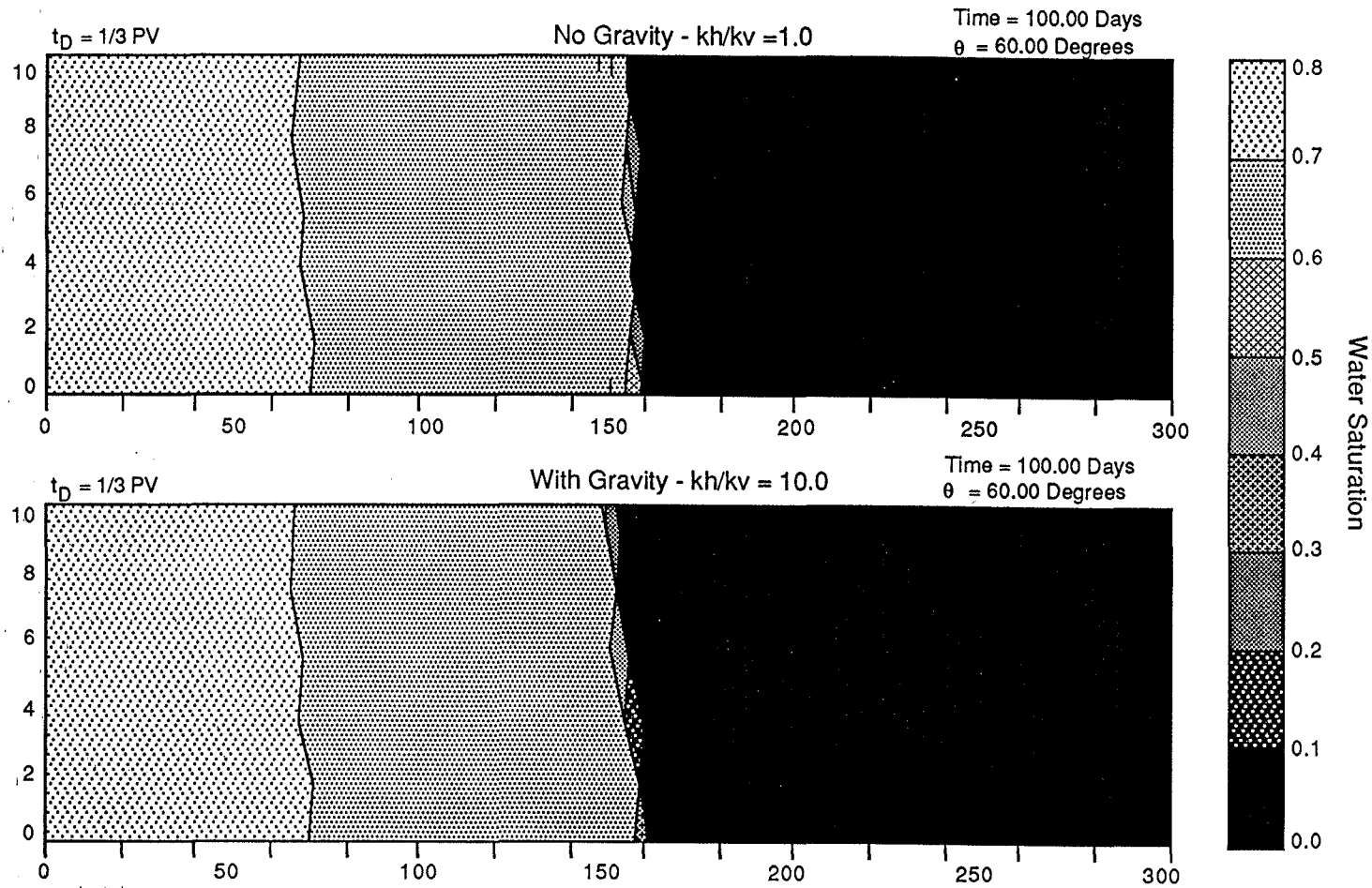
Figure III-18 : Cross-Bed Sand Waterflood
Grid Orientation Effect

41
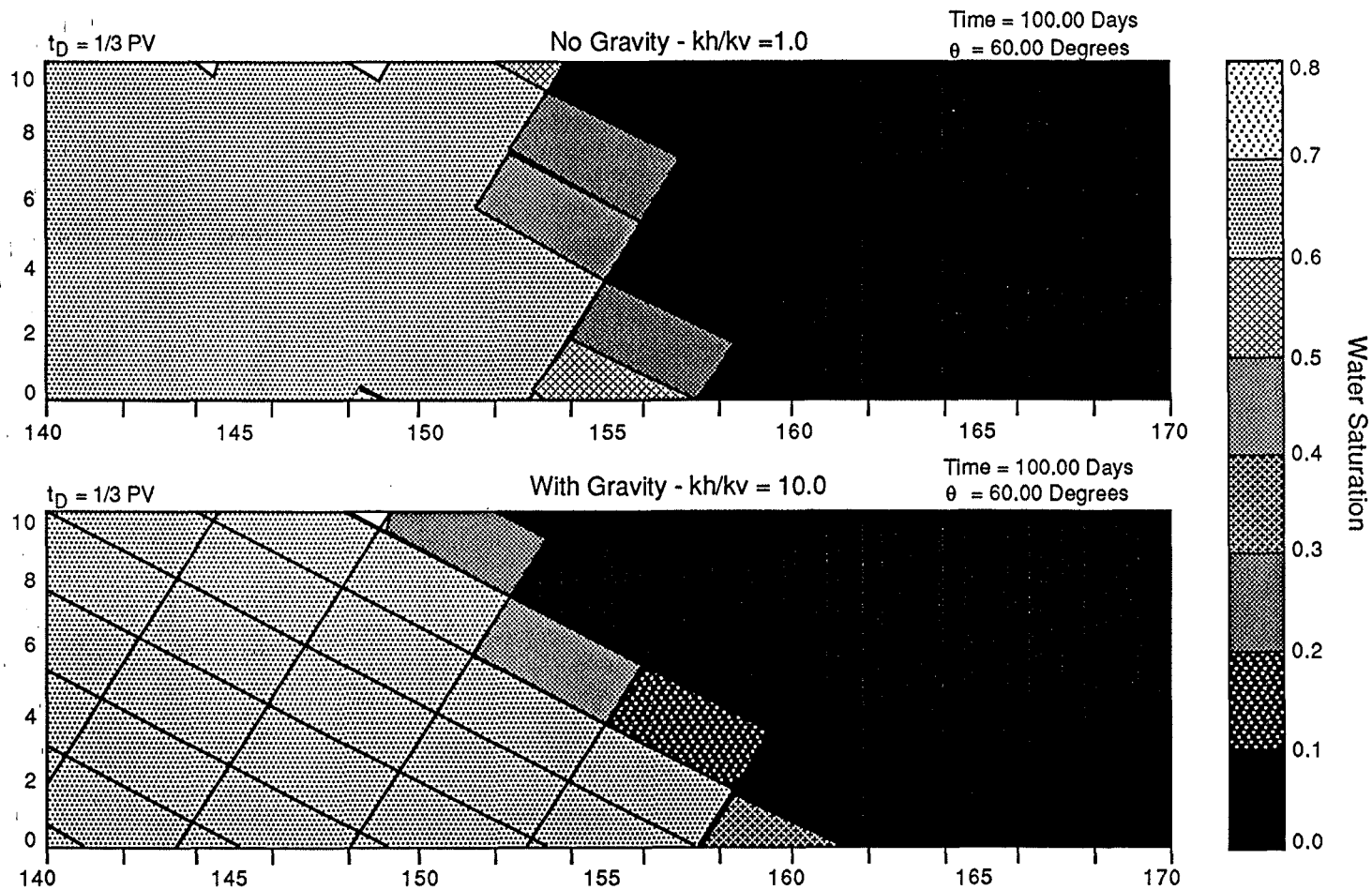
Figure III-19 : Cross-Bed Sand Waterflood
Directionality Effect

t_D = 1/3 PV   Flood Direction - Right to Left   Time = 100.00 Days
θ = 60.00 Degrees

t_D = 1/3 PV   Flood Direction - Left to Right   Time = 100.00 Days
θ = 60.00 Degrees

Water Saturation

42
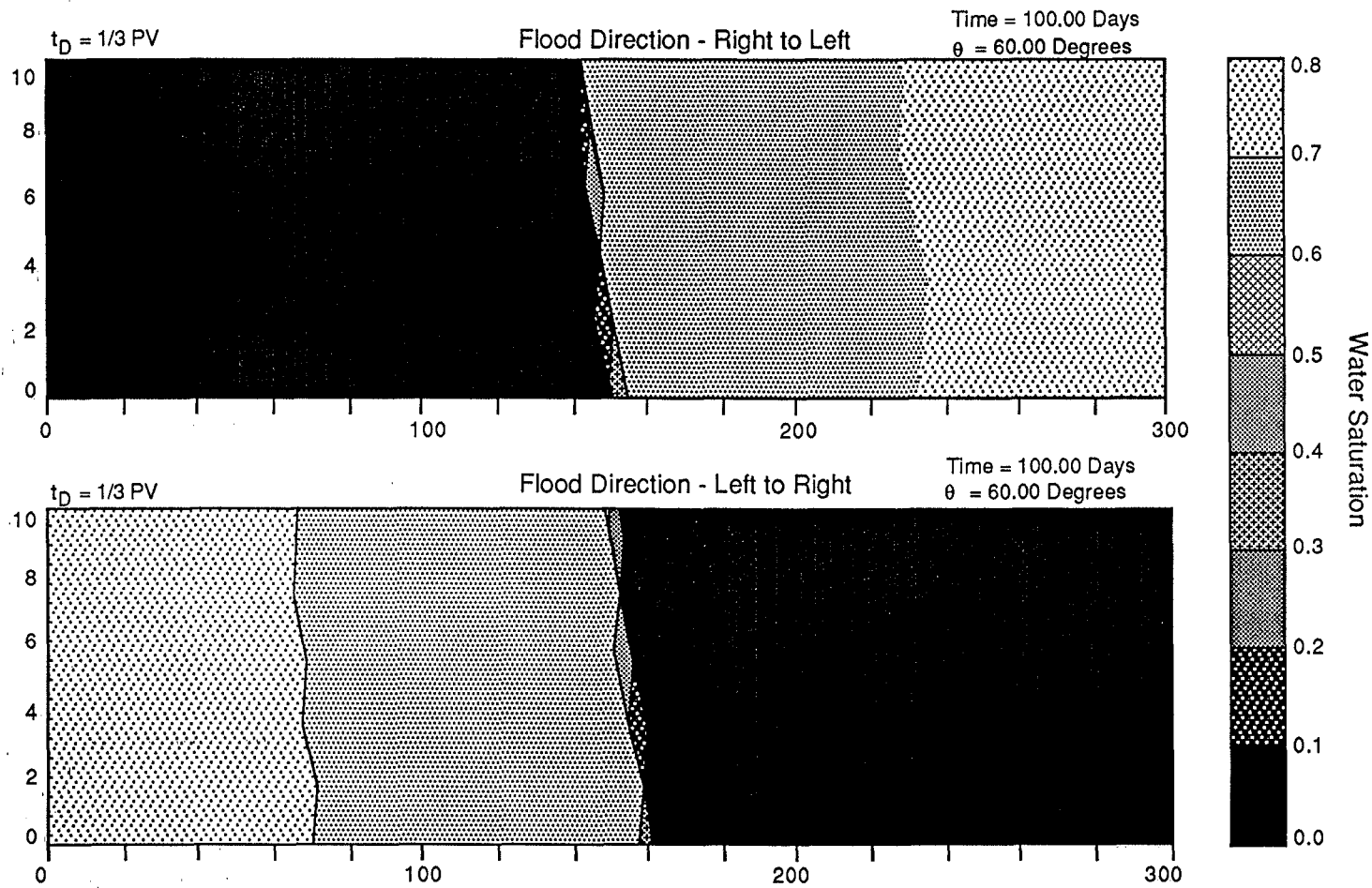
Figure III-20 : Cross-Bed Sand Waterflood
Directionality Effect

t_D = 1/3 PV   Flood Direction - Right to Left   Time = 100.00 Days
θ = 60.00 Degrees

t_D = 1/3 PV   Flood Direction - Left to Right   Time = 100.00 Days
θ = 60.00 Degrees

Water Saturation

43
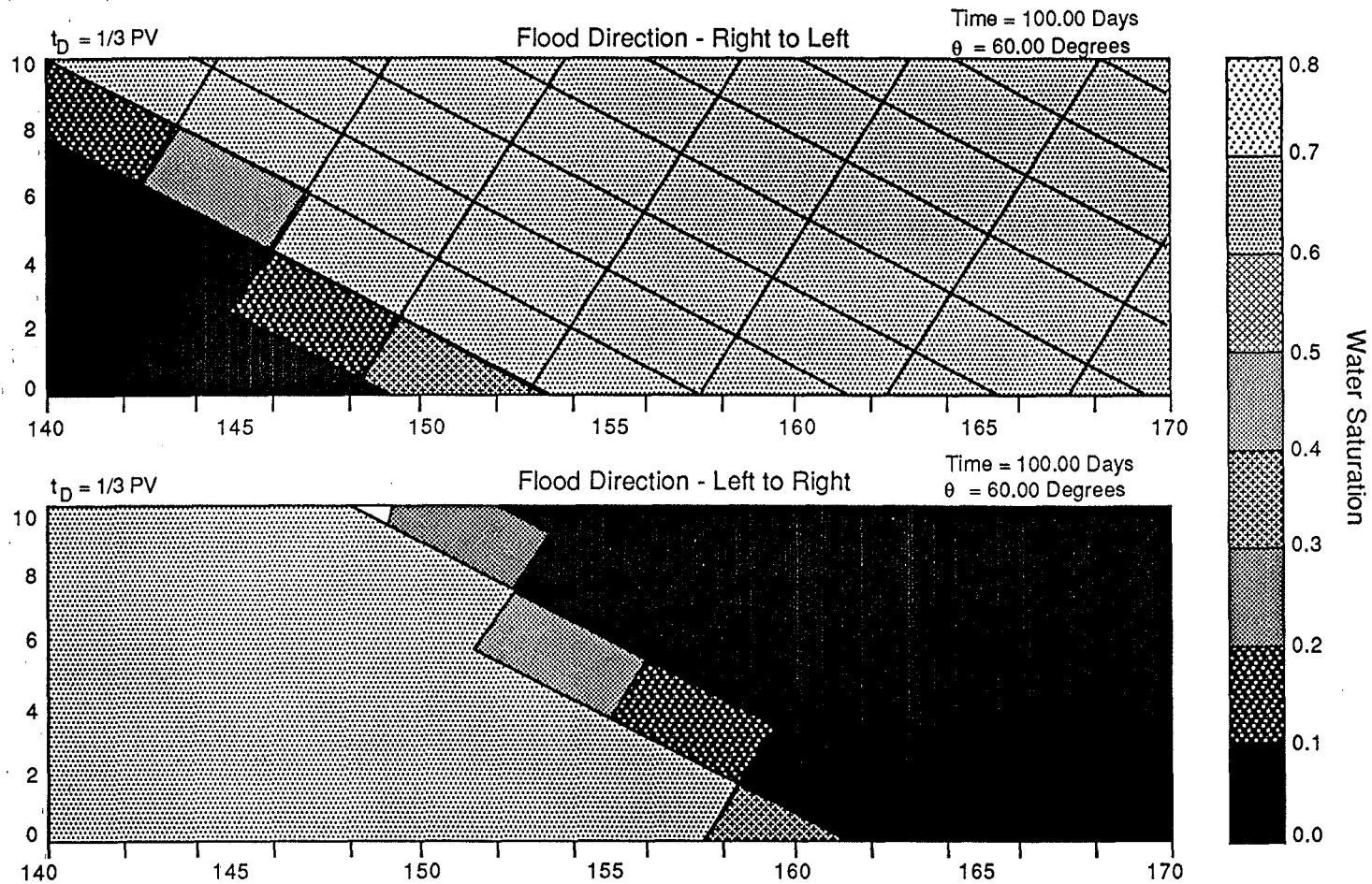
statement is in doubt. A major geologic concern is the fluid movement at the top and bottom of the system. Here, impermeable boundaries confine fluid to stay within the system. Shales generally underlay cross bedded units so that the impermeable lower boundary is not a bad assumption. Cross beds often have an erosional surface and another cross bed set overlaying them, so the upper boundary can be assumed to be a barrier also. In some realistic examples, however, the upper and/or lower boundaries have some permeability, so that under some conditions, fluid may prefer to leave the system instead of flowing across the low interbed permeability region. This can greatly alter expected flow patterns in the reservoir, and should be considered.

CHAPTER IV

IMMISCIBLE DISPLACEMENTS

IV.A - Introduction

This section investigates ways to perform grid block averaging for immiscible displacements based on the pseudo function approach. The idea behind pseudo functions (relative permeabilities and capillary pressures) is to characterize the waterflood recovery of a two-dimensional (2-D) reservoir with averages such that a one-dimensional (1-D) displacement, using these properties, approximates the same recovery curve. The objective of this section is to discuss desirable features of pseudo curves, give the pseudo fractional flow of a particular stratified reservoir, and to compare this to some common analytical methods to generate pseudos.

IV.B - Approach

We consider an ordered or graded stratification, with no stochastic variations, because some common depositional units, channel and barrier bar sands, are described as fining upward or downward. The permeability in these fining sequences decreases in the direction of increasing fineness due to increasing shale content and decreasing grain size.

Our 2-D reservoir consists of 10 homogeneous layers with constant properties. The permeability contrast from top to bottom is 1:10, increasing linearly downward with an average permeability, k, of 55 md. The permeability is anisotropic, however,

so that the horizontal and vertical permeabilities may be different. The reservoir is horizontal. The rock relative permeability curve is (Fig. IV-1) the same for all layers, as are the irreducible saturations of oil and water. There is no free gas. The capillary pressure function varies with horizontal permeability according to the Levertt J-function so that each layer has a different curve (Fig. IV-2).

IV.C - Simulator Used

We use a 2-D cross-sectional IMPES numerical simulator written by the author (see appendices for a description) to generate production curves and averaged fractional flow curves. Such simulators are subject to truncation error; however, the stratification renders the averaged water/oil displacement front so disperse that this is not a major difficulty here. Since the simulation includes capillary pressure, gravity, and allows the possibility of non-pistonlike displacements within a layer, the overall production curves represent actual flow quite generally.

For each run we generate pseudo fractional flow curves by techniques described below. These curves are then compared to those from three common analytical displacement theories: Dykstra-Parsons[7] (DP), Hearn[13], and a generalized vertical equilibrium (VE) theory given by Coats *et al.*[12]. See Jones[14] for an exposition of the VE theory.

Relative Permeability Curves
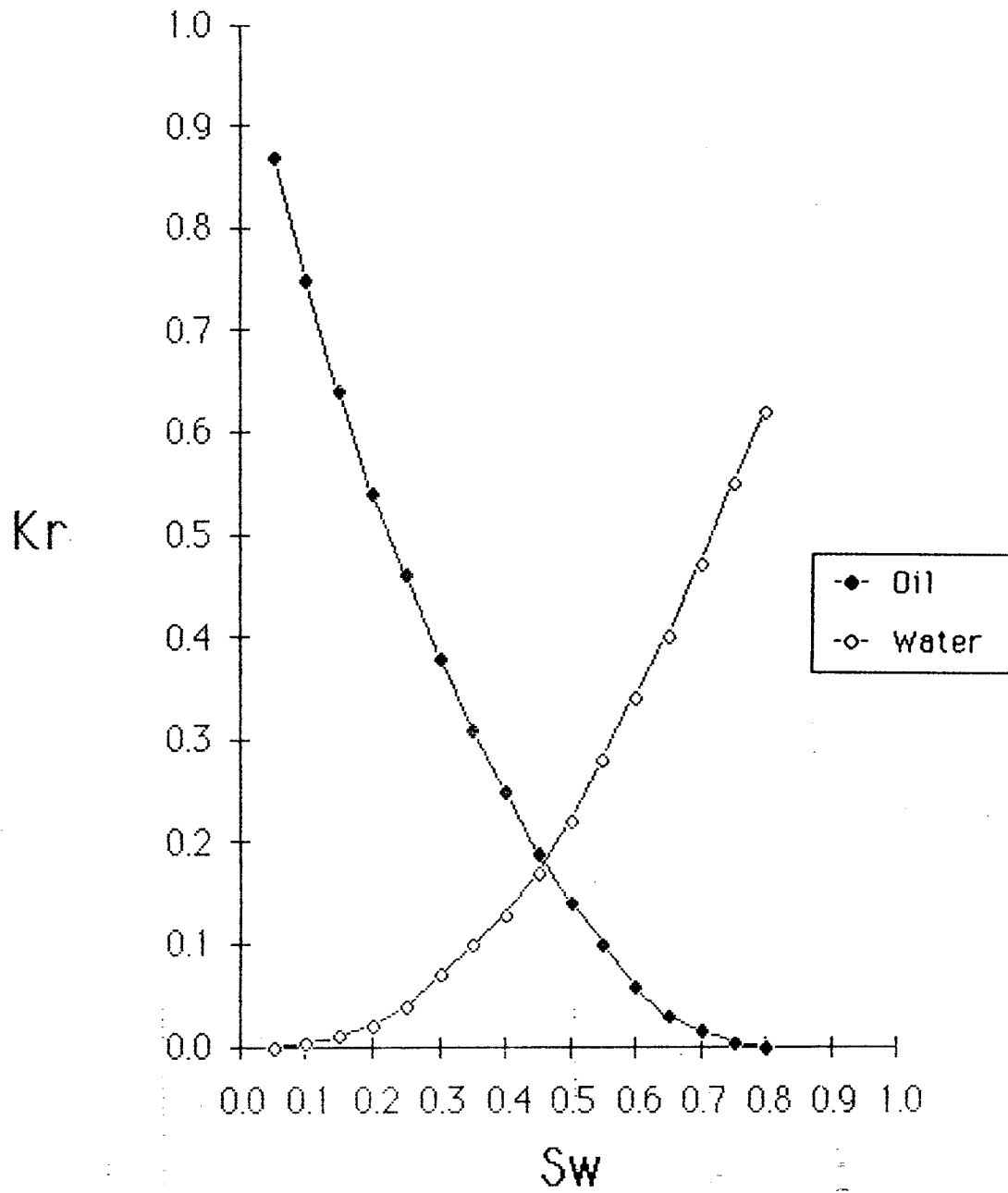
Figure IV-1 : Input Relative Permeability Curves

Capillary Pressure Curves
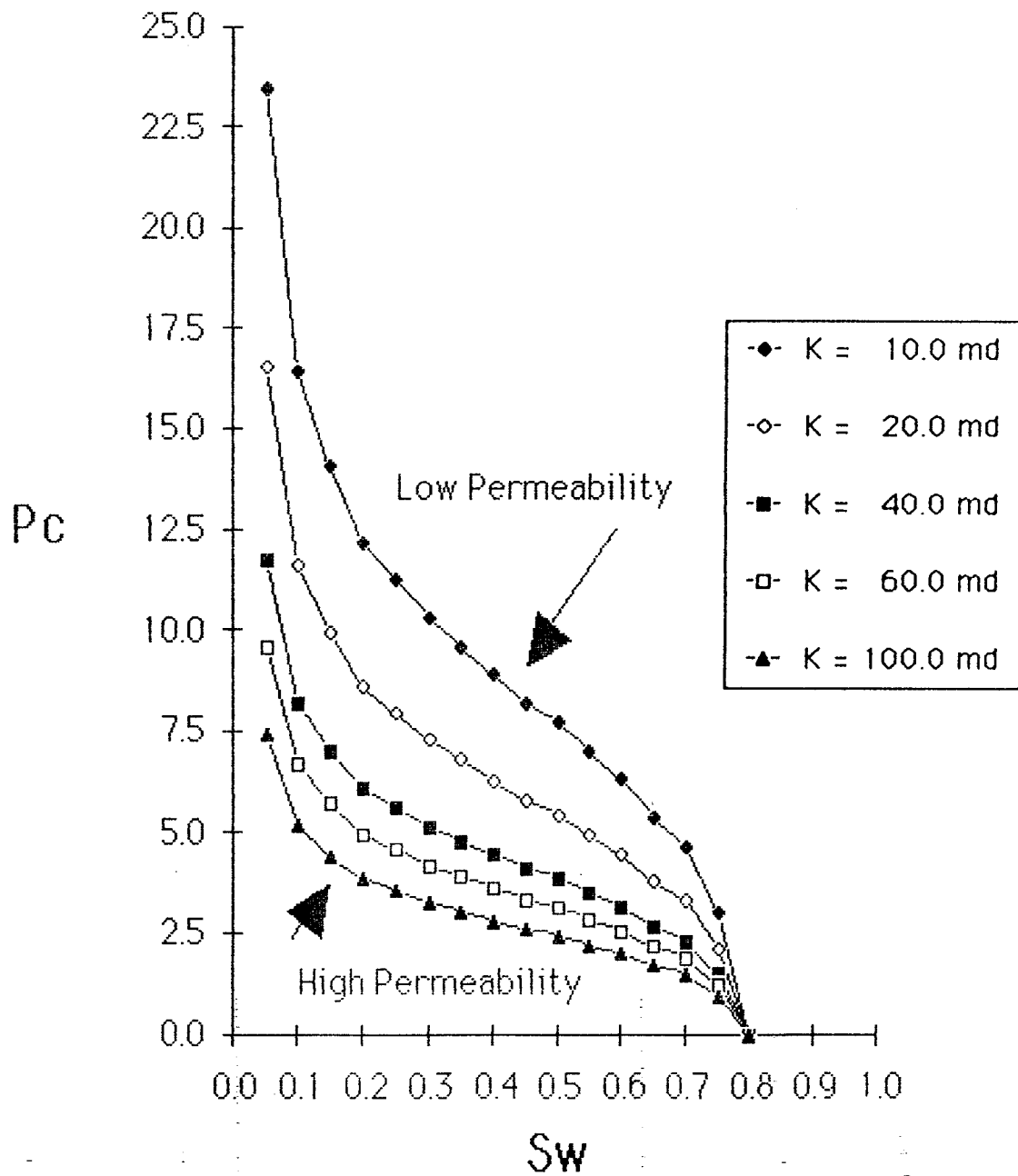
Figure IV-2 : Input Capillary Pressure Curves

IV.D - Simulation Curves

We present our simulation results in terms of pseudo fractional flow curves at a given time and mobility ratio. The pseudo or averaged water fractional flow (f_w) is defined as:

$$f_w = \frac{\sum\limits_{i=1}^{n} u_{wi}\, h_i}{\sum\limits_{i=1}^{n} (u_{wi} + u_{oi})\, h_i} = \frac{\sum\limits_{i=1}^{n} u_{wi}\, h_i}{u_T} \qquad \text{(IV-1)}$$

where

f_w =   water fractional flow

u_{wi} =   water flux in layer i

u_{oi} =   oil flux in layer i

u_T =   total fluid flux across a vertical cross-section

h_i =   thickness for layer i

n =   number of layers

i =   layer index

This is equivalent to the more common defintion

$$u_w = f_w\, u_T \qquad \text{(IV-2)}$$

where

u_w =   total water flux across a vertical cross-section

$$= \sum\limits_{i=1}^{n} u_{wi} \qquad \text{(IV-3)}$$

The average water saturation, S_w, is a thickness average of the layer water saturations across a vertical cross section or:

$$\overline{S_w} = \frac{\sum_{i=1}^{n} S_{w,i}\, h_i\, \phi_i}{\sum_{i=1}^{n} h_i\, \phi_i} \qquad \text{(IV-4)}$$

where

$\overline{S_w}$ = average water saturation

$S_{w,i}$ = water saturation in layer i

h_i = thickness of layer i

n = number of layers

i = layer index

There are two ways to calculate an f_w - S_w curve from a 2-D simulation. The first is to evaluate the water fluxes and saturations at a fixed position. The entire curve is generated as fronts in each layer pass the position with increasing time. If the fixed position is at the effluent end of the reservoir, this method must necessarily give an accurate pseudo curve since it is the production response which we wish to represent in the first place. Generating a complete pseudo curve in this manner is time consuming, however, since the entire water/oil front must pass the fixed position. The pseudo curve generated in this manner may not be scalable to a reservoir with different dimensions, but this is most apparent from the second approach. Since this method creates a time averaged fractional flow curve, a time parameter is meaningless for fixed postion curves.

The second approach, that is adopted here, is to evaluate the water fluxes and saturations along several cross-sections at a fixed time. The displacement front need

not clear the effluent end at all to generate a complete curve by this method. Indeed, the method works best when the front is entirely contained in the reservoir (before breakthrough). More importantly, the second approach allows us to see how the fractional flow curves change with time. Displaceable pore volumes of water injected, t_D, will be the time parameter in these figures. R_L is a measure of vertical communication and will be defined later in this chapter.

The end-point mobility ratio, M, associated with each run is an end point mobility ratio calculated as follows:

$$M = \frac{\lambda_{rw}^{o}}{\lambda_{ro}^{o}} = \frac{k_{rw}^{o}}{k_{ro}^{o}} \frac{\mu_o}{\mu_w} \tag{IV-5}$$

where

$$M = \text{end-point mobility ratio}$$

$$k_{rw}^{o} = \text{water relative permeability at residual oil saturation}$$

$$k_{ro}^{o} = \text{oil relative permeability at residual water saturation}$$

$$\mu_w = \text{water viscosity}$$

$$\mu_o = \text{oil viscosity}$$

Variations in M were achieved by varying μ_o while keeping all other variables constant.

IV.E - Results

The most general pseudo relative permeabilities should be independent of reservoir dimensions, particularly system length. Most analytical theories have been

based on the assumption of perfect vertical communication. Using highly idealized displacements, Zapata[9] has shown that even if vertical communication is poor, the pseudo function approach should be valid as long as the reservoir's aspect ratio is large (as is usually the case). For very short times, however, the averaged f_w - S_w curve should be time-dependent, even in the best of circumstances.

We tested this notion on more complicated waterfloods in our simulator runs. Figure IV-3 shows pseudo fractional flow curves at three different times based on our simulator results. Before approximately 0.25 pore volumes (PV) injected, the curves shift with time as the reservoir becomes equilibrated. After some time, however, the curves converge to a "stabilized" curve (Fig. IV-4). This stabilized curve is the one which we will use in later comparisons.

The results in Figs. IV-3 and IV-4 were with zero vertical permeability. The apparent stabilization with time contradicts the DP theory which allows the layer flow rates (and, hence, the water fluxes) to vary with time when the mobility ratio is not unity. Other runs with some vertical permeability showed even greater stability than this one with zero communication.

Figure IV-5 shows the results of a DP calculation (no simulation) in the same reservoir as Fig. IV-3. (The agreement with the simulation is shown below in Fig. IV-8). Even with this extreme mobility ratio of 0.1, the f_w - S_w curves vary only a little. Thus, while it is true that pseudo functions cannot rigorously be used in the absence of vertical communication, the variation will be modest for even the most extreme mobility ratios. For mobility ratios closer to unity, Fig. IV-6, the variation is not discernable.

Simulation Fractional Flow

M = .10
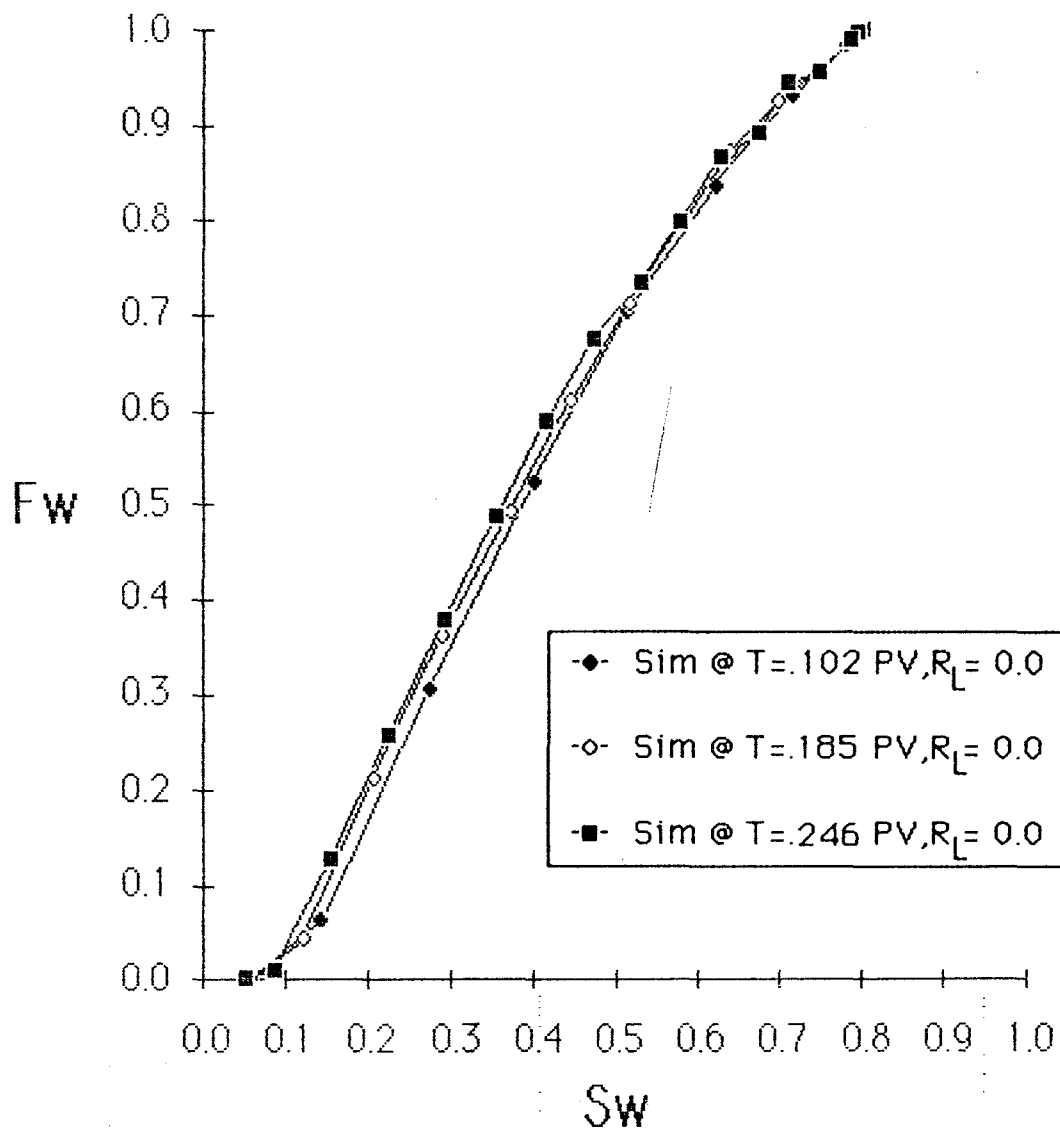
Figure IV-3 : Simulation Behavior at Early Times
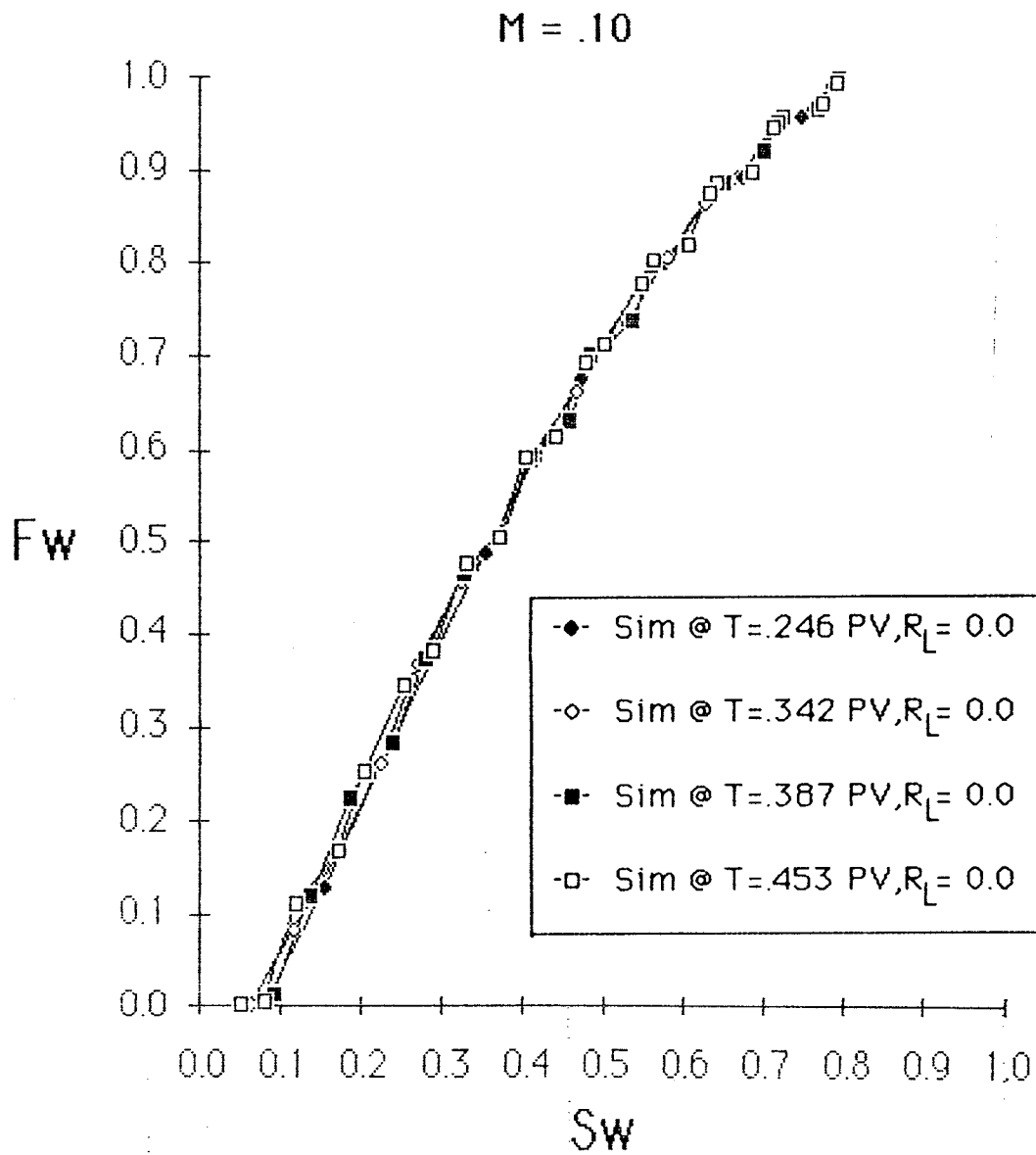
Figure IV-4 : Simulation Behavior at Intermediate Times

Simulation Fractional Flow

M = .10
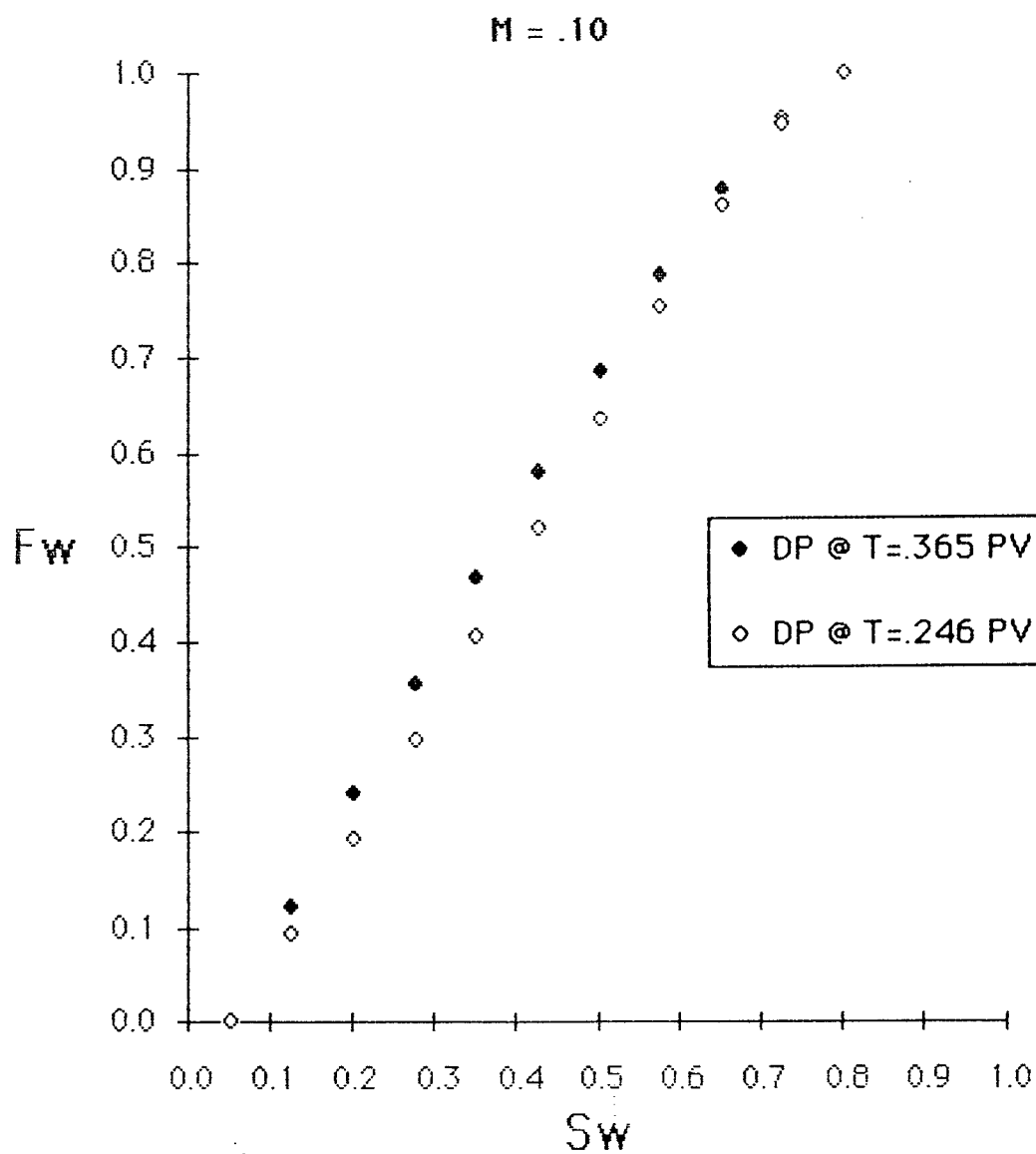
Figure IV-5 : Dykstra-Parsons Variation with Time at
M=0.1

Simulation Fractional Flow

$\overline{M} = .710$
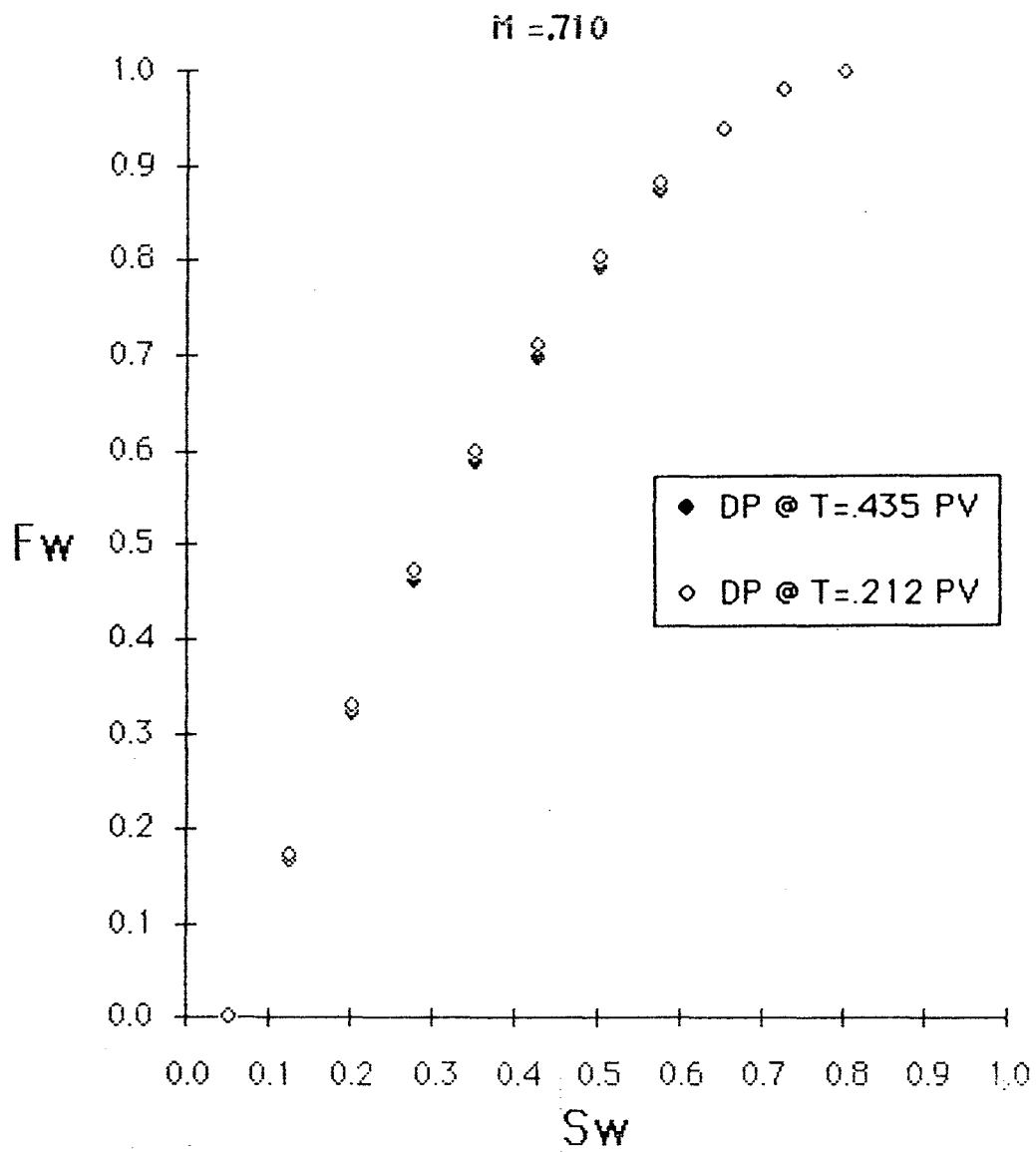
Figure IV-6 : Dykstra-Parsons Variation with Time at
M=0.71

These results suggest that the pseudo function approach might be more widely valid that previously supposed.

An early analytical method is that of Hearn[13] which assumes that each layer is in perfect communication with every other layer. This results in instantaneous redistribution of fluids vertically to satisfy pressure gradients between layers. Gravity and capillary pressure are neglected, and a pistion-like displacesment is assumed in each layer as in the DP method. A comparison between Hearn and DP should show the effect of viscous crossflow[9]; a comparison between Hearn and the VE theory (of which Hearn is a special case) should show the effects of capillary pressure and gravity.

Figure IV-7 shows the f_w - S_w curve calculated by the Hearn and VE methods. When the mobility ratio is low the two methods agree well; when it is high there is deviation, particularly at low water saturations. Displacements with mobility ratios near one are less dominated by viscous forces; hence, gravity and capillary forces -- the major differences between Hearn and VE -- are emphasized. Figure IV-7 also shows the sensitivity of both approaches to mobility ratio.

Even though both Hearn and DP yield stabilized f_w - S_w curves, the two approaches do not agree when the mobility ratio is greatly different from one. When M = 1.0, crossflow does not occur. As M increases, the effect of crossflow, which the Hearn vs. DP comparison issustrates, increases. Figure IV-8 shows a comparison between the VE, Hearn, DP and simulation (k_v = 0) curves. Note that the simulator predicts a curve much closer to the DP result, as it should. This figure suggests that vertical permeability (perhaps scaled by the aspect ratio) is a determining factor in

Simulation Fractional Flow
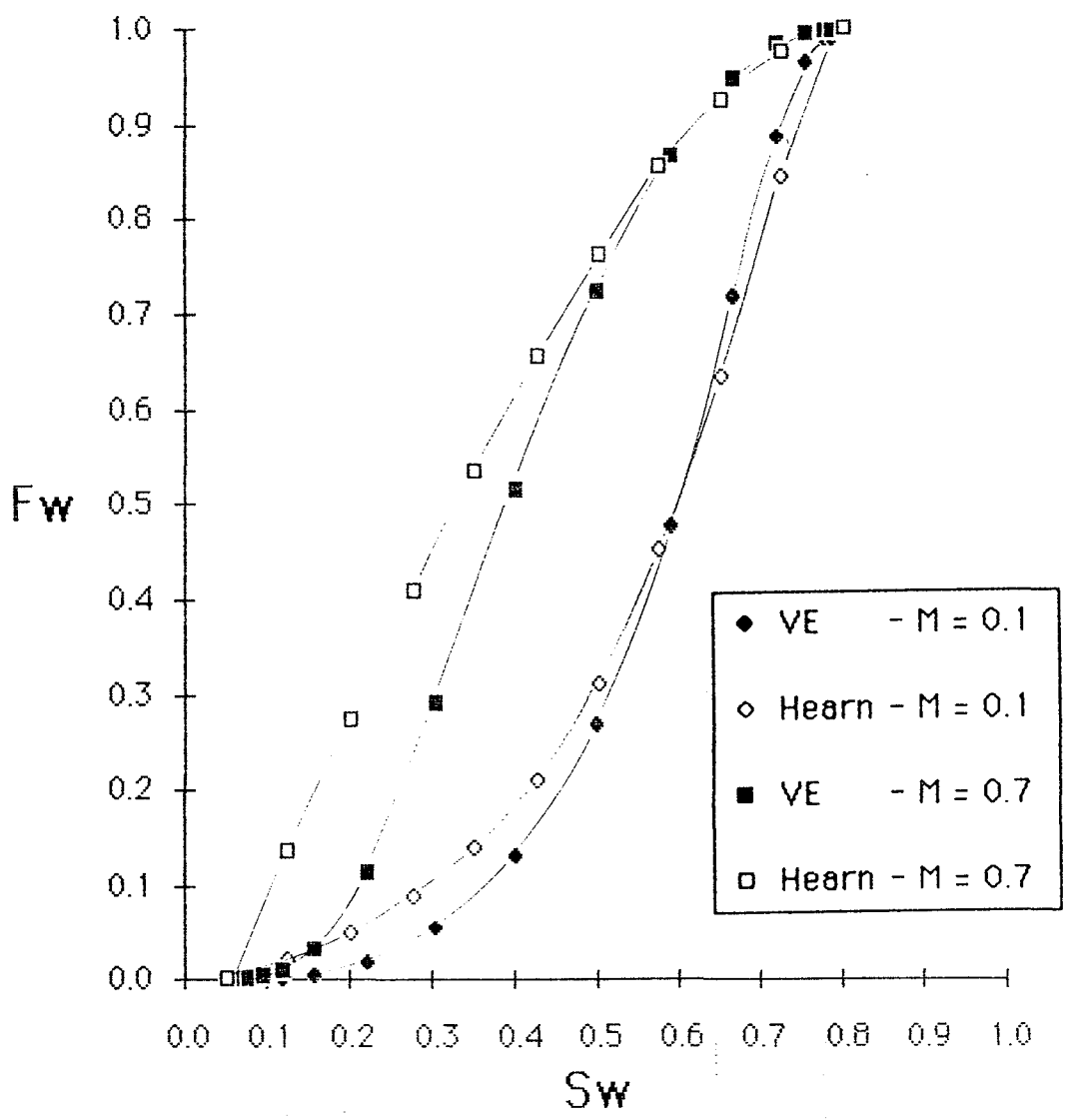
Figure IV-7 : Hearn vs. VE

Simulation Fractional Flow

M = .10
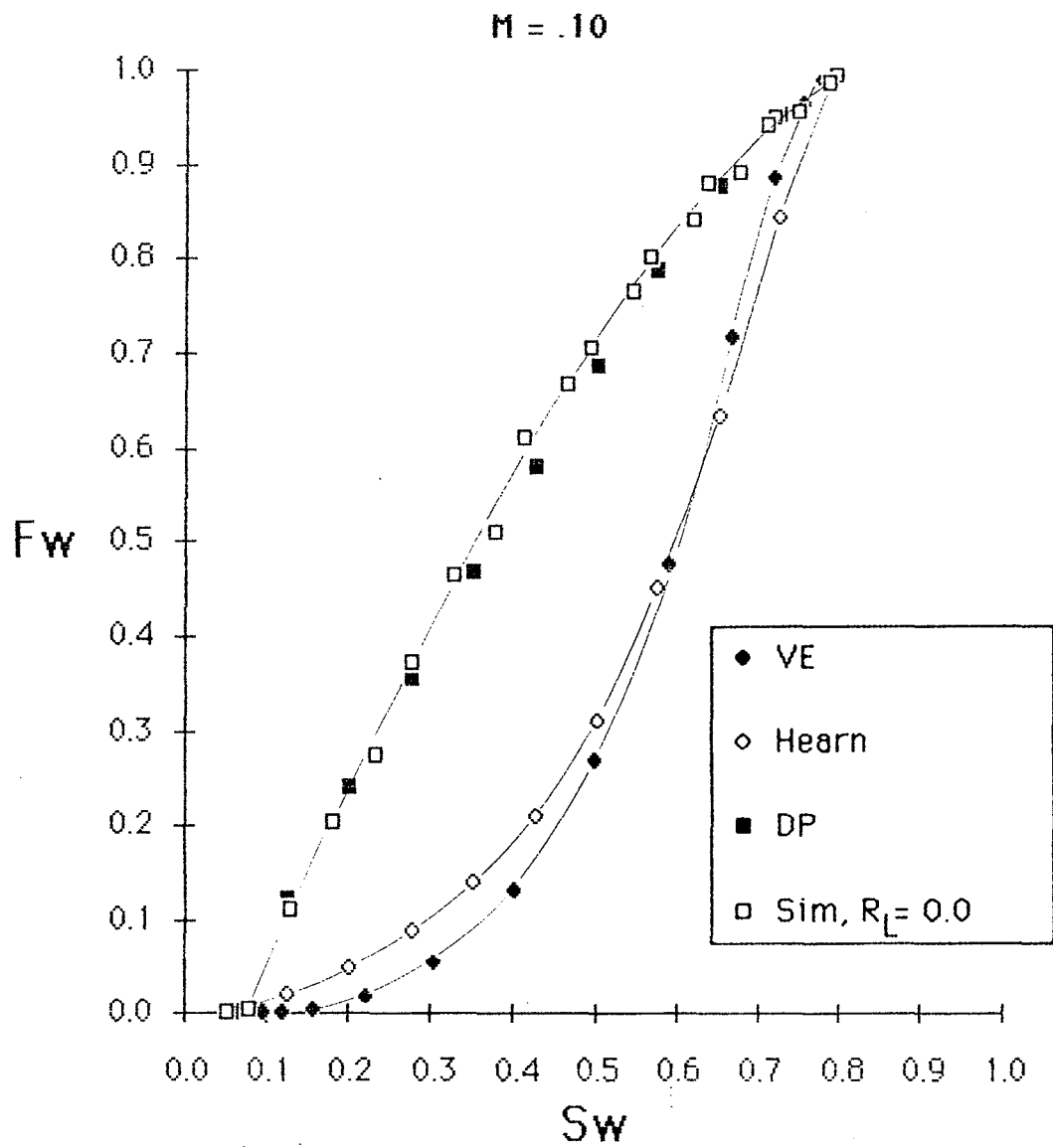
Figure IV-8 : Comparison of Theories at M=0.1

selecting which pseudo generation approach to use. The choice becomes less important as the mobility ratio approaches unity inasmuch as all curves approach the same result, Fig. IV-9. The unit mobility ratio limit is the Stiles model.[8]

A possible yardstick with which to differentiate the pseudo generation techniques is R_L.

$$R_L = \left(\frac{L}{H}\right)\left(\frac{\hat{k}_v}{\bar{k}_h}\right)^{\frac{1}{2}} \tag{IV-6}$$

where

L =   length of system

H =   height of system

$\hat{k}_v$ =   harmonic mean of vertical permeabilities

$\bar{k}_h$ =   arithmetic mean of horizontal permeabilities

Under Zapata's idealized conditions of no gravity or capillary pressure, the following quidelines were suggested:

1) $R_L < 1$ is Dykstra-Parsons ($R_L = 0$, zero vertical communication)

2) $R_L > 10$ is Vertical Equilibrium ($R_L = \infty$, infinite vertical communication)

The R_L quideline should scale, such that if R_L is the same for two runs, the resulting fractional flow curves should be the same, regardless of the different system shape or permeability anisotropies. The scalability is restricted to cases with the same mobility ratio, relative permeability curves, and capillary pressure curves, as these parameters are not included in the defining equation above.

Simulation Fractional Flow

M = .71
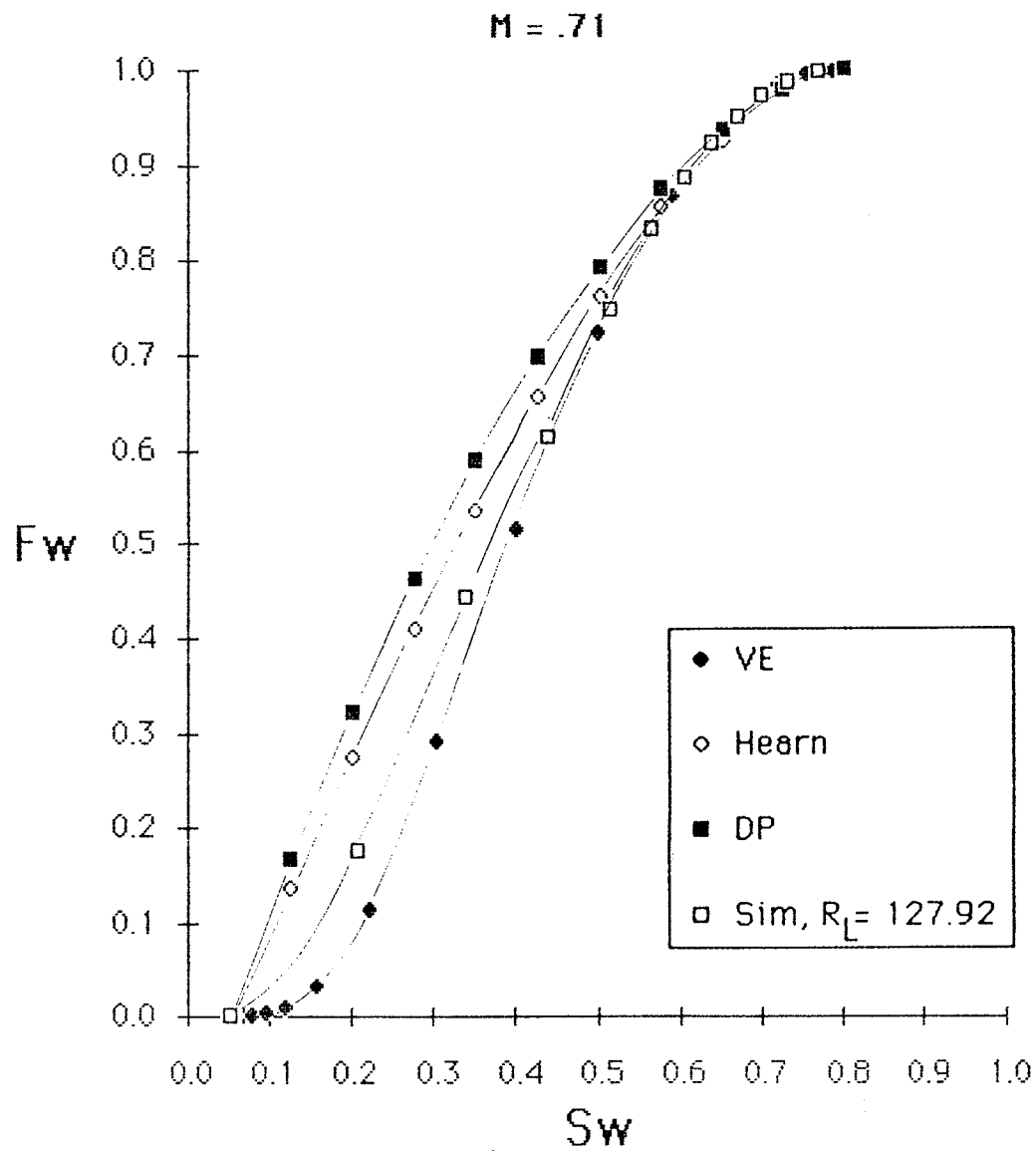
Figure IV-9 : Comparison of Theories at M=0.71

To test the scalability of the R_L guideline, we made two runs with the same R_L=12.79, but with different grid block dimensions (300' x 10' vs. 210' x 7'). The reservoir velocity was maintained at 1 ft/day and the permeabilities were held the same. Figure IV-10 shows that the two runs produced nearly identical fractional flow behavior. This demonstrates the lack of sensitivity of the results to grid size, as long as the aspect ratio is maintained.

We also made two runs with the same R_L, but different vertical permeability configurations, Fig. IV-11. That these two curves agree well indicates that R_L is insensitive to how vertical permeability is distributed, as long as the harmonic mean is the same.

We also tested the ability of the R_L yardstick to predict whether a reservoir will act more like one with no vertical communication, or one with infinite vertical communication. This test is not as complete as is necessary to draw firm conclusions, but it does illustrate some interesting behavior. In Fig. IV-12, a case with R_L=.4 is shown to have nearly an identical fractional flow curve as a case with R_L=0. Both of these cases are very well approximated by the DP theory, Fig. IV-13, indicating that R_L does not have to be absolutely zero for a system to act as if R_L=0. This supports the idea that $R_L < 1$ is well approximated by the DP theory.

Supporting the other yardstick, ($R_L > 10$ approximates VE) was not as successful. Cases were run with R_L = 3, 7.47, 9.05, 12.79, 23.64, and 128, Figs. IV-14 and IV-15. If the guideline were valid, all of these cases with $R_L > 10$ would fall on the VE curve. As Fig. IV-14 shows, however, the fractional flow curves do vary significantly at M = 0.1. In a blow-up, Fig. IV-15, all of these simulation curves

Simulation Fractional Flow

M = .10
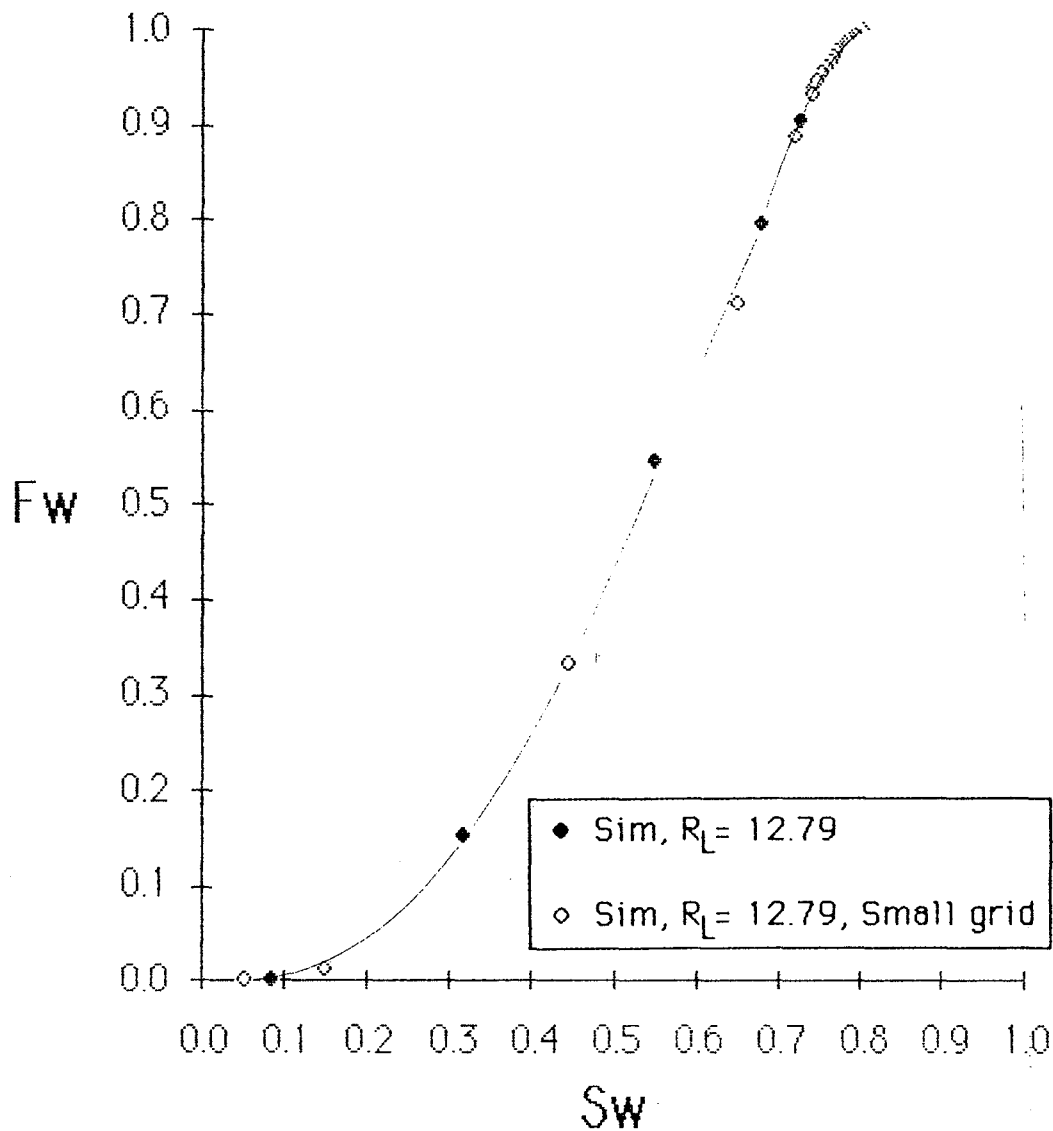
Figure IV-10 : Grid Size Comparison

Simulation Fractional Flow

M = .10

Legend:
- ● Sim, R_L= 7.47, k_V= kh/10.
- ○ Sim, R_L= 7.47, k_V= 3.414
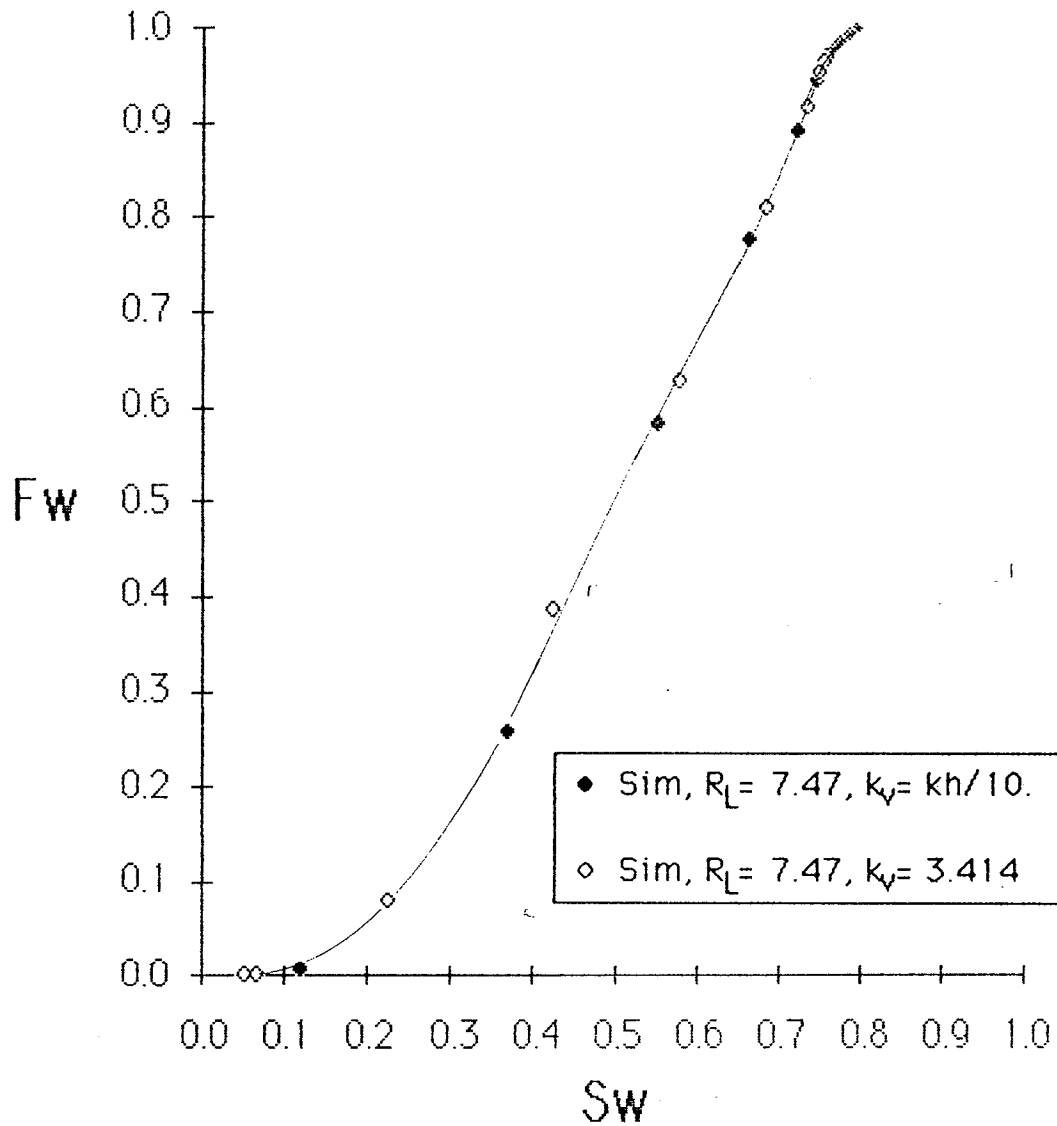
Figure IV-11 : Comparison of Vertical Permeability
Configurations

Simulation Fractional Flow

M = .10
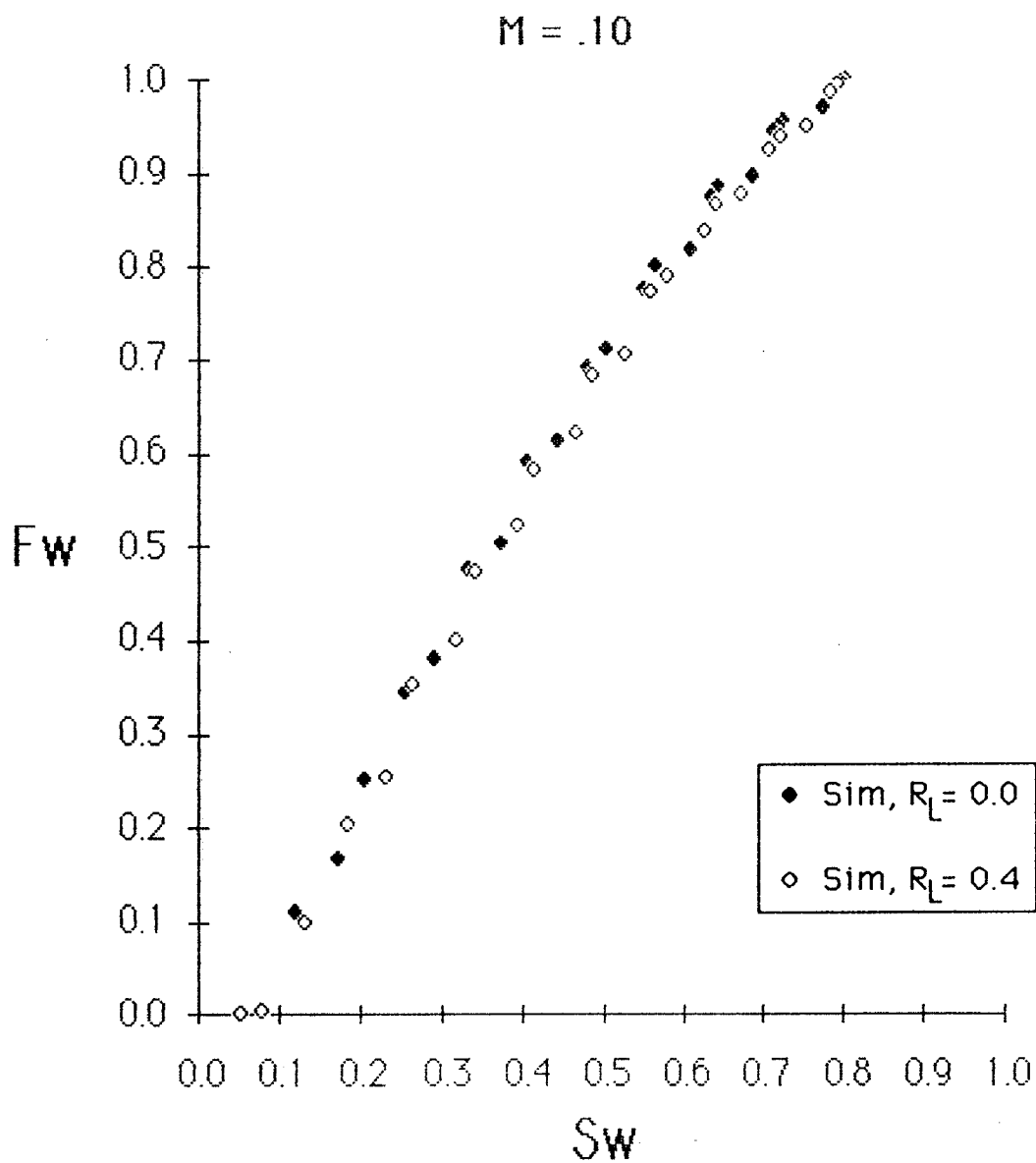
Figure IV-12 : Simulation Results at Low Vertical
Permeability

Simulation Fractional Flow

M = .10
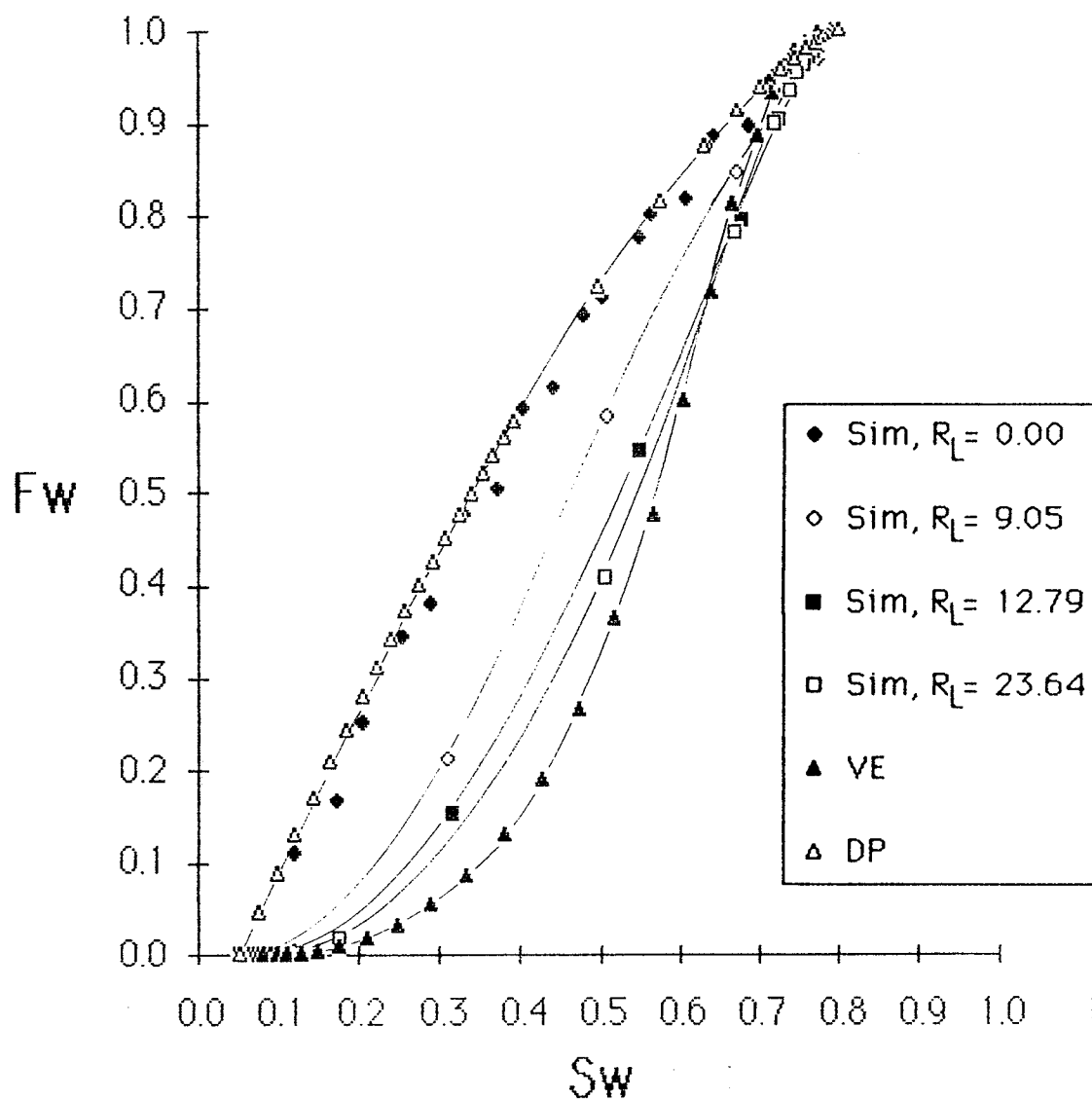
Figure IV-13 : Simulation vs. Theory

Simulation Fractional Flow

M = .10
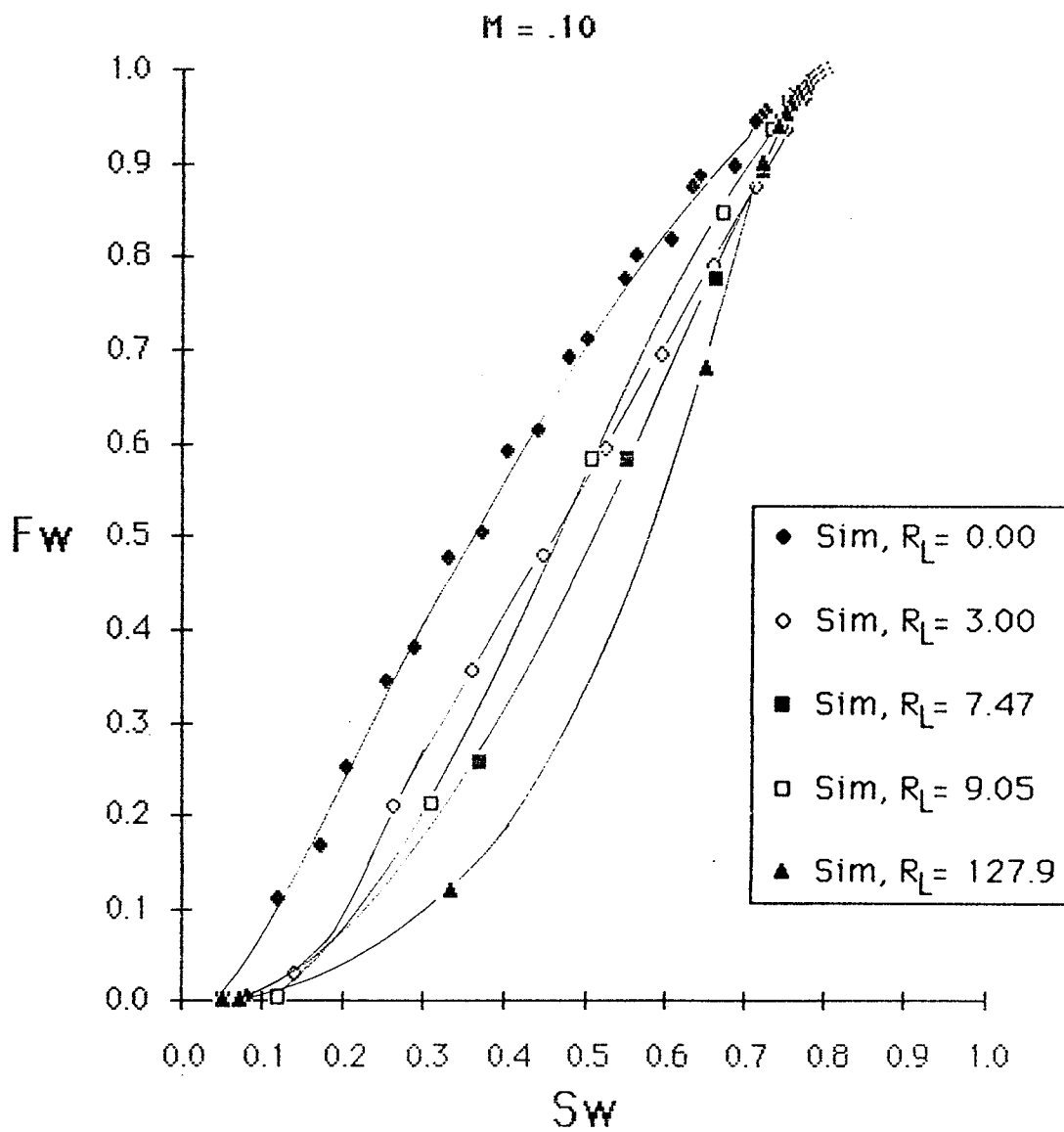
Figure IV-14 : Simulation Results Over Wide Range of
Vertical Permeabilities
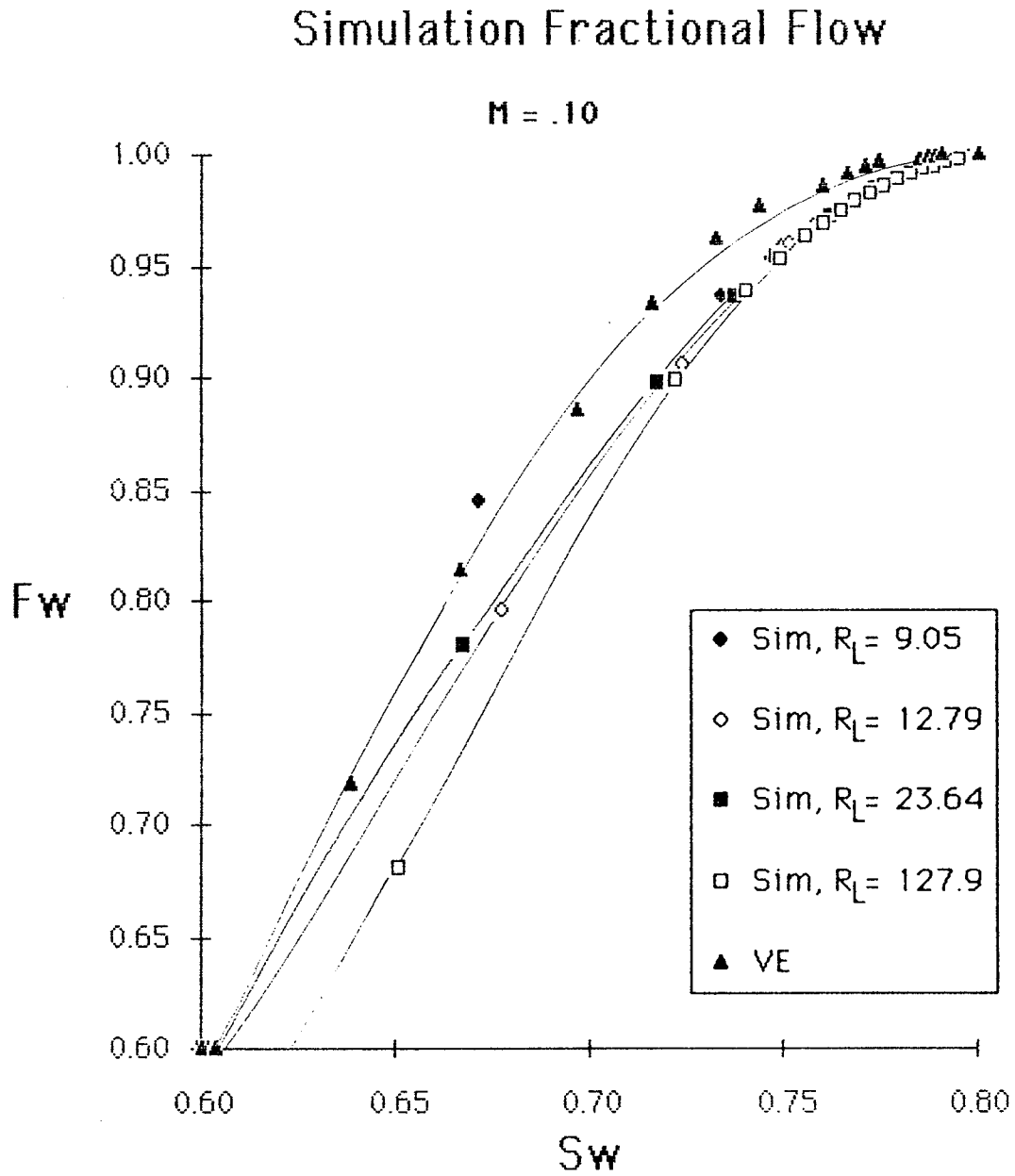
Figure IV-15 : Simulation Results at High Vertical
Permeability

seem to converge near $S_w = 1-S_{or}$, but not to the VE curve. Figure IV-16 shows that these curves also have very nearly the same tangent point, so that they will have nearly identical oil production histories using the Buckley-Leverett graphical method. The curve for $R_L = 3$ clearly has a different tangent, although it does display similar behavior near $S_w = 1-S_{or}$. $R_L = 7.47$ and 9.05 are essentially the same as the curves with $R_L > 10$. This indicates that an $R_L = 5$ or 7 may be a better yardstick. A reason for this ambiguity may be that the reservoir approach truely infinite communication asymptotically with R_L^q. Regardless of the precise cut-off R_L to be used, this study shows that the $R_L > 7$ guideline does predict similar behavior, but that VE is not the best curve to use.

This is encouraging from a practical simulation view for two reasons. First, most reservoirs reach $R_L = 7$ with even very little vertical permeability, so that the need for detailed vertical permeability information is relaxed. Second, experience shows that the greater the vertical permeability, the greater the run time on the simulator. If VE is not an adequate pseudo, then a simulation run with $R_L = 7$ will give as good a pseudo as a costlier simulation run with $R_L = 100$. Therefore, one pseudo may be used for many grid blocks in a system since the pseudo applies to a very wide range of vertical permeability values. This can greatly increase the confidence in pseudos, decrease the cost of generating them, and reduce the number of different pseudos that must be generated for a grid system.

Since vertical equilibrium has long been accepted as the best way of generating pseudo curves for cases of good communication, it is very interesting that the simulation curves did not match the VE curves. The differences between simulation and VE curves is discussed below.

Simulation Fractional Flow

M = .10
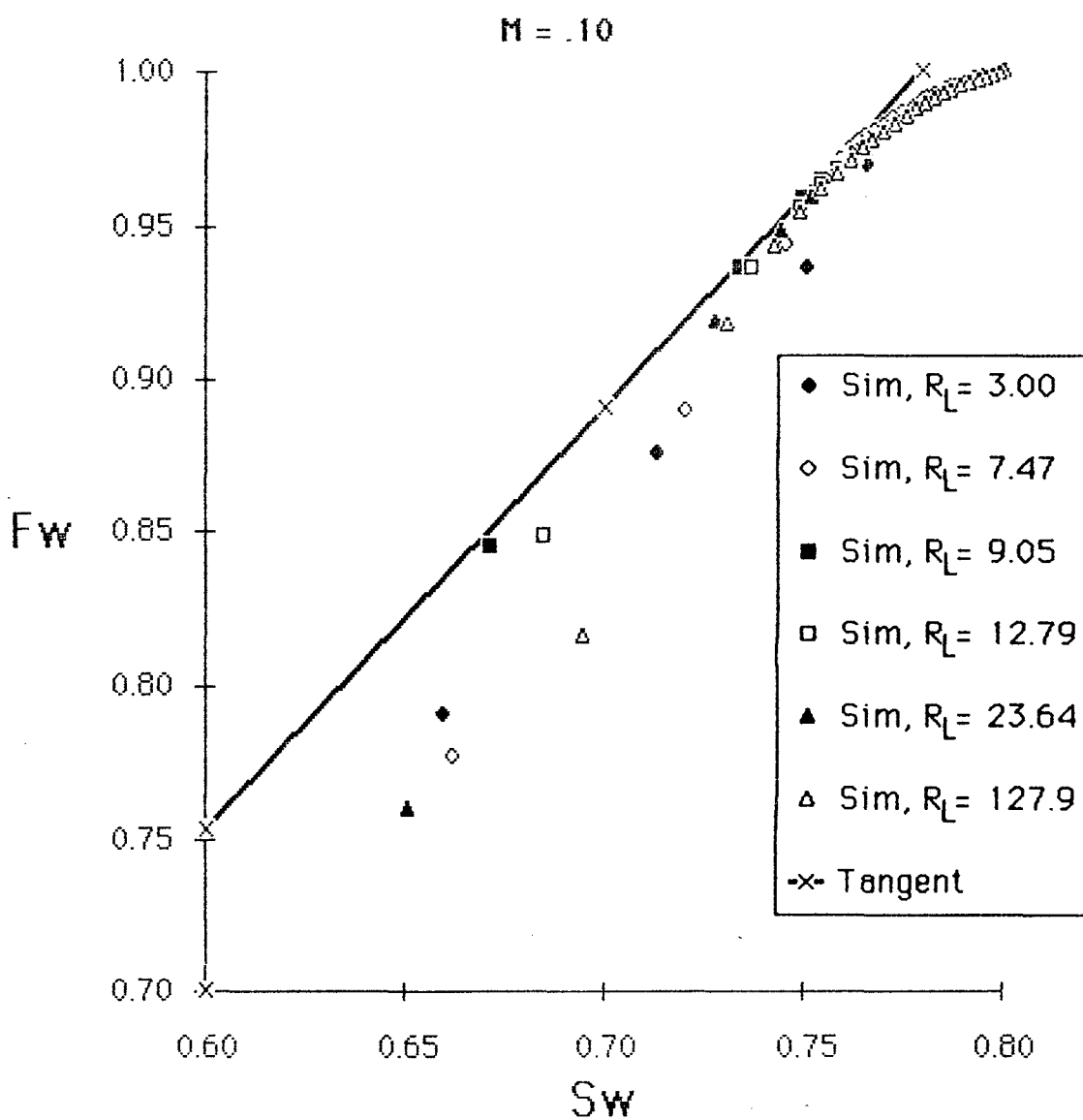
Figure IV-16 : Simulation Results With Buckley-Leverett
Tangent Line

Simulation Fractional Flow

M = .10
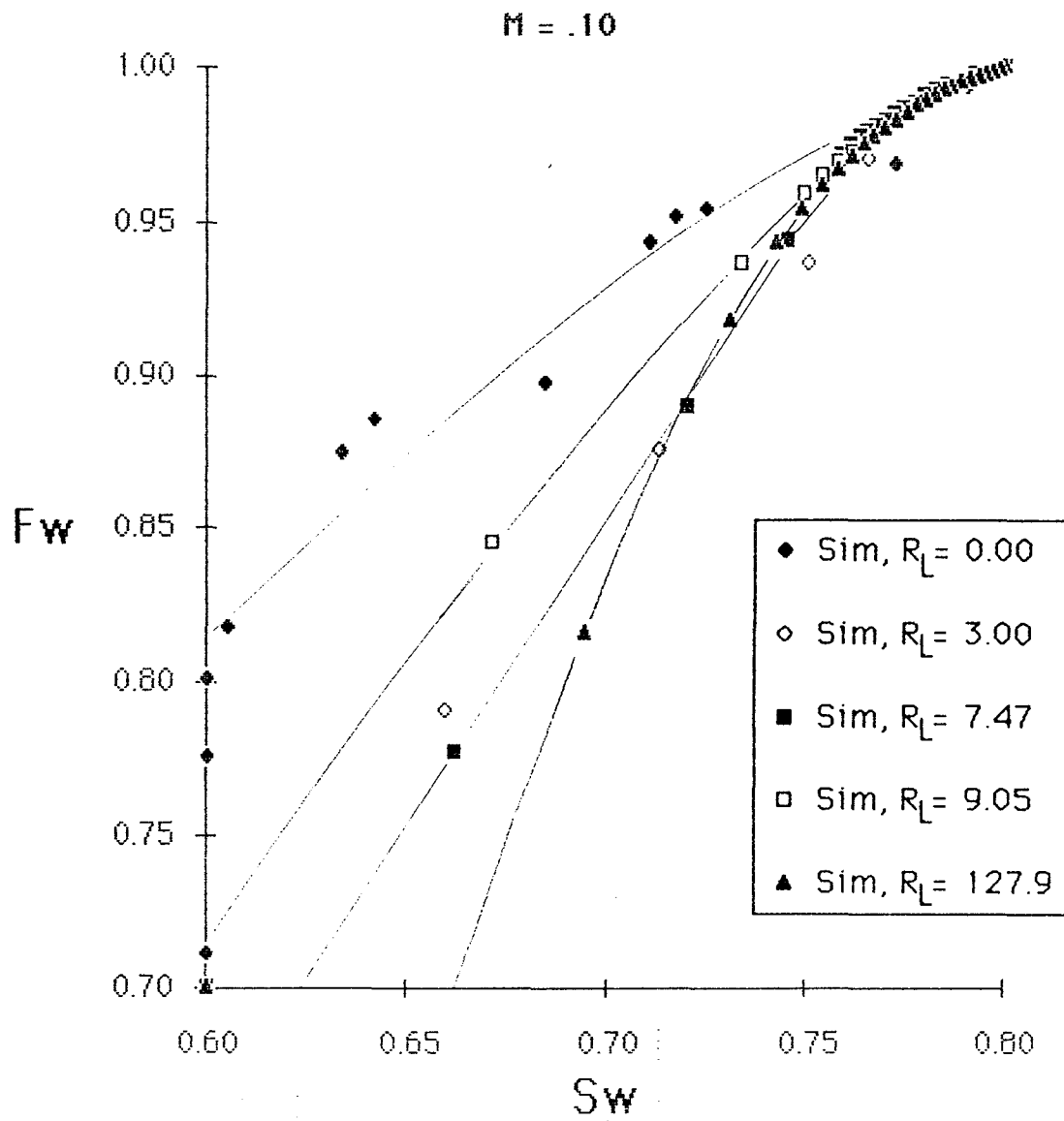
Figure IV-17 : Expanded View of Fig. IV-14

IV.F - Vertical Equilibrium

Vertical equilibrium is a condition in which the vertical distribution of saturations is determined by the equilibrium between gravity and capillary forces. This implies that vertical communication is good enough to allow redistribution of the oil and water phases vertically in a shorter time than the fluids can move horizontally. In a finite difference simulator, fluid is only allowed to move into an adjacent grid block during a single time step. This restriction limits the ability of a simulator to duplicate VE behavior with practical time step sizes. However, with very large vertical permeability and a small time step, it should be possible to approximate the VE curve.

A simulation with a very large vertical permeability compares very favorably with the VE curve at $M = 0.1$, Fig. IV-18. An enlargement of the high saturation end of the curve, Fig. IV-19, indicates, however, that the curve has a different shape and thus will have significantly different production curves. A tangent line used to determine water breakthrough in the Buckley-Leverett graphical technique indicates an earlier breakthrough for VE than for the simulation curve. Also, a tangent line at $S_w = 1-S_{or}$ indicates that the VE curve predicts a much longer time to sweepout than the simulation curve. These two deviations of the VE theory from the simulation may be due to some non-physical assumptions made in the VE development, and in the inability of the simulator to achieve instantaneous redistribution.

In the derivation of VE, k_z is assumed large, so that

Simulation Fractional Flow

M = .10
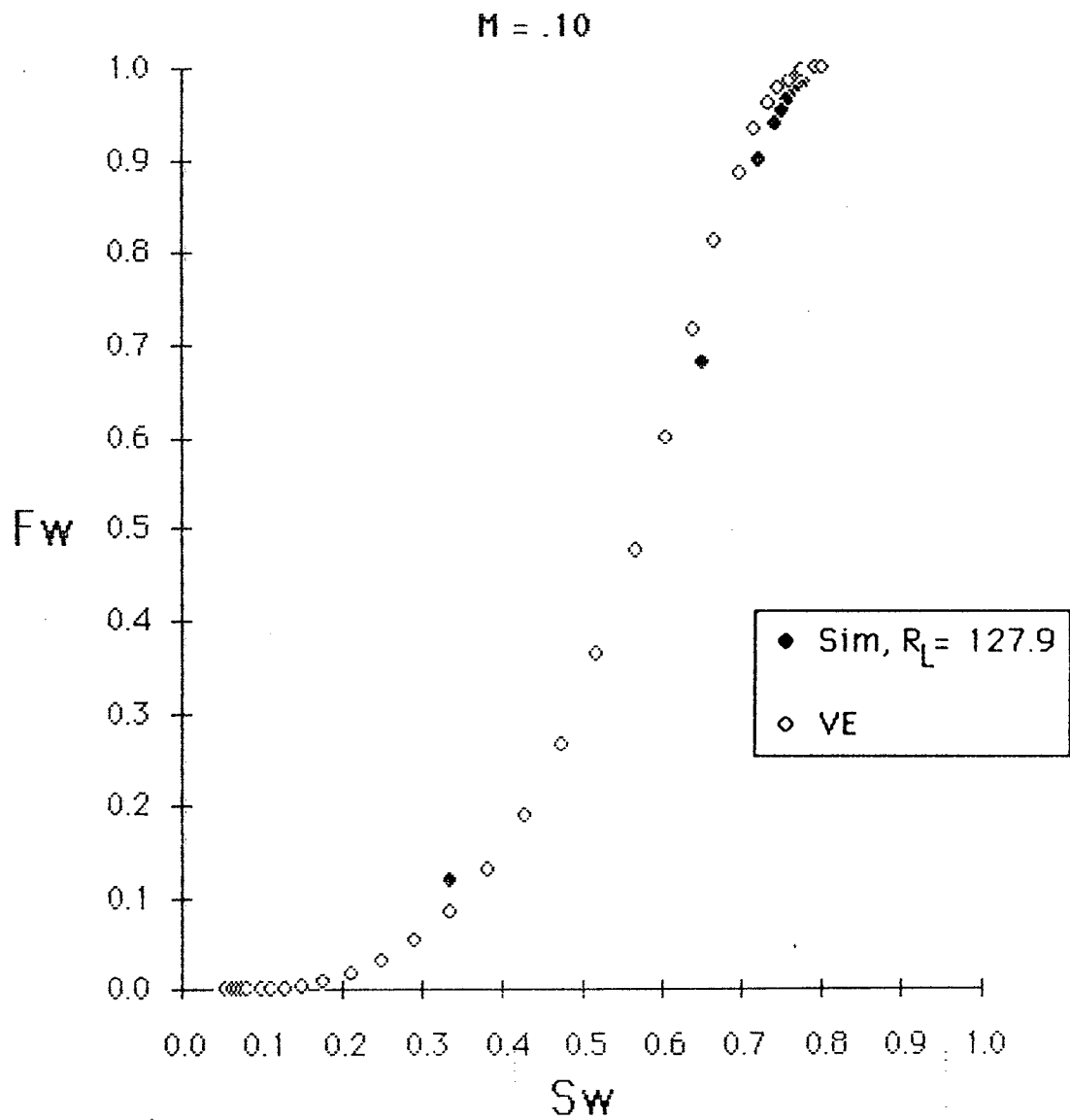
Figure IV-18 : Vertical Equilibrium vs. High R_L
Simulation

Simulation Fractional Flow

M = .10
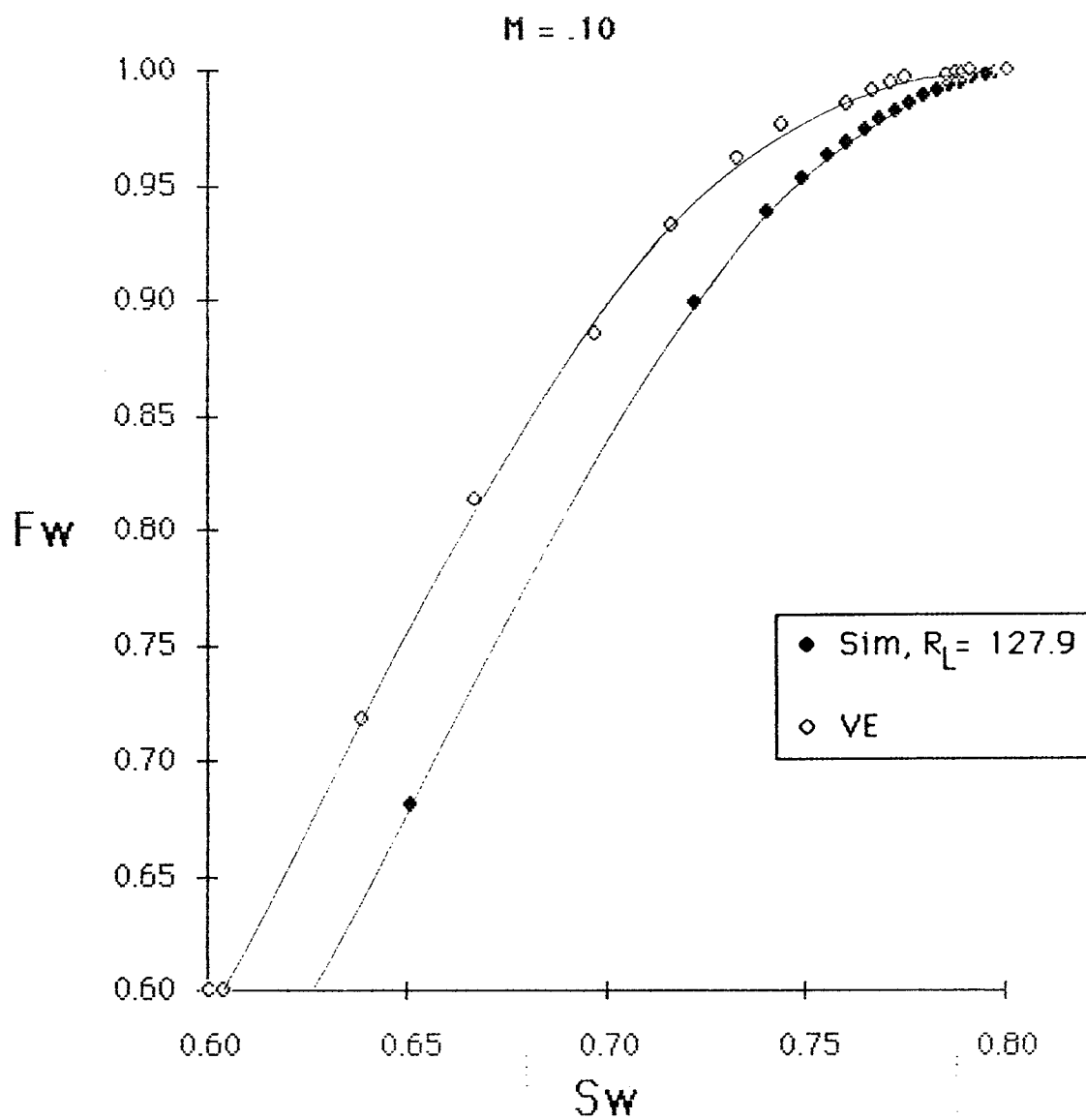
Figure IV-19 : Expanded View of Fig. IV-18

$$\frac{\partial p_w}{\partial z} + \rho_w \; g \cos \alpha = 0 \qquad\qquad : \text{Consistent Units} \qquad\qquad \text{(IV-7)}$$

where

$\dfrac{\partial p_w}{\partial z}$ = water phase vertical pressure gradient

ρ_w = water phase density

g = gravitational constant

α = dip angle (0 = horizontal)

However, the product $k_z \lambda_{rw}$ must be large for the above result to be valid, not just k_z. Clearly, when S_w is near S_{wr}, λ_{rw} is near zero, so that $k_z \lambda_{rw}$ cannot be large and the above assumption is invalid. The same arguements apply to the oil gradient equation, so that it is not valid near $S_w = 1\text{-}S_{or}$. If our interest were in finding the pressure distribution of one phase alone, this would pose no problem for we could apply the oil gradient near $S_w = S_{wr}$ and the water gradient near $S_w = 1\text{-}S_{or}$. However, we need to know both phase pressures so that we can calculate the capillary pressure. From this capillary pressure and the P_c vs S_w curves, we can calculate the water saturation distribution. Clearly, VE is only valid at points in the reservoir where $S_{wr} < S_w < 1\text{-}S_{or}$. At this point, however, no work has been completed to determine how far S_w must be from the endpoints to ensure a proper saturation distribution.

The two deviations listed above can be directly related to this question, since they both occur in the saturation regions in which the VE assumption is invalid. The breakthrough time is determined by the behavior of the flood front in the reservoir -

where S_w is near S_{wr}. VE makes the aforementioned non-physical assumptions when the water saturation is in this range. It is unclear how this will influence the saturation distribution or the fractional flow curve. The simulator restricts movement of water in this region by the low mobility in this saturation range, so that VE is able to move fluids at low saturations better than the simulator can.

The sweepout time is determined by the behavior of the fluids behind the front as the reservoir fills up with water. An interesting inconsistency in the VE theory develops when $S_w = 1-S_{or}$ at more than one layer vertically. When $P_c=0$ at $S_w = 1-S_{or}$, water and oil phase pressures are equal. When this condition occurs at more than one location vertically, the basic equation of VE, Eq. IV-7, is necessarily violated, unless the fluid densities are equal. This leads to a delay in the time needed to completely saturate a vertical column and thus a longer time is needed to sweep the reservoir.

These two explanations for the differences between simulation and VE theory assume that the simulation is correct. While it is true that the simulation does not make any restrictions on the pressure profiles, it does have a finite ability to redistribute fluids vertically. In fact, when at or very near $S_w = S_{wr}$, there is little or no water movement due to the low mobility of the water phase, even if there are large capillary, gravity, or viscous driving forces. Comparisons between simulation and VE vertical pressure profiles, Fig. IV-20, show that VE is an adequate approximation only in areas behind the front which have been well swept, but have not yet reached $S_w = 1-S_{or}$ in the bottom layer. Since this area is relatively unimportant to front development, it is not surprising that the breakthroughs do not match well. Despite the problems that a simulator has in distributing fluids vertically and matching VE, it must be assumed that the sumulator can better model the complex flow in the reservoir, and thus should be
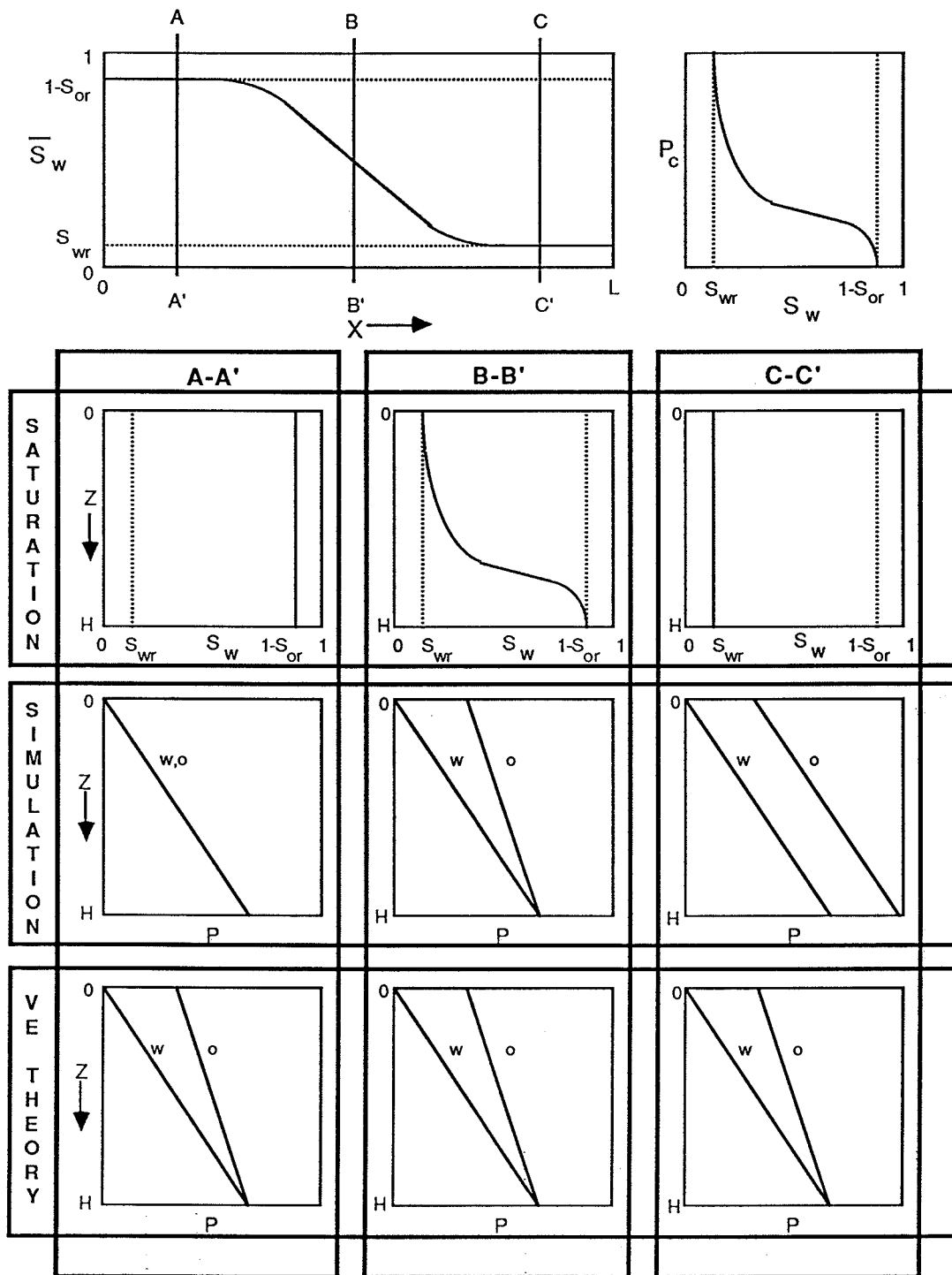
Figure IV-20 : Schematic Phase Pressure Diagram
Illustrating the Difference Between Simulation
Results and VE Theory

regarded as more realistic. Instantaneous redistribution is, therefore, a theory which one can not expect to duplicate in nature or in the laboratory.

CHAPTER V

CONCLUSTIOS AND RECOMMENDATIONS

V.A - Conclusions

Based on the simulations run for this study, the following conclusions can be drawn:

1) Oil displacement can be affected by a graded permeability heterogeneity. Channel sands, with the high permeability on the bottom, generally will greatly reduce displacement efficiency when compared to a homogeneous system. Barrier bars, with the low permeability on the top, will usually also reduce displacement efficiency, but usually not as severely as a channel sand.

2) The gravity number, N_g, and mobility ratio, M, can be used qualitatively to measure the degree of displacement efficiency reduction.

3) As N_g approaches zero, a channel sand will behave like the inverse of a barrier bar since viscous forces dominate the displacement.

4) As an extrapolation of an observed trend, a channel sand will sweep only the bottom layer, whereas a barrier bar will approach a piston-like displacement as N_g gets large.

5) When M < 1, displacement efficiency with a graded permeability heterogeneity is good since the water does not tend to bypass the oil.

6) When M > 1, displacement inefficiencies caused by the stratification or gravity number are magnified due to the additional tendency of water to bypass the oil on the microscopic scale.

7) Cross bedding with unit mobility ratio and zero gravity number will not significantly alter displacement efficiency. In combination with mobility ratio or gravity number effects, however, cross bedding may lead to substantial differences.

8) Generating pseudo functions from smaller-scale simulations is probably the preferred approach because these can handle a large variety of permeability configurations, or heterogeneities. When this is not possible, analytical approaches are required.

9) When vertical communication is good, the pseudo function approach becomes quite accurate because a single or stabilized fractional flow curve can represent the entire displacement. When vertical communication is poor, the fractional flow curve changes with time, but the change is relatively slow so that the pseudo function approach is still valid for practical use.

10) The extent of vertical communication determines which analytical approach is appropriate. R_L is a good yardstick for determining the extent of vertical communication. While Dykstra-Parsons represents behavior well when R_L < 1, Vertical Equilibrium does not best represent behavior when R_L > 10, even though stabilized conditions are reached.

11) The R_L value of 10 is conservative, and may be reduced to near 5 with confidence that all cases when $R_L > 5$ can be represented by the same pseudo curve.

V.B - Recommendations

With the experience gained during the course of this study, the author makes the following recommendations:

1) This study should be extended to more thoroughly examine the effects of the parameters studied here. A quantitative measure of these effects may be possible if the fractional flow curve is fitted to a parametric equation and the value of the parameters determined empirically.

2) Although this study concluded that cross bedding was not significant, future work should investigate the representation of cross beds in both grid block pseudo curves and directly into numerical simulators.

3) A very fine grid simulation should be compared to coarse grid simulations, one which utilizes pseudo curves and another which does not. This entails access to a supercomputer, but should indicate the sensitivity of a reservoir scale simulation to stratification within a grid block.

4) Stratified systems are only one of many heteogeneities that exist in nature. Future work should investigate the representation of these complex heterogeneities.

These recommendations presuppose the importance of these parameters to oil displacements. It should be kept in mind that the input data to the reservior characterization is often crude itself, so that an extremely precise characterization is perhaps not necessary. It is obviously important to identify the sensitivity of simulations to the grid data. We may very well find that the averaging performed by crossflow within the reservoir is significant to a degree that renders precision unnecessary.

NOMENCLATURE

Symbols

A	=	Cross sectional area
f_w	=	Water fractional flow
g	=	Gravitational constant
h	=	layer thickness
H	=	System height
k	=	Permeability
k_r°	=	Endpoint relative permeability
L	=	System length
M	=	Mobility Ratio
n	=	Number of layers
N_g	=	Gravity number
P_c	=	Capillary pressure
q	=	Volumetric flow rate
R_L	=	Vertical Equilibrium yardstick
S	=	Saturation
t	=	Time
u	=	Darcy Velocity (q/A)
W	=	System width
x	=	Distance in x-direction
y	=	Distance in y-direction
z	=	Distance in z-direction

Greek

α = Dip angle

ϕ = Porosity

ρ = Phase density

γ = Phase specific gravity

λ = Phase mobility

μ = Viscosity

Subscripts

x = x-direction

y = y-direction

z = z-direction

w = water phase

o = oil phase

or = residual oil

T = total

D = dimensionless

h = horizontal

v = vertical

wr = residual water

Superscripts

$^{-}$ = Arithmetic average

$^{\wedge}$ = Harmonic average

APPENDICES

APPENDIX A

SIMULATOR DESCRIPTION

The simulator used in this study is a 2-D cross sectional, 2-phase Black Oil model which is a simplification of a 3-D, 3-phase model. The simplification was made to reduce run time and storage requirements for this work, and was achieved by reducing the y-dimension to 1 block. Most of the code is written to accomodate a 3-D system. The solution technique is typical of IMPES simulators, so that only the following details will be discussed here:

    - 3-D well model

    - automatic time step selector

    - restart option

    - material balance checking

    - relative permeability and capillary pressure treatment.

A.1 - 3-D WELL MODEL

The extension of a 2-D areal to a 3-D model is not trivial, although it is basically just a bookkeeping problem. The main difficulty comes in describing the well model for the vertical direction, and then incorporating it into the solution matrix. The solution presented here assumes a stack of layers, each of which acts like a 2-D areal well model described well by Peaceman[20]. These layers are connected at the wellbore, which gives extra constraints due to the hydrostatic pressure of the fluids in the

wellbore, and the common production or injection of fluids, as described by Zapata [9].
These conditions lead to the following basic equations:

$$q_k = F_{lk}(P_{wk} - P_k) \quad k=1,nz \qquad \text{: Areal well model} \qquad \text{(A-1)}$$

$$Q = \Sigma q_k \qquad\qquad k=1,nz \qquad \text{: Common production} \qquad \text{(A-2)}$$

$$P_{wk} = P_{BH} - \gamma_F \Delta D_k \qquad\qquad \text{: Hydrostatic equilibrium} \qquad \text{(A-3)}$$

The aim of the following mathematical development is to derive an equation for q_k which incorporates Q and constrains wellbore pressures to hydrostatic equilibrium. First, substituting Eq. A-3 into Eq. A-1 gives

$$q_k = F_{lk}(P_{BH} - \gamma_F \Delta D_k - P_k) \qquad\qquad \text{(A-4)}$$

Substituting Eq. A-4 into Eq. A-2 gives

$$Q = \Sigma F_{lk}(P_{BH} - \gamma_F \Delta D_k - P_k)$$

or,
$$Q = \Sigma F_{lk} P_{BH} - \Sigma F_{lk} \gamma_F \Delta D_k - \Sigma F_{lk} P_k \qquad\qquad \text{(A-5)}$$

Equation A-5 can be solved for PBH so that

$$PBH = \frac{Q + \Sigma F_{lk} \gamma_F \Delta D_k + \Sigma F_{lk} P_k}{\Sigma F_{lk}} \qquad\qquad \text{(A-6)}$$

Substituting Eq. A-6 into Eq. A-4 gives us our desired result,

$$q_k = F_{lk}\left(\frac{Q + \Sigma F_{lk} \gamma_F \Delta D_k + \Sigma F_{lk} P_k}{\Sigma F_{lk}} - \gamma_F \Delta D_k - P_k\right) \qquad \text{(A-7)}$$

To improve the well model, we can treat the P_k pressure terms at the new time level and thus make the well model implicit.

$$q_k = F_{lk} \left(\frac{Q + \Sigma F_{lk} \gamma_F \Delta D_k}{\Sigma F_{lk}} - \gamma_F \Delta D_k \right) - F_{lk} \left(P_k - \frac{\Sigma F_{lk} P_k}{\Sigma F_{lk}} \right) \quad \text{(A-8)}$$

The last term in Eq. A-8 includes a summation over all of the stacked grid blocks in a particular well. This shows up in the solution matrix as terms which do not fall on the normal diagonals, but which do remain within the outside bands, if the blocks are numbered in column major order.

If a rate constraint is given so that Q is given, and P_{BH} is unknown, the A matrix and B vector (Ax = B) will be augmented as follows:

$$b_k = b_k + F_{lk} \left(\frac{Q + \Sigma F_{lk} \gamma_F \Delta D_k}{\Sigma F_{lk}} - \gamma_F \Delta D_k \right) \quad \text{(A-9)}$$

$$A_{k,k} = A_{k,k} + F_{lk} - \frac{F_{lk}}{\Sigma F_{lk}} \qquad \text{: Diagonal terms} \qquad \text{(A-10)}$$

$$A_{k,i} = A_{k,i} - \frac{F_{lk} F_{li}}{\Sigma F_{lk}} \qquad \text{: Off-diagonal terms, } i \neq k \quad \text{(A-11)}$$

If a bottom hole pressure constraint is given, then P_{BH} is known, and the arrays are augmented as follows:

$$b_k = b_k + F_{lk} \left(P_{BH} - \gamma_F \Delta D_k \right) \qquad \text{(A-12)}$$

$$A_{k,k} = A_{k,k} + F_{lk} \qquad \text{: Diagonal terms} \qquad \text{(A-13)}$$

The F_{lk} terms are calculated as a normal areal Peaceman flow coefficient with an enhancement needed for the grid system we used. Our purpose was to impose the wellbore pressure on the face of a grid block instead of in the center of the grid block. This involved calculating a skin factor which would, theoretically, move the well where we wanted it. The skin factor was then added into the Peaceman well model flow coefficient.

The skin factor adjustments were calculated by considering the following system:

Figure A-1 : Plan View of System Considered
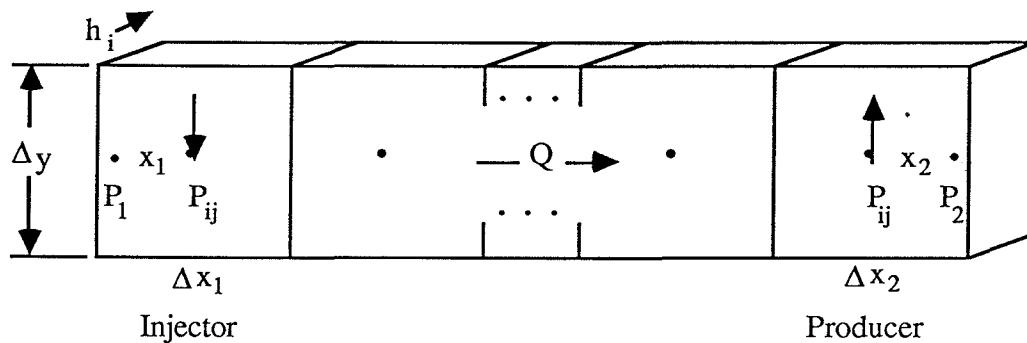
where P_{ij} is the grid block pressure

P_1, P_2 are wellbore pressures in wells 1 and 2, respectively

Assuming steady state flow within a grid block,

$$q = F_1 (P_w - P_{ij}) = \frac{kA}{\mu} \frac{(P_1 - P_{ij})}{x_1} \qquad \text{: Injector} \qquad (A-14)$$

Flow Coefficient   Darcy's Law for linear system

$$q = F_1 (P_{ij} - P_w) = \frac{kA}{\mu} \frac{(P_{ij} - P_2)}{x_2} \qquad \text{: Producer} \qquad (A-15)$$

where

$$F_1 = \frac{2\pi k h}{\mu (\ln\frac{r_0}{r_w} + S)}$$

$$A = h \Delta y$$

Since both these equations lead to the same skin factor, we will consider only the injector equation here. P_1 is an arbitrary position in the grid block a horizontal distance x_1 from the center of the block where we wich to place the well. If we let $P_w = P_1 = P$, then

$$\frac{2\pi k h}{\mu} \frac{(P - P_{ij})}{(\ln\frac{r_0}{r_w} + S)} = \frac{k h \Delta y}{\mu} \frac{(P - P_{ij})}{x_1} \qquad (A-16)$$

Simplifying and solving for S, we find that

$$S = \frac{2\pi x_1}{\Delta y} - \ln\frac{r_0}{r_w} \qquad (A-17)$$

For our special case in which the well pressure is on the block face, $x_1 = \Delta x_1/2$, and

$$S = \frac{\Delta x}{\Delta y} \pi - \ln\frac{r_0}{r_w} \qquad (A-18)$$

This result has not been rigorously tested, but the data available indicates that our original purpose has been accomplished.

This skin factor is used in the flow coefficient as

$$F_l = \frac{2\pi\, k\, h}{\mu\, (\, \ln\frac{r_0}{r_w} + S\,)} \qquad : \text{Single phase} \qquad (A\text{--}19)$$

$$F_l = \frac{2\pi\, k\, h}{\mu\, (\, \ln\frac{r_0}{r_w} + S\,)}\ (\lambda_o + \lambda_w) \qquad : \text{2 phase (oil/water)} \qquad (A\text{--}20)$$

$$F_l = \frac{2\pi\, k\, h}{\mu\, (\, \ln\frac{r_0}{r_w} + S\,)}\ (\lambda_o + \lambda_w + \lambda_g) \qquad : \text{3 phase} \qquad (A\text{--}21)$$

where

$$\lambda_j = \frac{k_{rj}}{\mu_j}, \quad \text{for } j = \text{oil (o), water (w), or gas (g).}$$

In each of these terms, the denominator reduces to

$$\frac{\Delta x}{\Delta y}\ \pi \qquad\qquad\qquad (A\text{--}22)$$

when the skin factor derived above is substituted. This provides a simplification since r_0 is not needed. This simulator provides input flags to select this skin factor method or a more traditional approach which calculates r_0 for the desired geometry.

Two major problems arise when implementing this 3-D well model. First is the assignment of the different phase flow rates as a fraction of the total rate in a well. The second is the evaluation of the fluid density in the wellbore, γ_F. This second problem is more difficult and will be handled last.

A few assumptions have been made to simplify the allocation of the total rate into the phase rates. In an injection well, it is assumed that the oil and gas fractions of the total injection rate are input parameters and remain constant with time. Usually, these fractions will both be zero so that only water is injected. At the production wells, the total rate produced from a layer is partitioned by the ratio of phase mobility to total fluid mobility. The mobilities are calculated at grid block pressure and saturation. Both of these assumptions are reasonable.

The evaluation of the wellbore fluid density is difficult in a production well, but easy in an injector. In the injector, we use our input oil and gas fractions mentioned above to multiply the phase densities. Usually, $\gamma_F = \gamma_w$ since we inject water only. The production well treatment is broken into the rate constraint case and the pressure constraint case. When rate constrained, no pressures are known, so that a ratio of the phase mobility is the best possible method.

$$\gamma_F = \gamma_o\frac{\lambda_o}{\lambda_{tot}} + \gamma_w\frac{\lambda_w}{\lambda_{tot}} + \gamma_g\frac{\lambda_g}{\lambda_{tot}} \tag{A-23}$$

When pressure constrained, however, both the wellbore and grid block pressures are known, so that a flow rate can be calculated into each layer for each phase. This procedure starts at the known bottom hole pressure and proceeds up the well as follows:

Figure A-2 : Schematic of Calculation Procedure

① Given wellbore pressure, P_w

② Calculate phase and total flow rates

③ Calculate $\gamma_F = \gamma_o \dfrac{q_o}{q_{tot}} + \gamma_w \dfrac{q_w}{q_{tot}} + \gamma_g \dfrac{q_g}{q_{tot}}$

where the rates are actually cumulative

from the bottom of the well

④ Calculate P_w from hydrostatic equilibrium

for the next block up the well

⑤ Repeat
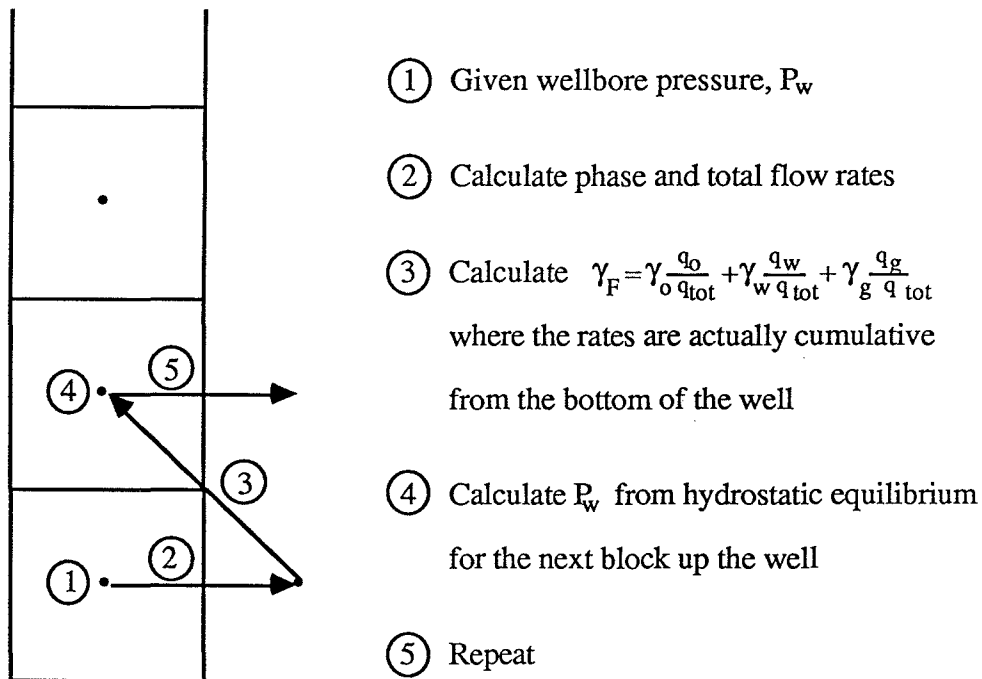
This procedure is explicit since it uses pressures at the current time level. However, we assume that the wellbore fluid density will not change drastically during a time step.

A.2 - Time Step Selection

Two levels of time step selection are provided in this simulator. Within a time step, the time step size will be reduced as needed to keep the maximum pressure and saturation changes within user defined limits. In the management routine following the time step, some simple stability criteria are used to select the step size for the next time step.

The pressure and saturation change limits are included to maintain accuracy and stability in the actual solutions obtained during a time step. The saturation constraint is designed to reduce the effect of calculating saturations explicitly by limiting how much saturation can change in a grid block over one time step. If the saturation change is greater than this limit at the end of the time step, both pressure and saturation values are reset to their values before the time step and the step is repeated with a smaller time step until the limit is met. The pressure change constraint is similar to the saturation change constraint in purpose and execution. Here, however, the check is made before the new saturations for a time step are calculated, but after converged pressures are found. Also, the purpose is to limit the effects of time averaging due to the implicit calculation of pressures instead of the errors made in the explicit calculation of saturations.

In the management routine, three criteria are used to predict a stable time step size. The first limits the amount of fluid relative to the grid block size which will remain in a grid block during a time step. At the end of a time step, the water and oil flow rates in the x and z directions are calculated for each grid block. The net flow of oil and water in each direction is added together to give the net rate of fluid which will remain in the grid block. This rate is then related to the pore volume of that grid block, and a time step is calculated such that no more than 1/4 of the pore volume will remain during a time step[21]. The minimum time step of those calculated for each grid block is then the maximum time step allowed without violating this stability criteria.

The second and third criteria increase the current step size so that the maximum pressure or saturation change will approach the user defined limits for the changes. This gives a much needed mechanism for the time step to increase while constraining the increase to acceptable limits.

At the end of the management routine, the minimum step of these three methods is selected as the step size to use for the next time step.

A.3 - Restart Option

A restart option allows a run which has been terminated for any reason to be continued where it left off. This is very important when running large jobs, in particular where allowable run time for a single job is limited by the system and allowing the continuation of runs for longer simulated times after seeing the results of the first run. Therefore, a restart option is included to reduce costs due to duplicate runs and to allow running of long jobs.

The restart is very simple both conceptually and in practice. Whenever the program is requested to print the pressure, saturation, and well information, the pressure and saturation grids, time, time step size, and other necessary information are updated on a restart file. To run a program with a restart file, simply set the restart flag so that some of the input data will be read from the restart file instead of the standard input file. This makes the restart utility very easy to use.

A.4 - Material Balance Checking

Material balance checking is not performed by the simulator during run time. Instead, the simulator dumps critical data to a material balance file at every time step. This file is then processed by a material balance post-processor to generate a detailed report of fluids present and produced at each step. This information is used to calculate a material balance on each phase as follows:

$$\text{Balance} = \frac{\text{Initial - Current phase in place}}{\text{Injected - Produced phase}} \cdot \qquad (A\text{-}24)$$

Clearly, this balance should equal 1.0 for each phase at each time, and a major deviation from 1.0 indicates some instability in the problem.

A.5 - Relative Permeability and Capillary Pressure Treatment

Relative permeability and capillary pressure curves are allowed to vary across the system by assigning each grid block to one of possibly several input curves. Relative permeability can be input as a table (S_w, k_{ro}, k_{rw}) or as parameters of the equations

$$k_{ro} = k_{ro}^{\circ} (1 - S)^{m} \qquad (A\text{-}25)$$

$$k_{rw} = k_{rw}^{\circ} (S)^{n} \qquad (A\text{-}26)$$

$$S = \frac{S_w - S_{wr}}{1 - S_{or} - S_{wr}} \qquad (A\text{-}27)$$

Capillary pressure must be input as a table. Evaluation of tabulated curves uses a midpoint search to bracket the input saturation, and then a linear interpolation to find the correct permeability or capillary pressure. Since a linear interpolation is used between successive table entries, care sould be taken when creating the input table to ensure accuracy.

APPENDIX B

SAMPLE INPUT FILES

B.1 - Main Input File

```
1  0  0.0  0.0  0  0.0  0      ; IMB,ICHECK,QOINJ,QGINJ,IRATE,TIME,ISTART
0.0  1.E-5  3500.0             ; CW,CF,PREF
1.0 0.8 1.0  50.  .05          ; SGW,SGO,SGG,DPLIM,DSLIM
14.7  1.00  1.0  5.0E-2        ; PSW,BWS,WVISC,EPS
1  0                           ; IRTKR,IRTPC
16                             ; NSAT FOR KR TABLE #1
.05  .87  .00                  ;
...                            ; NSAT LINES OF SW,KRO,KRW FOR KR TABLE #1
.80  .00  .62                  ;
0  1                           ; IRTKR,IRTPC
16                             ; NSAT FOR PC TABLE #1
.05  23.4521                   ;
...                            ; NSAT LINES OF SW,PC FOR PC TABLE #1
.80  0.0000                    ;
0  2                           ; IRTKR,IRTPC
16                             ; NSAT FOR PC TABLE #2
.05  16.1234                   ;
...                            ; NSAT LINES OF SW,PC FOR PC TABLE #2
.80  0.0000                    ;
0  0                           ; IRTKR,IRTPC -FLAG TO END KR AND PC INPUT
2                              ; NSAT2
0.0  0.  0.  0.                ; NSAT2 LINES OF SW,KRO,KRG,PCOG
1.0  0.  0.  0.                ;
2                              ; NPRE
2000.0  1.40  100.0  1.0       ; NPRE LINES OF P,$\mu_O$,$R_S$,$B_O$
5000.0  1.40  100.0  1.0       ;
300.0 2000.0 10 220.0 .75 2000.0; PMIN,PMAX,NGAS,TEMPF,SPGR,PBUB
30  1  10  0  0  0  1000.0     ; NX,NY,NZ,IOPT,JOPT,KOPT,DTOP
100.0  1.0  10.0               ; DX,DY,DZ
0                              ; IACT
5                              ; ITYPE FOR P
3200.0  0.00 0.0 0.43333       ; VALUE,XGRAD,YGRAD,ZGRAD
1                              ; ITYPE FOR SW
0.05                           ; VALUE
1                              ; ITYPE FOR SO
0.95                           ; VALUE
1                              ; ITYPE FOR POR
0.20                           ; VALUE
1                              ; ITYPE FOR IKR
1                              ; VALUE
5                              ; ITYPE FOR IPC
1  0.0  0.0  0.1               ; VALUE,XGRAD,YGRAD,ZGRAD
5                              ; ITYPE FOR XKX
10.0  0.0  0.0  1.0            ; VALUE,XGRAD,YGRAD,ZGRAD
0                              ; IISO
5                              ; ITYPE FOR XKY
10.0  0.0  0.0  1.0            ; VALUE,XGRAD,YGRAD,ZGRAD
1                              ; ITYPE FOR XKZ
100.0                          ; VALUE,XGRAD,YGRAD,ZGRAD
$
```

Description of Reservoir Represented in Main Input File

This input file creates a grid with 30 - 100' blocks in the x-direction, 10 - 10' blocks in the z-direction, and a unit thickness block in the y-direction, all of which are active. Therefore, the overall grid dimensions are 3000' x 1' x 100'. The pressure array is initialized to 3200 psia at the top of the reservoir and grades linearly to the bottom with a gradient of 0.433 psi/ft. There are no pressure gradients in the x-direction. Water saturation is 5% everywhere with no gas, so that oil saturation is 95% everywhere. The porosity is constant at 20%. All blocks use the same relative permeability table, but each layer has a different capillary pressure table, numbered from 1 at the top to 10 at the bottom (only two capillary pressure tables are shown in the input file for brevity). X-direction permeability is 10 md at the top, grades linearly to 100 md at the bottom, and is homogeneous within a layer. Y-direction permeability is the same as x-direction permeability. Z-direction permeability is set to 100 md everywhere.

Main Input File Record Descriptions

```
RECORD 1 :   IMB,ICHECK,QOINJ,QGINJ,IRATE,TIME,ISTART
(1 LINE)     IMB      -   MATERIAL BALANCE FLAG
                      =   0     NO HISTORY DATA KEPT
                      =   1     HISTORY DATA OUTPUT TO UNIT IMAT
             ICHECK   -   CHECK FLAG
                      =   0     NO CHECKING DESIRED
                      =   1     CHECK WELL PROPERTIES GIVEN IN /TARGET/
             QOINJ    -   OIL FRACTION OF INJECTION STREAM
             QGINJ    -   GAS FRACTION OF INJECTION STREAM
             IRATE    -   GRID BLOCK FLOW RATE PRINT FLAG
                      =   0     NO PRINTING OF GRID BLOCK FLOW RATES
                      =   1     PRINTS ENTIRE ARRAY OF OIL AND WATER FLOW
                                RATES
             TIME     -   TIME AT WHICH TO START SIMULATION (DAYS)
             ISTART   -   RESTART FLAG
                      =   0     GRID BLOCK DATA READ FROM THIS FILE
                      =   1     GRID BLOCK DATA READ FROM THE RESTART FILE
```

```
RECORD 2 :    CW,CF,PREF
(1 LINE)      CW      -  WATER COMPRESSIBILITY (1/PSIA)
              CF      -  FORMATION COMPRESSIBILITY (1/PSIA)
              PREF    -  REFERENCE PRESSURE FOR POROSITY FUNCTION
                      =  -1   CONSTANT POROSITY FLAG

RECORD 3 :    SGW,SGO,SGG,DPLIM,DSLIM
(1 LINE)      SGW     -  WATER SPECIFIC GRAVITY (WATER=1)
              SGO     -  OIL SPECIFIC GRAVITY (WATER=1)
              SGG     -  GAS SPECIFIC GRAVITY (AIR=1)
              DPLIM   -  LIMIT ON GRID BLOCK PRESSURE CHANGE PER TIME STEP
              DSLIM   -  LIMIT ON GRID BLOCK WATER SATURATION CHANGE PER
                         TIME STEP

RECORD 4 :    PSW,BWS,WVISC,EPS
(1 LINE)      PSW     -  REFERENCE PRESSURE FOR WATER FORMATION VOLUME
                         FACTOR FUNCTION
              BWS     -  REFERENCE WATER FORMATION VOLUME FACTOR
              WVISC   -  CONSTANT WATER VISCOSITY VALUE
              EPS     -  CONVERGENCE TOLERANCE FOR PRESSURE EQUATION

RECORD 5 :    RELATIVE PERMEABILITY(KR) AND CAPILLARY PRESSURE(CP) TABLES
              (OIL/WATER SYSTEM)

              IRTKR   -  RELATIVE PERMEABILITY (KR) ROCK TYPE ID
              IRTPC   -  CAPILLARY PRESSURE (PC) ROCK TYPE ID
              NSAT    -  NUMBER OF DATA LINES IN A TABLE
              DATA LINE DEFINITIONS VARY ACCORDING TO IRTKR AND IRTPC AS:
              IRTKR = 0,  IRTPC = 0 - NO MORE TABLES TO READ
              IRTKR > 0,  IRTPC = 0 - KR TABLE #IRTKR
                                    - SW,KRO,KRW
              IRTKR = 0,  IRTPC > 0 - PC TABLE #IRTPC
                                    - SW,PC
              IRTKR > 0,  IRTPC > 0 - BOTH KR TABLE #IRTKR AND PC TABLE
                                      #IKRPC
                                    - SW,KRO,KRW,PC
              IRTKR < 0,  IRTPC = 0 - KR FUNCTION #IRTKR
                                    - SWR,SOR,N,M,KRW*,KRO*
              IRTKR < 0,  IRTPC > 0 - KR FUNCTION #IRTKR FOLLOWED BY
                                      PC TABLE #IRTPC
                                    - SWR,SOR,N,M,KRW*,KRO*
                                    - NSAT
                                    - SW,PC
                          IRTPC < 0 - ERROR

              *NOTE : MAXIMUM OF 100 DIFFERENT TABLES AND FUNCTIONS FOR KR
                      AND PC, BUT LIMITED TO 1000 TOTAL DATA LINES.

RECORD 6 :    WATER SATURATION TABLE 2 (GAS/OIL/WATER SYSTEM)
(NSAT2+1 LINES)
              NSAT2   -  NUMBER OF TABLE ROWS(>0)
              SATTAB2 -  SATURATION,KRO,KRG,PCOG
              *NOTE : DATA NOT CURRENTLY USED, BUT MUST EXIST IN DATA SET.

RECORD 7 :    PRESSURE TABLE
(NPRE+1 LINES)
              NPRE    -  NUMBER OF TABLE ROWS(>0)
              PRETAB  -  PRESSURE,$\mu_O$,$R_S$,$B_O$
```

```
RECORD 8 :      GAS PROPERTIES TABLE
(1 LINE)        PMIN    -   MINIMUM PRESSURE
                PMAX    -   MAXIMUM PRESSURE
                NGAS    -   NUMBER OF TABLE ROWS(>0)
                TEMPF   -   SYSTEM TEMPERATURE(°F)
                SPGR    -   GAS SPECIFIC GRAVITY(AIR=1)
                PBUB    -   BUBBLE POINT PRESSURE(PSIA)
                GASTAB  -   PRESSURE,Z-FACTOR,CG,MU (IS GENERATED BY SUB
                            SETGAS)
                *NOTE : DATA NOT CURRENTLY USED, BUT MUST EXIST IN DATA SET.

RECORD 9 :      GRID NUMBER INPUT - NX,NY,NZ,IOPT,JOPT,KOPT,DTOP
(1 LINE)        NX,NY,NZ- NUMBER OF GRID BLOCKS IN X, Y, AND Z DIRECTIONS
                IOPT
                JOPT    -   GRID SPACING FLAGs IN X, Y, AND Z DIRECTION
                KOPT
                DTOP    -   DEPTH TO TOP OF FORMATION (FEET)

RECORD 10 :     GRID SIZE INPUT - DEPENDS ON VALUES OF IOPT, JOPT, AND KOPT
                                  FLAGS
                IOPT
                JOPT    =  0   CONSTANT SIZE IN ALL DIRECTIONS
                KOPT    -      DX,DY,DZ (FEET)
                OR
                IOPT    =  0   CONSTANT SIZE IN X DIRECTION
                        -      DX
                        =  1   VARIABLE SIZE IN X DIRECTION
                        -      DX(1),DX(2),...,DX(NX)
                FOLLOWED BY
                JOPT    =  0   CONSTANT SIZE IN Y DIRECTION
                        -      DY
                        =  1   VARIABLE SIZE IN Y DIRECTION
                        -      DY(1),DY(2),...,DY(NY)
                FOLLOWED BY
                KOPT    =  0   CONSTANT SIZE IN Z DIRECTION
                        -      DZ
                        =  1   VARIABLE SIZE IN Z DIRECTION
                        -      DZ(1),DZ(2),...,DZ(NZ)

RECORD 11 :     GRID BLOCK ACTIVITY FLAG - IACT
(1 LINE)        IACT    -   ACTIVITY FLAG
                        =  0   ALL GRID BLOCKS ARE ACTIVE
                        =  1   SOME GRID BLOCKS ARE INACTIVE

RECORD 12 :     ACTIVE GRID BLOCK INPUT - DEPENDS ON VALUE OF IACT FLAG
                IACT    =  0   NO LINES ARE READ FOR THIS RECORD
                        =  1   (KF,KL) I = 1
                               (KF,KL) I = 2
                               ...
                               (KF,KL) I = NX
                                    KF = FIRST ACTIVE GRID BLOCK IN A
                                         COLUMN
                                    KL = LAST ACTIVE GRID BLOCK IN A
                                         COLUMN

RECORD 13 :     GRID BLOCK PRESSURE VALUES, P

RECORD 14 :     GRID BLOCK WATER SATURATION VALUES, SW

RECORD 15 :     GRID BLOCK OIL SATURATION VALUES, SO

RECORD 16 :-    GRID BLOCK POROSITY VALUES, POR

RECORD 17 :     GRID BLOCK RELATIVE PERMEABILITY ID VALUES, IKR
```

RECORD 18 : GRID BLOCK CAPILLARY PRESSURE ID VALUES, IPC

RECORD 19 : GRID BLOCK X-DIRECTION PERMEABILITY VALUES, XKX

```
RECORD 20 :   IISO
(1 LINE)      IISO    -    ISOTROPIC PERMEABILITY FLAG
                      =  0     ANISOTROPIC - READ KY AND KZ ALSO
                      =  1     ISOTROPIC   - SET KY = KZ = KX
```

RECORD 21 : GRID BLOCK Y-DIRECTION PERMEABILITY VALUES, XKY
(ONLY IF IISO = 0)

RECORD 22 : GRID BLOCK Z-DIRECTION PERMEABILITY VALUES, XKZ
(ONLY IF IISO = 0)

```
RECORDS 13-22 USE THE SAME FORMAT (EXCEPT FOR RECORD 20) :
              ITYPE    -   DATA FLAG
              DATA LINES VARY ACCORDING TO ITYPE FLAG AS :
              ITYPE    =  1    CONSTANT VALUE FOR ALL BLOCKS
                       -       VALUE
                       =  2    CONSTANT VALUES ON ROWS
                       -       VAL(1),VAL(2),...,VAL(NZ)
                       =  3    CONSTANT VALUES ON COLUMNS
                       -       VAL(1),VAL(2),...,VAL(NX)
                       =  4    NO CONSTANT VALUES
                       -       VAL(KF),VAL(KF+1),...,VAL(KL) I = 1
                       -       VAL(KF),VAL(KF+1),...,VAL(KL) I = 2
                       -       ...
                       -       VAL(KF),VAL(KF+1),...,VAL(KL) I = NX
                       =  5    CONSTANT GRADIENTS IN X, Y, AND Z DIRECTIONS
                       -       VALUE,XGRAD,YGRAD,ZGRAD
                               VALUE =  DATA VALUE IN UPPER LEFT CORNER OF
                                        GRID
                               XGRAD
                               YGRAD = GRADIENTS OF DATA (DATA VALUE/FOOT)
                               ZGRAD
                       <  0    AFTER READING DATA ACCORDING TO ABS(ITYPE)
                               ABOVE, INDIVIDUAL GRID BLOCK VALUES CAN BE
                               READ
                       -       NVAL            THE NUMBER OF VALUES TO READ
                       -       I,J,K,VALUE  BLOCK LOCATION AND NEW VALUE
```

B.2 - Well Input File

```
2   0                         ; NWELL,ISKIN
1   1  1   .50  1000.0        ; M,I,J,R,SKINN
2  30  1   .50  1000.0        ; M,I,J,R,SKINN
*                             ; CHARACTER INITIATING AN OUTPUT
OPTION
1  1  1  1  20  20  3000.     ; IWELL,IDELF,IPWHAT,NPWHAT,IPTYPE,NPT
YPE,
                                   TMAX
2                             ; NUPS
1  1  1     3.562  0  0  0.0  ; K,I1,M1,T1,I2,M2,T2
2  1 -3 2300.000  0  0  0.0   ; K,I1,M1,T1,I2,M2,T2
1.E-3  .95                    ; T1,T2
1  1  0  1  1                 ; IOPT(1),...,IOPT(5)
0  0  0  0  0  1  1           ; NOPT(1),...,NOPT(7)
$
```

Description of Wells Represented in Well Input File

This input file describes two wells in the system - one located at (I,J) location (1,1) and the other at (30,1). Note that the grid system is 30 x 1 x 10 with just 1 block in the y-direction. Each well has a radius of 0.5 feet. The skin factor of 1000.0 is used as a flag to the well model routine to adjust the flow coefficient as described in the Simulator Description of the Appendix.

The simulation run will cease at t = 3000.0 days and produce printer and plotter output every 20 time steps. Well number 1, located at (1,1), will inject 3.562 RB/D and produce with a bottom hole pressure constraint of 2300.0 psi at well number 2, located at (30,1). These values will be constant throughout the simulation as all check parameters are zero (note also that flag ICHECK is zero in the main input file). Time step size is initialized to 0.001 days and will be adjusted automatically according to the stability factor (the ratio of dimensionless time step to dimensionless grid block size), which is input as 0.95. The printed output will include the pressure array, water saturation array, cumulative rates per well, and well data per layer. The plot output will

include the pressure array and the water saturation array, but is not currently affected by the values of NOPT input above.

Well Input File Record Descriptions

```
RECORD 1 :    NWELL,ISKIN
(1 LINE)      NWELL    -    NUMBER OF WELLS IN SYSTEM
              ISKIN    -    SKIN FACTOR FLAG
                       =    0    SAME SKIN FACTOR APPLIES TO ALL LAYERS
                                 IN A WELL
                       =    1    READ A SEPARATE SKIN FACTOR FOR EACH LAYER
                                 IN A WELL

RECORD 2 :    M,I,J,R,SKINN
(1 LINE)      M        -    WELL NUMBER FOR THIS LINE
              I        -    X BLOCK LOCATION OF WELL
              J        -    Y BLOCK LOCATION OF WELL
              R        -    WELL RADIUS (FEET)
              SKINN    -    SKIN FACTOR - VALUE DEPENDS ON ISKIN FLAG
                           ISKIN = 0      SKINN IS THE SKIN FACTOR
                                 = 1      DUMMY VALUE WHICH IS NOT USED

RECORD 3 :    SKIN FACTOR FOR EACH LAYER IN THE WELLS - ONLY IF
              ISKIN FLAG = 1
              M        -    WELL NUMBER FOR THIS LINE
              SKIN(M,KF)
              SKIN(M,KF+1)
              . . .    -    SKIN FACTOR FOR EACH LAYER IN WELL NUMBER M
              SKIN(M,KL)
                           WHERE    KF = FIRST ACTIVE GRID BLOCK IN WELL M
                                    KL = LAST ACTIVE GRID BLOCK IN WELL M

RECORD 4 :    ICHR   INITIATES AN OUTPUT OPTION SECTION OF DATA
(1 LINE)      ICHR     -    SINGLE CHARACTER IN COLUMN 1
                       =    $    TERMINATES INPUT FROM THIS FILE
                       =    *    SIGNALS PROPER START OF DATA
                       ≠    *    SKIPS THIS LINE AND READS NEXT
```

```
RECORD 5 :      IWELL,IDELF,IPWHAT,NPWHAT,IPTYPE,NPTYPE,TMAX
(1 LINE)        IWELL   -   WELL UPDATE FLAG
                        =   0   NO NEW WELL DATA WILL BE READ
                        =   1   WELL DATA WILL BE UPDATED
                IDELF   -   TIME STEP UPDATE FLAG
                        =   0   NO NEW TIME STEP DATA WILL BE READ
                        =   1   TIME STEP DATA WILL BE UPDATED
                IPWHAT  -   PRINT OPTION UPDATE FLAG
                        =   0   NO NEW PRINT OPTION DATA WILL BE READ
                        =   1   PRINT OPTION DATA WILL BE UPDATED
                NPWHAT  -   PLOT OPTION UPDATE FLAG
                        =   0   NO NEW PLOT OPTION DATA WILL BE READ
                        =   1   PLOT OPTION DATA WILL BE UPDATED
                IPTYPE  -   PRINT FREQUENCY FLAG
                        =   0   TIME AT WHICH TO PRINT WILL BE READ
                        >   0   SPECIFIES THE TIME STEP INCREMENT FOR
                                PRINTING
                NPTYPE  -   PLOT FREQUENCY FLAG
                        =   0   TIME AT WHICH TO PLOT WILL BE READ
                        >   0   SPECIFIES THE TIME STEP INCREMENT FOR
                                PLOTTING
                TMAX    -   TIME TO PAUSE OR STOP SIMULATION (DAYS)
                        -   WHEN TMAX IS REACHED, THIS FILE IS ACCESSED
                            AGAIN, ALLOWING THE USER TO UPDATE THE WELL,
                            TIME STEP, AND OUTPUT OPTIONS, AND RUN THE
                            SIMULATION TURNING WELLS ON OR OFF, AND
                            CHANGING TIME STEP SIZE, JUST TO MENTION A
                            COUPLE OF USES

RECORD 6A:      WELL UPDATE DATA - ONLY IF IWELL = 1
(1 LINE)        NUPS    -   NUMBER OF WELL UPDATES TO READ

RECORD 6B:      K,I1,M1,T1,I2,M2,T2
(1 LINE)        K       -   WELL NUMBER TO UPDATE
                I1      -   CHANGE WELL DATA FLAG
                        =   0   NO CHANGE MADE TO WELL DATA
                        =   1   WELL DATA WILL BE CHANGED TO M1 AND T1
                M1      -   REPLACES IFLAG(K) WHEN I1 = 1
                T1      -   REPLACES WELVAL(K) WHEN I1 = 1
                I2      -   CHANGE CHECK DATA FLAG
                        =   0   NO CHANGE MADE TO CHECK DATA
                        =   1   CHECK DATA WILL BE CHANGED TO M2 AND T2
                M2      -   REPLACES ICH(K) WHEN I2 = 1
                T2      -   REPLACES CHK(K) WHEN I2 = 1

RECORD 7 :      TIME STEP DATA - ONLY IF IDELF = 1
(1 LINE)        T1      -   NEW TIME STEP IF T1 > 0
                T2      -   NEW STABILITY FACTOR IF T2 > 0

RECORD 8 :      PRINT OUTPUT OPTIONS - ONLY IF IPWHAT = 1
(1 LINE)        IOPT    -   ARRAY OF LENGTH 5 ACTING LIKE 5 DIP SWITCHES
                            (0-OFF/1-ON)
                        1   PRESSURE ARRAY
                        2   WATER SATURATION ARRAY
                        3   OIL SATURATION ARRAY
                        4   CUMULATIVE WELL DATA
                        5   WELL DATA PER LAYER

RECORD 9 :      PLOT OUTPUT OPTIONS - ONLY IF NPWHAT = 1
(1 LINE)        NOPT    -   ARRAY OF LENGTH 7 ACTING LIKE 7 DIP SWITCHES
                            (0-OFF/1-ON)

                *NOTE-: THIS FEATURE IS NOT IMPLEMENTED.  THE VALUES OF NOPT
                        ARE NEVER USED
```

```
RECORD 10:    OUTPUT TIME DATA - ONLY IF IPTYPE = 0 OR NPTYPE = 0
(1 LINE)      T1      -    TIME AT WHICH TO PRINT (DAYS) IF IPTYPE = 0,
                           ELSE NOT USED
              T2      -    TIME AT WHICH TO PLOT (DAYS) IF NPTYPE = 0,
                           ELSE NOT USED
```

BIBLIOGRAPHY

1. Buckley, S.E. and Leverett, M.C., "Mechanism of Fluid Displacement in Sands," *Trans.*, AIME (1942) **146**, 107-16.

2. Welge, H.J., "A Simplified Method for Computing Oil Recovery by Gas or Water Drive," *Trans.*, AIME (1952) **195**, 91-8.

3. Collins, R.E., *Flow Through Porous Media*, Petroleum Publishing Co., Tulsa (1976).

4. Craig, F.F., Jr., *The Reservoir Engineering Aspects of Waterflooding*, Monograph Series, SPE, Dallas (1971) **3**.

5. Dake, L.P., *Fundamentals of Reservoir Engineering*, Elsevier Scientific Publishing Co., New York (1978).

6. Lake, L.W., and Pope, G.A., *Fundamentals of Enhanced Oil Recovery*, Chapter 6 (in progress).

7. Dykstra, H. and Parsons, R.L., "The Prediction of Oil Recovery by Water Flood," Secondary Recovery of Oil in the United States, API (1950) pp.160-174.

8. Stiles, W.E., "Use of Permeability Distribution in Waterflood Calculations," *Trans.*, AIME, (1949) **186**, 9-13.

9. Zapata, V.J., "The Effects of Viscous Crossflow on Sharp Front Displacements in Two-Layered Porous Media," MS thesis, U. of Texas, Austin, Tx. (1979).

10. Reznic, A.A., Enick, R.M., and Panvelker, S.B.,"An Analytical Extension of the Dykstra-Parsons Vertical Stratification Discrete Solution to a Continuous, Real-Time Basis," *Soc. Pet. Eng. J.*, (December 1984) 643-55.

11 Coats, K.H., Nielson, R.L., Terhune, M.H., and Weber, A.G.,"Simulation of Three-Dimensional, Two-Phase Flow in Oil and Gas Reservoirs," *Soc. Pet. Eng. J.*, (December 1967) 377-88.

12. Coats, K.H., Dempsey, J.R., and Henderson, J.H., "The Use of Vertical Equilibrium in Two-Dimensional Simulation of Three-Dimensional Reservoir Performance," *Soc. Pet. Eng. J.*, (March 1971) 63-71.

13. Hearn, C.L., "Simulation of Stratified Waterflooding by Pseudo-Relative Permeability Curves," *J. Pet. Tech.*, (July 1971) 805-13.

14. Jones, R.S., Jr., "A Predictive Model for Water and Polymer Flooding," MS thesis, U. of Texas, Austin, Tx (April 1984).

15. Lake, L.W., and Pope, G.A., *Fundamentals of Enhanced Oil Recovery,* Chapter 6.5 (in progress).

16. Berruin, N.and Morse, R.A.,"Waterflood Performance of Heterogeneous Systems," *J. Pet. Tech.,* (July 1979) 829-36.

17. Haldorsen, H.H., and Lake, L.W., "A New Approach to Shale Management in Field-Scale Simulation Models," *Soc. Pet. Eng. J.,* (August 1984) 447-57.

18. Jones, J.R., Jr., Scott, A.J., Lake, L.W., and Waggoner, J.R., "Reservoir Characterization For Numerical Simulation of Mesaverde Meanderbelt Sandstone, Northwest Colorado," paper SPE 13052 presented at the 1984 SPE Annual Technical Conference and Exhibition, Houston, Sept. 16-19.

19. Lasseter, T.J., Waggoner, J.R., and Lake, L.W., "Reservoir Heterogeneities and Their Influence on Ultimate Recovery," presented at the 1985 NIPER Reservoir Characterization Technical Conference, Dallas, Texas, Apr. 29.

20. Peaceman, D.W.,"Interpretation of Well-Block Pressures in Numerical Reservoir Simulation," *Soc. Pet. Eng. J.,* (June 1978) 183-94.

21. Todd, M.R., O'Dell, P.M., and Hirisaki, G.J.,"Methods for Increasing Accuracy in Numerical Reservoir Simulators," *Soc. Pet. Eng. J.,* (December 1971) 515-30.

22. Weber, K.J.,"Influence on Fluid Flow of Common Sedimentary Structures in Sand Bodies," paper SPE 9247 presented at the 1980 SPE Annual Technical Conference and Exhibition, Dallas, Sept. 21-24.

23. Kortekaas, T.F.M.,"Water/Oil Displacement Characteristics in Cross-Bedded Reservoir Zones," paper SPE 12158 presented at the 1983 SPE Annual Technical Conference and Exhibition, San Francisco, Oct. 5-8.

VITA

John Raymond Waggoner was born in Ithaca, New York on December 27, 1959, the son of James A. and Mary S. Waggoner. After completing his secondary education at Memorial High School, Houston, Texas, in 1978, he entered the University of Texas (UT) in Austin, Texas, where he received his B.S. in Petroleum Engineering in May, 1982. In September, 1982, he entered graduate school at the University of Texas in Petroleum Engineering. During the summers of 1981 through 1983, he worked for Conoco Research and Development in Ponca City, Oklahoma, on a different project each year. In 1981, his work concerned well-to-well tracer studies and their use in determining heterogeneities between wells. In 1982, his work concerned the history match of a surfactant flood pilot study to characterize the reservoir heterogeneity. In 1983, he designed some core cleaning equipment and studied the cleaning effectiveness of a variety of solvents. Following his wedding to Lauren Green on May 26, 1984, he worked the rest of the summer for Schlumberger-Doll Research (SDR) in Ridgefield, Connecticut, simulating the effect of reservoir heterogeneity on vertical water saturation profiles. Based on this work at SDR, he co-authored a paper with Dr. Thomas Lasseter of SDR and Dr. Larry Lake of UT entitled "Reservoir Heterogeneities and Their Influence on Ultimate Recovery".

Permanent Address: 849 Pecanwood
                                Houston, Texas 77024

This thesis was typed by John R. Waggoner.